l'université nantes angers le mans
COMMUNAUTÉ D'UNIVERSITÉS ET ÉTABLISSEMENTS

UNIVERSITÉ DE NANTES

Thèse de Doctorat

Razmig KANDILIAN

Mémoire présenté en vue de l'obtention du
grade de Docteur de l'Université de Nantes
sous le label de L'Université Nantes Angers Le Mans

École doctorale : Sciences pour l'ingénieur, Géosciences, Architecture

Discipline : *Sciences pour l'ingénieur*
Spécialité : *Génie des procédés*
Unité de recherche : *Laboratoire GEPEA, UMR-CNRS 6144*

Soutenue le *23 juillet, 2015*

Etude du couplage entre limitation azotée et transfert de lumière pour la production de lipides par microalgues en photobioréacteur

JURY

Rapporteurs :	**Giles PELTIER**, Directeur de recherche, CEA Cadarache, Institut de Biologie Environnementale et Biotechnologie **Vincent GOETZ**, Directeur de recherche, CNRS, Laboratory PROMES
Examinateurs :	**Jack LEGRAND**, Professeur, Université de Nantes **Laurent PILON,** Professeur, University of California Los Angeles **Alberto BRUCATO,** Professeur, Università di Palermo
Directeur de Thèse :	**Jeremy PRUVOST**, Professeur. Université de Nantes

Résumé de la thèse

Etude du couplage entre limitation azotée et transfert de lumière pour la production de lipides par microalgues en photobioréacteur

By
Razmig Kandilian
Université de Nantes
Le laboratoire de Génie des procédés – environnement – agro-alimentaire (GEPEA)

L'accroissement de la demande d'énergie combiné aux préoccupations sur la disponibilité à long terme des ressources pétrolières, ainsi que les dommages environnementaux liés à la combustion des combustibles fossiles ont forcé les sociétés à chercher des carburants alternatifs et durables. Sur les cinq dernières décennies, la population mondiale a plus que doublé, et il est prévu qu'elle augmentera de 1,4 milliard de personnes d'ici à 2035 [BP(2014)]. Simultanément, la demande d'énergie ainsi que les émissions de CO_2 devraient augmenter de 41% et 29%, respectivement [BP(2014)]. La planète reçoit 2850 Peta W d'énergie via le rayonnement solaire. Pourtant, selon l'administration de l'information de l'énergie des États-Unis, les énergies renouvelables représentaient seulement 11% de l'énergie totale produite aux États-Unis en 2013 [Administration(2013)]. À noter que cette même année, la biomasse était la source d'environ 49% de la production d'énergie renouvelable aux États-Unis. Le reste provenait du vent (17%), du solaire thermique et photovoltaïque (3.4%), géothermique (2,4%), et hydrothermique (28%). En 2009, le transport a été responsable de 29% de la consommation de l'énergie totale aux Etats-Unis, dont le transport terrestre a constitué approximativement 80% de celui-ci. L'utilisation mondiale des carburants liquides devrait augmenter de 19 millions de barils par jour en 2035, et cela principalement en raison du secteur des trans-

ports. De même, en Europe, la part totale des énergies renouvelables était de 14,1 en 2012 % [EU(2013)]. Cela a été répartie comme suivant : 5.1 % de l'énergie solaire, 65,5 % de la biomasse et des déchets, 3,2 % de l'énergie géothermique, 10 % de l'énergie du vent, et 16,2 % pour l'hydro-électricité. En outre, la part des énergies renouvelables dans le secteur des transports dans l'UE était seulement de 5,4 % en 2013 [EU(2013)].

Malgré l'introduction des voitures électriques, le pétrole liquide reste difficile à remplacer commercialement par une autre source d'énergie disponible, vue sa densité énergétique élevée et sa facilité de stockage. La grande majorité du pétrole est fournie par les combustibles fossiles, ce qui a mené à la pollution et au changement climatique [IPCC(2007)]. Cela a amené à la recherche de solutions alternatives, comme la production de carburants liquides issus de la biomasse "biocarburants". Ainsi, différents pays de par le monde ont fixé des objectifs d'incorporation de ces biocarburants. Par exemple, l'EISA (Energy Independence and Security Act of 2007), a fixé les normes des carburants renouvelables imposant 136 million de mètres cubes de biocarburants renouvelables pour être mélangés avec des carburants de transport vendus aux États-Unis en 2022 [Ferrell and Sarisky-Reed(2010)]. De la même façon, la législation actuelle de l'Union européenne exige qu'au moins 10 % de l'énergie utilisée dans le secteur du transport doit provenir de sources renouvelables d'ici à 2020 [EU(2009)].

Les biocarburants de première génération sont produits via la voie de fermentation du sucre, de l'amidon ou de la cellulose afin de produire l'éthanol, le propanol et le butanol [Chisti(2007)]. Or, ils sont apparus défavorables, en raison de l'utilisation de l'alimentation humaine et animale comme matière première pour la production de biocarburants en plus de leur rendement énergétique faible. Ils ont donc été remplacés par des biocarburants dits de deuxième génération, qui utilisent le soja, le canola, le palmier, le jatropha, le maïs, ainsi que l'huile de cuisson usée comme matière première pour produire des biocarburants comme le biodiesel. L'utilisation de ces plantes pour produire des carburants a toute fois suscité

des controverses en raison de l'utilisation de cultures terrestres, d'eau douce, et de vastes surfaces de terres arables pour produire des quantités suffisantes de carburants [Chisti(2007)]. Ainsi, l'huile de palme, considérée comme ayant l'un des meilleurs rendements, peut fournir un rendement annuel maximal de 2400 litres d'huile par hectare. Pour produire la quantité utilisée annuellement pour la transportation dans le pays (833 million m^3 de carburants), une surface terrestre trois fois plus grande que celle disponible aux États-Unis sera nécessaire. En Outre, 30% du maïs cultivé aux États-Unis est utilisé pour la production d'éthanol. Afin de répondre aux mandats fédéraux d'EISA 2022, plus de 100% du maïs produit aux États-Unis devraient être convertis en biocarburants pour produire les 136 m^3 d'éthanol. Par conséquent, au maximum 56 des 136 m^3 de biocarburants mandatés par EISA ont ainsi été autorisés à être convertis en bioéthanol. Le reste devrait provenir de biodiesel à base de microalgues [Ferrell and Sarisky-Reed(2010)]. De même, l'Union européenne a plafonné la quantité d'éthanol qui peut être utilisée comme combustible dans le secteur du transport pour un maximum de 7 % [EU(2009)].

Les microalgues possèdent des productivités dix fois plus grande que les plantes supérieures et elles peuvent être cultivées dans des eaux usées ainsi que sur des terres arides. Ces organismes unicellulaires utilisent l'énergie solaire pour convertir le CO_2 en biomasse, avec une efficacité de 10 à 100 fois supérieure à celle des plantes supérieures [Ke(2001),Chisti(2007),Carvalho *et al.*(2011)]. Les microalgues utilisent de l'eau comme source d'électrons, la lumière du soleil comme source d'énergie, et le CO_2 comme source de carbone inorganique pour produire de l'oxygène, de l'amidon, des glucides, et des lipides. Une partie de ces lipides, en particulier les triglycérides, peut être extraite de la cellule et convertie en biodiesel par transestérification. L'analyse du cycle de vie (LCA) effectuée dans les travaux de Liu *et al.* [Liu *et al.*(2013b)], a démontré que le biodiesel dérivé de microalgues, se caractérise par des émissions des gaz à effet de serre (GES), nettement plus faible que l'éthanol et le pétrodiesel.

Cependant, il a au mieux un rendement énergétique compris entre 1 et 3, ce qui est beaucoup plus faible que les carburants pétroliers [Liu *et al.*(2013b)]. Certaines espèces comme la microalgue marine *Nannochloropsis oculata* et la microalgue verte *Botryococcus braunii* peuvent accumuler jusqu'à 30 à 70% de poids sec en lipides [Hodgson *et al.*(1991), Rodolfi *et al.*(2009)]. Les lipides peuvent être convertis en biodiesel et la biomasse résiduelle peut être fermentée pour produire du biogaz ou vendue comme engrais car elle est riche en phosphate et en azote. Alternativement, la biomasse peut être convertie en pétrole brut via la liquéfaction hydrothermique. Cette dernière est un processus qui expose la biomasse humide, qui contient jusqu'à 20% de sa poids sec en solides, à des températures jusqu'à 350 ^{o}C et des pressions 10-20 MPa pour produire de l'huile brute "biocrude" se caractérisant par un pouvoir calorifique supérieur compris entre 35 et 40 MJ /kg. Cependant, l'huile produite via la liquéfaction hydrothermique contientde l'azote et de l'oxygène jusqu'à 11 et 6% au poids sec, respectivement [Frank *et al.*(2013)]. Cela n'est pas toutefois souhaitable, car elle entraîne une augmentation des émissions de NO_x lorsque le carburant produit est brûlé [Frank *et al.*(2013)]. Ainsi, l'huile doit être traitée et l'excès d'oxygène et d'azote doit être retiré ce qui conduit au final à augmenter le coût de production [Frank *et al.*(2013)]. Donc, la production de biodiesel par extraction des lipides, suivie par leur transestérification, reste une option attrayante.

Actuellement, la production de la biomasse microalgale dans des PBRs exposés aux conditions solaires n'est pas rentable. À titre d'exemple, le rendement théorique maximum de biodiesel est estimé à 350000 L/ha·an, alors que les rendements réels sont au mieux de 50000 L/ha·an [Chisti(2013)]. De même, le rendement théorique de la biomasse avec une fraction massique de lipides allant jusqu'à 40% du poids sec, est estimé à 0,095 kg/m^2·j alors que la productivité typique en PBRs est inférieure à 0,025 kg/m^2·j [Chisti(2013)]. Ces réductions au niveau de la productivité en biomasse et par conséquent de biodiesel, sont souvent attribués

à l'inefficacité de l'utilisation de la lumière dans les PBRs [Chisti(2013)]. Par conséquent, malgré la grande efficacité photosynthétique des micro-organismes, le biodiesel microalgal demeure approximativement trois fois plus coûteux à produire que le pétrole [Jones and Mayfield(2012)]. Chisti [Chisti(2012)] a déterminé que le coût de production de la biomasse composée de 40.% du poids sec de lipides, doit être inférieur à 0,50 $ pour que le biodiesel microalgal soit économiquement compétitif avec 100 $ par baril du pétrole brut. Or, les estimations actuelles des coûts de production de la biomasse sèche varient de 5 $ à 100 $ par kg [Chisti(2012), Chisti(2013)]. Alternativement, Stephens *et al.* [Stephens *et al.*(2010)] a illustré la production de biodiesel à grande échelle ($\geq$ 500 ha), et il a démontré que les systèmes de production de microalgues peuvent être rentables, s'ils ont également été utilisés pour la co-production des produits à haute valeur ajoutée (HVA), tels que les protéines végétales hydrolysées (PVH) ou le bêta-carotène qui peut être vendu pour 600 $/kg.

La productivité faible du PBR ainsi que le coût élevé de la production de biomasse, mettent en évidence l'importance de l'optimisation de l'utilisation de la lumière dans les PBRs. Le but de cette étude a donc été de comprendre comment le taux d'absorption de la lumière par les cellules affecte leur production de lipides, et de proposer des règles et des lignes directives afin d'optimiser le processus de production en photobioréacteurs. Pour cela, l'exécution de l'analyse du transfert radiatif dans les cultures de micro-algues, ainsi que la connaissance des caractéristiques radiatives des micro-organismes étaient nécessaires. La présente étude peut être divisée en deux parties. La première partie porte sur la détermination expérimentale et théorique des caractéristiques optiques des micro-organismes. Ensuite, la deuxième partie détaille l'influence de l'absorption de la lumière par les micro-organismes sur l'accumulation et la production de triglycérides.

Tout d'abord, l'étude présente la validation d'un modèle basé sur la théorie de Lorenz-Mie pour prédire les proprietes radiatives des micro-organismes en les comparant à celles mesurées

expérimentalement. Ainsi, toutes les propriétés radiatives (sections efficaces d'absorption et de diffusion, fonction de phase), ont été mesurées expérimentalement pour la microalgue *Chlamydomonas reinhardtii* cultivée dans les conditions optimales de croissance et dans des conditions de limitation nutritive, et également pour *Chlorella vulgaris*. La validation a été réalisée avec succès pour *C. reinhardtii* en conditions optimales de croissance et en limitation azotée. Cependant, le modèle théorique n'a pas permis de prédire les proprietes de *C. vulgaris* avec précision. Cette dernière est cependant connue pour avoir une paroi cellulaire rigide et épaisse. La modélisation des cellules de *C.vulgaris* supposées comme étant des sphères enrobées d'une paroi avec une absorption nulle de la coque extérieur a entraîné une diminution de 15 % au niveau de l'absorption des sections par rapport à celle prévue pour les cellules de *C. vulgaris* modélisés comme des sphères homogènes. La diminution de la section efficace de l'absorption est due au "Package effect". Celui-ci provoque une diminution de la section efficace de l'absorption à la densité des pigments dans la cellule. Enfin, la vitesse moyenne d'absorpion des photons ainsi que la fraction éclairée du PBR ont été estimés en utilisant les propriétés radiatives déterminées par mesure ou par prédiction. Les différences relatives maximales dans ces paramètres étaient inférieures à 6%, 15% et 5% en utilisant repectivement les propriétés radiatives de *C. reinhardtii* cultivées dans des conditions de croissance optimale, *C. reinhardtii* cultivée en limitation azotée, et *C. vulgaris*.

Ensuite, une procédure expérimentale simple a été mise au point pour la récupération du spectre moyen d'absorption de la section efficace des suspensions de microalgues concentrées présentant des échantillons de diffusion uniques ou multiples. La méthode a combiné des mesures expérimentales de la transmittance hémisphérique normale et de la réflectance des suspensions dans des cuvettes classiques avec une méthode inverse basée sur un algorithme génétique et des expressions analytiques obtenues à partir du modèle à deux-flux modifié. La méthode a été validée par des mesures directes dela fonction de phase de diffusion et de la

section efficace d'absorption et de diffusion de la microalgue d'eau douce *Chlorella vulgaris*. Il a été possible de récupérer la section efficace d'absorption avec une précision suffisante pour une estimation correcte des vitesse d'absorption de photons locales et moyennes dans le PBR.

La deuxième partie du travail s'est focalisée sur la détermination de la relation entre le vitesse d'absorption de photons et la production de TAG pour deux espèces distinctes, à savoir, l'eustigmatophyceae d'eau de mer *Nannochloropsis oculata* et la microalgue d'eau douce *Parachlorella kessleri*, cultivées repectivement en batch et en continu. Tout d'abord, une relation a été déterminée entre la vitesse moyen d'absorption de photons par unité de masse de microalgues et la productivité quotidienne de TAG pour des cultures de *N. oculata*. Cette relation a indiqué que la carence azotée toute seule ne garantit pas un taux de production élevé de TAG. Les cinétiques de la biosynthèse de TAG sont apparues limitées par le vitesse d'absorption des photons des cultures. La productivité surfacique de TAG atteint une valeur maximale de 4.5 g/m^2·j pour un vitesse d'absorption de photons de 13 $\mu\text{mol}_h\nu$/g·s. En outre, un vitesse d'absorption initial de valeur critique supérieure à 13 $\mu\text{mol}_h\nu$/g·s a été requis pour déclencher une grande accumulation intracellulaire en TAG en carence soudaine et progressive d'azote. Cependant, pour les cultures batch, les concentrations de la biomasse et de pigments ont considérablement évolué avec le temps et menant à une évolution importante de la vitesse d'absorption de photons en cours de culture, ce qui a rendu difficile l'analyse de la vitesse d'absorption de photons sur l'accumulation de lipides TAG à l'intérieur de cellules. Cela a conduit à une incertitude quant à la relation entre la vitesse d'absorption de photons et la capacité des cellules à accumuler les TAG. Pour cela, la notion de vitesse d'absorption de photons critique a été proposée cela a permis de montrer que les cultures qui ont présenté tout au début de la carence azotée une valeur supérieure à celle de la valeur critique, étaient garanties d'atteindre une accumulation maximale en TAG.

Dans un second temps, afin de clarifier cette relation, l'accumulation ainsi que la productivité intracellulaire en TAG ont été étudiées en régime permanent pour des cultures continues de *P. kessleri*, limitées en azote, où tous les paramètres physiologiques restent constants au cours du temps. Les résultats obtenus suggèrent que la concentration intracellulaire de TAG pour les cultures continues de *P. kessleri* dépend de la vitesse moyen d'absorption des photons dans le PBR. Tout d'abord, il a été démontré que la définition correcte de la vitesse moyen d'absorption des photons MRPA doit être exprimée par kilogramme de biomasse catalytique plutôt que par kilogramme de biomasse totale. D'ailleurs, la intracellulaire de TAG ainsi que la productivité de TAG ne dépendent pas uniquement de la MRPA mais aussi de la concentration de nitrate dans la culture. En effet, pour une concentration d'azote relativement importante dans le milieu d'alimentation, à savoir, $[NO_3^-]$ $\geq$ 3,65 mM, les cellules recourent à stocker le carbone sous forme de carbohydrates. Cependant, avec la diminution de la concentration de nitrate dans le milieu d'alimentation, la concentration intracellulaireen sucres a diminué et la concentration de TAG dans les cellules a augmenté. L'accumulation de TAG dans les cellules ainsi que la productivité de TAG dans la culture sont influencées de façon complexe à la fois par la vitesse moyen d'absorption des photons MRPA et la concentration en nitrate dans le milieu d'alimentation. Ainsi, la vitesse d'absorption de lumière dans le PBR et la concentration de nitrate dans le milieu doivent être soigneusement contrôlés pour maximiser la productivité de TAG.

Au final, ce travail ouvre de nombreuses perspectives. Des études ultérieures qui s'intéressent des propriétés radiatives des micro-algues, devraient porter sur la détermination précise de l'épaisseur et la composition de la paroi cellulaire de *Chlorella vulgaris*. De plus, l'hypothèse de l'homogénéité de la cellule doit être étudiée d'une manière plus approfondie. Dans ce contexte, une question se pose : est-ce que toutes les cellules, quelles que soient leur forme et leur taille, peuvent être supposées d'être homogènes ? De plus, il serait nécessaire de

modéliser le chloroplaste comme étant une entité séparée avec une vision plus précise de l'organisation pigmentaire. Enfin, la relation entre la vitesse spécifique d'absorption de photons et l'accumulation et la productivité de TAG doit être confirmée à grande échelle et en conditions solaires, avec donc des variations importantes de flux lumineux qui complexifieront l'optimisation du transfert de rayonnement pour la production de lipides par microalgues. Le procédéde production continue de biodiesel peut également être amélioré par l'optimisation de l'apport en azote (concentration d'alimentation en nitrate et taux de dilution appliqué à la culture). Cela nécessitera le développement et l'élaboration des modèles cinétiques prédisant la concentration en biomasse et en pigments en fonction de la concentration en nitrates. Enfin, la réussite du développement des procédés en aval downstream (récolte extraction des lipides, conversionen biodiesel, etc.) pourrait être la clé pour une production économiquement rentable du biodiesel microalgal.

Vita

2009 B.S., Mechanical Engineering, Summa Cum Laude

University of California Los Angeles

Los Angeles, CA

2011 M.S., Mechanical Engineering

University of California Los Angeles

Los Angeles, CA

2014 Ph.D., Mechanical Engineering

University of California Los Angeles

Los Angeles, CA

Archival publications

1. R. Kandilian, R.-L. Heng, L. Pilon, Absorption and scattering by fractal aggregates and by their equivalent coated spheres, Journal of Quantitative Spectroscopy and Radiative Transfer, Volume 151, Pages 310-326, 2015.

2. R. Kandilian, T.-C. Tsao, L. Pilon, Control of incident irradiance on a batch operated flat-plate Photobioreactor, Chemical Engineering Science, Volume 119, Pages 99-108, 2014.

3. R. Kandilian, J. Pruvost, J. Legrand, L. Pilon, Influence of light absorption rate by *Nannochloropsis oculata* on triglyceride production during nitrogen starvation, Bioresource Technology, Volume 163, Pages 308-319, 2014.

4. R. Kandilian, E. Lee, L. Pilon, Radiation and optical properties of *Nannochloropsis oculata* grown under different irradiances and spectra, Bioresource Technology, Volume 137, Pages 63-73, 2013.

5. I.M. McKinley, R. Kandilian and L. Pilon, Waste heat energy harvesting using the Olsen cycle on $0.945Pb(Zn_{1/3}Nb_{2/3})O_3 0.055PbTiO_3$ single crystals, Smart Materials and Structures, Volume 21, Issue 3, 035015, 2012.

6. L. Pilon, H. Berberoğlu, R. Kandilian, Radiation transfer in photobiological carbon dioxide fixation and fuel production by microalgae, Journal of Quantitative Spectroscopy and Radiative Transfer, Volume 112, Issue 17, Pages 2639-2660, 2011.

7. R. Kandilian, A Navid, L Pilon, The pyroelectric energy harvesting capabilities of PMN-PT near the morphotropic phase boundary, Smart Materials and Structures, Volume 20, Issue 5, 055020, 2011.

Conference presentations

1. R. Kandilian, A. Taleb, C. El-Khouri, M. Onay, J. Legrand, J. Pruvost, TAG production by *Parachlorella kessleri* cultures in continuous PBRs, The 5^{th} International Conference on Algal Biomass, Biofuels and Bioproducts, 7–10 June, 2015, San Diego, California, USA.

2. R. Kandilian, J. Pruvost, A. Soulies, B. Rousseau, J. Legrand, L. Pilon, Simple method to measure the spectral absorption cross-section of microalgae, Computational Thermal Radiation in Participating Media V, 1–3 April, 2015, Albi, France.

3. R. Kandilian, J. Pruvost, A. Artu, C. Lemasson, J. Legrand, L. Pilon, Comparison of experimentally measured and theoretically predicted radiation characteristics of various photosynthetic microorganisms, Computational Thermal Radiation in Participating Media V, 1–3 April, 2015, Albi, France.

4. R. Kandilian, J. Pruvost, J. Legrand, L. Pilon, Optimization of triglyceride production with respect to light using *Nannochlorpsis oculata*, The 4^{th} International Conference on Algal Biomass, Biofuels and Bioproducts, 15–18 June, 2014, Santa Fe, New Mexico, USA.

Acknowledgements

First, I would like to thank my thesis advisor professor Jérémy Pruvost for his guidance. It has been a pleasure working under his supervision in the last three years. I would also like to thank professor Jack Legrand, the director of GEPEA laboratory, for welcoming me to the research laboratory in Saint Nazaire. I would also like to express my appreciation to professor Laurent Pilon for his guidance both at UCLA and in Saint Nazaire. His work ethic and academic integrity will always serve as an example for me. My thanks also go to Dr. Vincent Goetz and Dr. Giles Peltier for taking the time to review my manuscript and for their contribution as members of my thesis jury. Finally, special thanks to professor Alberto Brucato for serving as a member of my jury.

I would like to thank the technical support team at the GEPEA, Delphine Kucma, Raphaelle Touchard, Emmanuel Dechandol, Helen Marec, and Candice Perrier, without whom this work would not have been possible.

During my time in Saint Nazaire I had the honor of meeting many friends. I would like to acknowledge these individuals, especially, Alexandra Busnel, Antoine Soulies, Antoinette Kazbar, Arnaud Artu ,Astrid de Luca, Benjamin Moutel, Camille Lemasson, Camille Poret, Clement Dousset, Emilie Angles, Francois Le Borgne, Jeremy Monlyad, Jordan Tallec, Kenza Saadaoui, Mbalo Ndiaye, Nour Ayache, Oumniya Arab, Pauline Engeammes, Remy Coat, Sergio Rios, Thomas Rinaldi, and Valantina Hmaymes.

I would like to thank Aumaya Taleb for her endless support and patience. Her love and companionship were essential for completing this thesis.

Finally, I would like to dedicate this dissertation to my loving parents Vahe and Linda Kandilian. A special thanks to my brother and my sister-in-law Ohannes and Mary Kandilian, my sister Rebecca Kandilian.

I would like to acknowledge and thank the NSF-IGERT program Clean Energy for Green Industry at UCLA (NSF Award 0903720) for financial support. I am also grateful to the Embassy of France in the United States for awarding me the Chateaubriand Fellowship and thank the ANR-DIESALG project (ANR-12-BIME-0001-02) for supporting this study.

Table of Contents

List of Figures

List of Tables

Introduction

The ever-increasing demand for energy combined with concerns over the long term availability and the environmental damage caused by fossil fuels has forced society to seek alternative and sustainable fuel production sources. Over the last five decades, world population has more than doubled and it is projected to increase by an additional 1.4 billion people by the year 2035 [BP(2014)]. Simultaneously, energy demand and CO_2 emissions are projected to increase by 41% and 29%, respectively [BP(2014)]. Solar radiation supplies the planet with 2,850 Peta Watt of energy. Yet, according to the United States Energy Information Administration, renewable energy accounted for only 11% of the total energy generated in the United States in 2013 [Administration(2013)]. Biomass was the source of approximately 49% of all renewable energy production in the U.S. that year. The remaining came from wind (17%), solar thermal and photovoltaic (3.4%), geothermal (2.4%), and hydrothermal (28%). In 2009, transportation was responsible for 29% of the total energy consumption in the United States with approximately 80% of it due to terrestrial transportation. Similarly, in Europe, the total share of renewable energy in 2012 was 14.1% [EU(2013)]. This was distributed as 5.1% solar energy, 65.5% biomass and waste, 3.2% geothermal energy,10% wind energy, and 16.2% hydropower. Moreover, the share of renewable energy in the transportation sector in the EU in 2013 was only 5.4% [EU(2013)].

Worldwide use of liquid fuel is projected to rise by 72 million liters per day in 2035 primarily due to the transportation sector. Despite the introduction of electric cars, the high energy density and ease of storage, liquid petroleum remains difficult to replace by any other commercially available energy source. The vast majority of the petroleum is supplied by fossil fuels which have led to pollution and climate change [IPCC(2007)]. On the other hand, liquid biofuels produced by photosynthetic microorganisms may be one of the renewable energy sources that satisfy the transportation fuel needs of the future. Therefore, the Energy Independence and Security Act (EISA) of 2007 established the renewable fuel standards mandating 136 million cubic meters of renewable biofuels to be blended with transportation

fuels sold in the U.S. by year 2022 [Ferrell and Sarisky-Reed(2010)]. Similarly, current European Union legislation requires at least 10% of the energy used in the transportation sector to come from renewable sources by 2020 [EU(2009)].

First-generation biofuels were produced by fermentation of sugar, starch, or cellulose to produce ethanol, propanol, and butanol [Chisti(2007)].These were unfavorable due to the use human and animal feed as a feedstock for biofuel production in addition to being unsustainable if mass-produced. Therefore, they have been superseded by second-generation biofuels that use soybean, canola, palm, jatropha, corn, as well as waste cooking oil as the feedstock to produce biofuels such as biodiesel. The use of these plants to produce fuels again proved controversial due to the use of food crops, freshwater, and large areas of arable land to produce fuels [Chisti(2007)]. The best agricultural crop, the palm oil, can yield a maximum of 2,400 liters of oil per acre per year. An arable land three times as large as that available in the U.S. is necessary to produce the 830 million cubic meters of transportation fuel the country uses yearly using palm oil. Moreover, 30% of the corn grown in the U.S. is used for ethanol production. In excess of 100% of the corn produced in the U.S. must be converted to biofuels to produce the 136 million cubic meters of ethanol to meet the 2022 EISA federal mandates. Therefore, at most 56 of the 136 million cubic meters of biofuels mandated by EISA are allowed to be bioethanol. The remainder is projected to come from microalgae-based biodiesel [Ferrell and Sarisky-Reed(2010)]. Similarly, the European Union has capped the amount of ethanol that can be used as fuel in the transportation sector to a maximum of 7% [EU(2009)].

Recent life cycle analysis (LCA) suggests that CO_2 emissions bioethanol produced from corn falls short of the U.S. legislative mandate of 60% reduction in greenhouse gas (GHG) emission compared to gasoline [Liska *et al.*(2014)]. By contrast, microalgae feature productivity ten times larger than higher plants and they can be cultivated in waste-water as well as on arid-land. These single cell organisms use solar radiation to convert CO_2 to biomass with efficiency 10 to 100 times larger than that of higher plants [Chisti(2007), Pilon *et al.*(2011), Carvalho *et al.*(2011), Ke(2001)]. Microalgae use water as their electron source,

sunlight as their energy source, and CO2 as their inorganic carbon source and produce oxygen, starch, carbohydrates, and lipids [Ke(2001)]. Some of these lipids, in particular triglyceride lipids, can be extracted from the cell and converted to biodiesel by transesterification. LCA analysis by Liu *et al.* [Liu *et al.*(2013b)] demonstrated that microalgae derived biodiesel has significantly lower GHG emission than both bioethanol and petroleum diesel. However, it has an energy return on investment between 1 and 3 which is much lower than petroleum fuels [Liu *et al.*(2013b)].

Some species such as the marine eustigmatophyceae *Nannochloropsis oculata* and the green microalgae *Botryococcus braunii* can contain up to 30 to 70% lipids by dry weight [Hodgson *et al.*(1991), Rodolfi *et al.*(2009)]. The lipids can be convereted to biodiesel and the remaining biomass can be fermented to produce biogas or sold as a fertilizer as it is rich in both phosphate and nitrogen. Alternatively, biomass can be converted to crude petroleum by hydrothermal liquefaction. The latter is a process that exposes wet biomass, 20 wt.% solids, to elevated temperatures (up to 350^{o}C) and pressures (10-20 MPa) to produce petroleum like biocrude oil that has a higher heating value between 35 and 40 MJ/kg. However, the oil produced using hydrothermal liquefaction contains nitrogen and oxygen of up to 11 and 6 wt.%, respectively [Frank *et al.*(2013)]. This is undesirable as it causes in increased NO_x emission when the produced fuel is burnt [Frank *et al.*(2013)]. Thus, the oil must be treated and excess oxygen and nitrogen removed which leads to increase in the production cost [Frank *et al.*(2013)]. Therefore, biodiesel production by lipid extraction and transesterification remains the most attractive option.

Currently, it is uneconomical to produce biomass in PBRs exposed to solar radiation. For example, maximum theoretical yield of biodiesel is reported to be 354,000 L/ha·year while actual yields are at best 50,000 L/ha^{-1}yr^{-1} [Chisti(2013)]. Similarly, theoretical yield of biomass with lipid mass fraction of 40 dry wt.% is reported to be 0.095 kg/m^2·day while the typical productivity in PBRs in less than 0.025 kg/m^2·day [Chisti(2013)]. These reductions in biodiesel and biomass productivity are attributed to inefficiency in light utilization by the PBRs [Chisti(2013)]. Consequentially, despite the large photosynthetic efficiency of

microorganisms, microalgae biodiesel remains approximately three times more expensive to produce than its petroleum counterpart [Jones and Mayfield(2012)]. Chisti [Chisti(2012)] determined that the cost of production for biomass composed of 40 dry wt.% lipids must be less than \$0.50 for microalgal biodiesel to be economically competitive with \$100 per barrel of crude oil. However, current estimates of dry biomass production costs range from \$5 to \$100 per kilogram [Chisti(2012), Chisti(2013)]. Alternatively, Stephens *et al.* [Stephens *et al.*(2010)] illustrated that biodiesel production by large-scale (> 500 hectare), microalgae production systems may be profitable if they were also used for co-producing high-value products such as acid-hydrolyzed vegetable protein (HVP) or beta-carotene which can be sold for \$600/kg. The low productivity of PBRs and the high cost of producing biomass highlight the importance of optimization of PBRs with respect to light.

The aim of this study was to understand how light absorption rate by the cells affects their lipid production and propose rules and guidelines for optimizing the biodiesel production process by. To do so, performing radiation transfer analysis in the microalgae cultures was necessary and therefore the knowledge of the radiation characteristics of the microorganisms. This study can be divided into two parts. The first part focuses on experimental and theoretical determination of the radiation characteristics of the microorganisms. Then, the second part details the influence of light absorption by the microorganisms on triglyceride accumulation and productivity. The manuscript is divided into five chapters preceded with an introduction and concluded by a chapter summarizing the main findings of the study and presenting perspectives and future work recommendations.

The first chapter presents a literature review and a summary of the state of the art of microalgae cultivation technologies. It provides an overview of cell and lipid metabolism and the essential triglyceride synthesis pathways. It also presents a framework for the remainder of the manuscript. The second chapter presents a comparison of theoretical and experimental determination of the radiation characteristics of microorganisms. Two distinct methods of radiation characteristics determination were applied to two different microorganisms to validate the model used for the theoretical approach. Chapter three presents a new simple

method of determining the absorption cross-section of microorganisms. A validation is presented for the new method by comparing it to the method used in Chapter two. Moreover, Chapter four characterizes the effects of light absorption rate by the microalgae *Nannochloropsis oculata* on triacylglycerol fatty acid productivity and accumulation in sudden nitrogen starvation batch cultures. Finally, Chapter five presents the effects of light absorption rate on the triglyceride productivity and accumulation of microalgae *Parachlorella kessleri* in nitrogen limited cultures in continuous production mode.

CHAPTER 1

Introduction

This chapter presents background information necessary to understand this study. First, it discusses the basics of photosynthesis and the metabolic pathways of fatty acid and lipid synthesis. Then it presents common methods of producing biomass and converting it to biofuels. The basics of radiation transport in photobioreactors and the radiation characteristics of the microorganisms are also presented.

1.1 Photosynthesis

Photosynthesis is the process that converts light energy into chemical energy in plants, green algae, cyanobacteria, and other photosynthetic microorganisms [Ke(2001)]. Photosynthesis occurs in the thylakoid membrane located inside the chloroplast in the two photosynthetic units called photosystem I (PS I) and photosystem II (PS II) [Ke(2001)]. Both PS I and PS II contain (i) a reaction center carrying out charge separation and electron transport and (ii) antenna featuring pigments responsible for absorbing light. The role of PS II is to split water into protons, oxygen, and electrons. PS I uses the electrons transported from PS II to carry out the redox reactions that result in CO_2 fixation [Ke(2001)]. The two main pigment molecules responsible for capturing light in photosynthetic green algae are Chlorophylls a and b [Ke(2001)]. Photosynthesis consists of two reactions : a light reactions followed by electron shuttling between the photosystems and a dark reaction [Ke(2001)].

1.1.1 Light dependent reactions

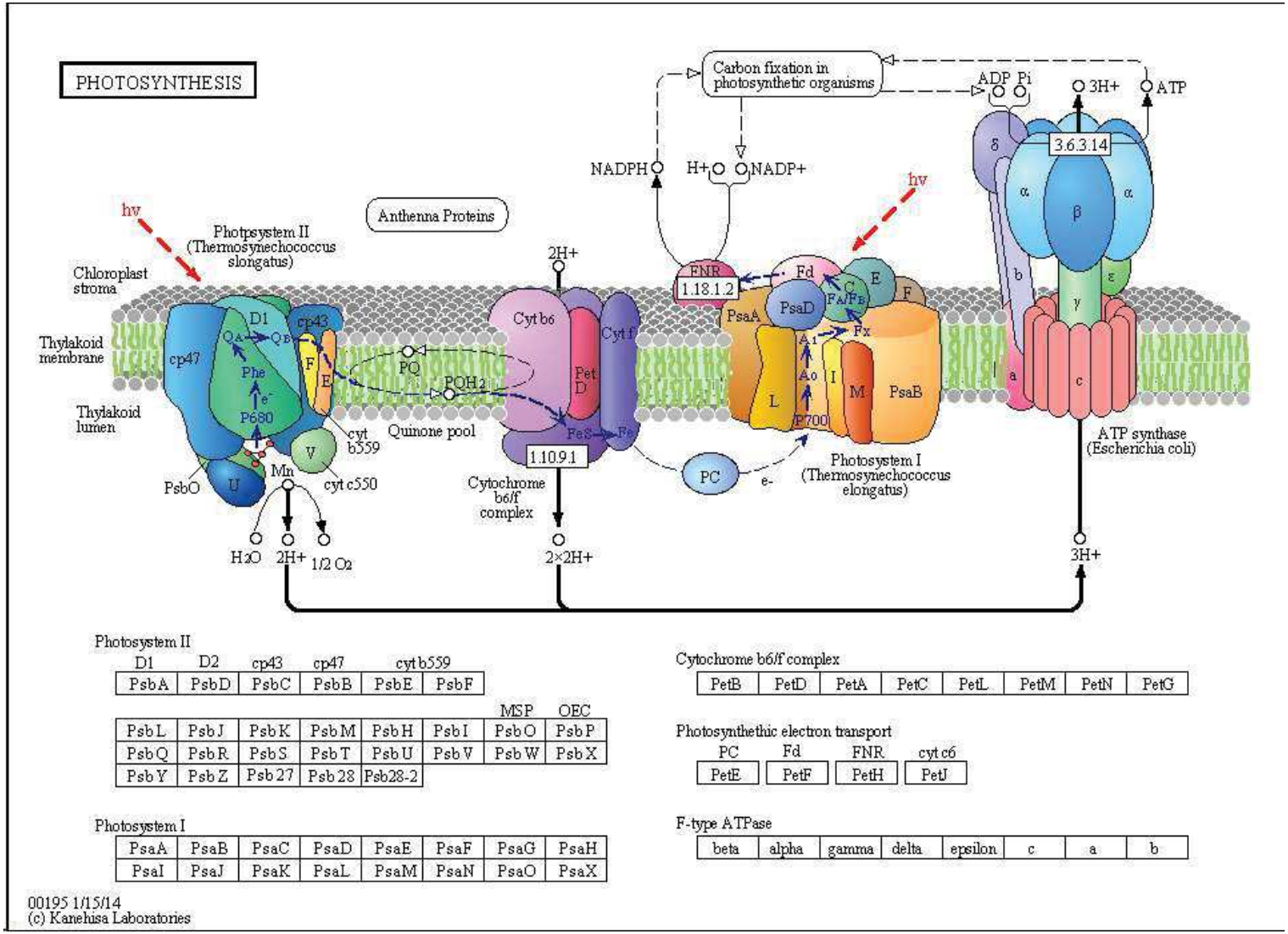

Figure 1.1: A schematic representation of the light reactions of the photosynthesis at the thylakoid membrane [Kanehisa Laboratories(2014)].

The light dependent reaction occurs in the grana and uses the absorbed light energy to produce the energy carrier molecules used in the light independent reaction. Figure 1.1 presents a schematic of the light dependent reaction of the photosynthesis at the thylakoid membrane. First, a photon strikes a chlorophyll*a* molecule in the PSII thereby exciting and freeing an electron. The electron is then passed to the metal-free chlorophyll variant called pheophytin which in turn passes it to a quinone molecule [Ke(2001)]. Through a series of electron transportation, described by the Z-scheme shown in Figure 1.2, the electron is transferred to a chlorophyll molecule in the PSI [Ke(2001)]. The proton gradient created across the chloroplast membrane is dissipated by the ATP synthase to form ATP [Ke(2001)]. The electron transported to PSI is then excited by a second photon absorbed by the chlorophyll molecule in the PSI. Hydrogen ions are moved across the thylakoid membrane into the lumen using the energy created by the electron acceptors. Finally using the transported electron, NADP is reduced to NADPH [Ke(2001)]. In the non-cyclic electron transport scheme, the electron lost by the chlorophyll*a* molecule is replaced by the splitting of a water molecule into H^+ and O_2. In the cyclic electron transport, the reaction only takes place in the PSI and is used to only create ATP. The electron excited by the light absorption is returned to the chlorophyll molecule in PSI and hence the water splitting step is unnecessary and it is omitted. In summary, the purpose of the the light reactions is to provide NADPH and ATP used to drive reduction of CO_2 as presented in the following equation [Ke(2001)]

$$2NADP^+ + 3H_2O + 2ADP + 2Pi \leftrightarrow 2NADPH + 3ATP + O_2 \tag{1.1}$$

1.1.1.1 Radiation harvesting pigments and photoadaptation

In the ideal case, the PS I and PS II each require only 4 moles of photons of wavelength equal to or smaller than 700 and 680 nm (red), respectively, to fix 1 mole of CO_2 [Ke(2001)]. Chlorophylls (chl) *a*, *b*, and *c* molecules are the primary pigments responsible for absorbing visible photons and transferring the charges to the reaction center. Carotenoids, on the other hand, can be divided into xanthophylls and carotenes [Ke(2001)]. Carotenes are photosyn-

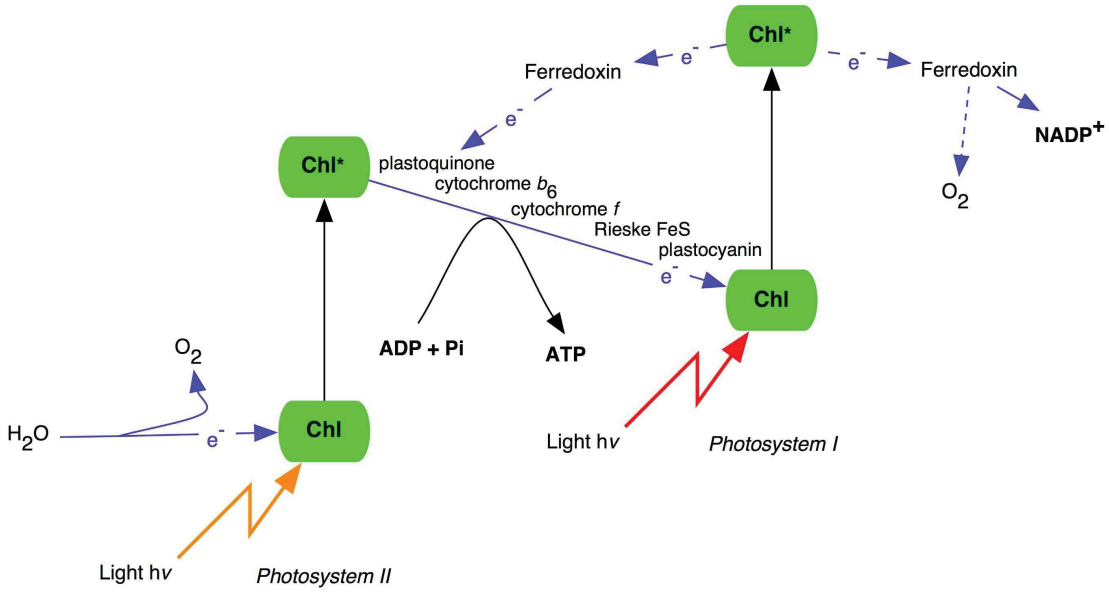

Figure 1.2: The Z-scheme describing the oxidation and reduction changes during the light reactions of photosynthesis [Allen(2004)].

thetic and absorb photons with wavelength corresponding to green and yellow colors and transfer the charges to chlorophyll molecules [Ke(2001)]. Xanthophylls, on the other hand, act to protect the photosynthetic apparatus against excessive light [Ke(2001)]. These photoprotective carotenoids quench poisonous free radicals and convert excess radiant energy into heat [Dubinsky and Stambler(2000), Lubián *et al.*(2000), Gentile and Blanch(2001)]. For example, *Nannochloropsis oculata* contain the pigments chlorophyll *a*, β-carotene, and the xanthophylls violaxanthin and vaucherxanthin but lack chlorophyll *b* [Cohen(1999)].

Microalgae experience photoacclimation and chromatic acclimation in response to different incident irradiance and spectrum, respectively [Dubinsky and Stambler(2000), Fisher *et al.*(1996), Gentile and Blanch(2001)]. For example, they tend to increase their pigment concentrations in light-limited conditions. However, this may not lead to significant changes in their radiation characteristics as increasing the concentration of chlorophylls also decreases their *in vivo* specific absorption coefficient due to mutual shading of pigment molecules [Dubinsky and Stambler(2000)]. The latter is partially responsible for what is known as the

package effect corresponding to the non-linear relationship between cell pigment concentrations and cell absorption cross-section [Jonasz and Fournier(2007)]. In addition, microalgae increase their photoprotective carotenoid concentration in response to large irradiance while reducing the amount of photosynthetic carotenoids through the so-called xanthophyll cycle [Dubinsky and Stambler(2000), Lubián *et al.*(2000), Gentile and Blanch(2001)]. The latter does not usually lead to changes in the overall carotenoid concentration as changes in the two types of carotenoids compensate each other [Dubinsky and Stambler(2000), Lubián *et al.*(2000)].

Moreover, photoacclimation and chromatic acclimation depend on the microalgae species. Even among *Nannochloropsis* species large difference in pigment expression exists. For example, Gentile and Blanch [Gentile and Blanch(2001)] observed an 80% and 60% decrease in chl*a* and vioxanthin, respectively, in batch grown *Nannochloropsis gaditana* when the incident irradiance on a 250 ml flask was increased from 70 μmol/m^{2}s to 880 μmol/m^{2}s. Fisher *et al.* [Fisher *et al.*(1996)] found that *Nannochloropsis sp.* grown under 30 μmol/m^{2}s, in continuous cultures, had a steady-state chlorophyll concentration 4.5 times larger than when grown under 650 μmol/m^{2}s. The low light-acclimated cells increased their number of photosynthetic units while the size of individual PSU remained constant. Lubián *et al.* [Lubián *et al.*(2000)] demonstrated that *N. oculata* had lower concentrations of carotenoids canthaxanthin and astaxanthin and larger chlorophyll *a* concentration per cell compared with *N. gaditana* and *N. salina* for cultures grown under the same conditions. The pigment concentrations of *Nannochloropsis sp.* depend also on the PBR thickness and the initial cell concentration [Fisher *et al.*(1996), Zou and Richmond(2000)]. Zou and Richmond [Zou and Richmond(2000)] showed that *Nannochloropsis sp.* had an order of magnitude larger steady-state chl*a* concentration per cell in cultures grown in 3 cm thick PBRs compared with those grown in 1 cm thick PBRs both exposed to 3000 μmol/m^{2}s. However, cells grown in 1 cm thick PBR had a larger carotenoid to chl*a* ratio. In addition, batch cultures of *Nannochloropsis sp.* with low initial cell density experienced a 5 day growth lag time while cultures with high initial cell concentration experienced no lag upon transfer to a PBR exposed to a

photon flux density of 3500 μmol/m^{2}s.

1.1.1.2 Photoinhibition

Exposing microalgae to large irradiance causes photo-oxidative damage in some of the PSII units. This so-called photoinhibition causes a decrease in the photosynthetic efficiency. This is primarily due to the destruction of one of the reaction center proteins, namely the 32 kDa protein D1 [Ke(2001), Baroli and Melis(1996)]. The chloroplast repairs such damage by destroying the affected D1 proteins and synthesizing new ones and integrating them into the affected PSII units. In fact, the cells continuously perform a damage repair cycle to repair the damaged PSII units [Melis *et al.*(1998), Baroli and Melis(1996)]. However, when the damage rate exceeds the repair rate, inhibition becomes apparent in the cells and the overall efficiency of the cells decreases [Ke(2001), Baroli and Melis(1996)]. In addition, long term exposure to intense light brings about physical changes in the thylakoid membrane such as a reduction in the number of PSI units while maintaining a large number of PSII units. The overall chlorophyll content can also decrease during the growth due to intense incident light and as a result, causing the photosynthetic rate to decrease [Ke(2001), Baroli and Melis(1996)]. This is sometimes referred to as chlorophyll bleaching [Baroli and Melis(1996), Björkman(1981)].

1.1.2 Light independent reactions

The carbon fixation reaction or the dark reaction uses carbon dioxide supplied by the atmosphere and reduces it to carbohydrates $(CH_2O)_n$ by the addition of hydrogen in a metabolic pathway known as the Calvin cycle [Ke(2001)]. The energy for this reaction comes from the NADPH and the ATP supplied by the light dependent reactions. The reaction can be expressed as [Ke(2001)]

$$3CO_2 + 6H^+ + 6NADPH + 9ATP \leftrightarrow C_3H_6O_7 - phosphate + 9ADP + 8Pi + 6NADP^+ + 3H_2O \tag{1.2}$$

Figure 1.3 illustrates the CO_2 fixation pathway used by plants and microalgae known as

the Calvin cycle. It consists of 13 reactions catalyzed by 11 enzymes and as previously mentioned it is independent of light. Ribulose1,5-biphosphate carboxylase/oxygenase (Rubisco) is the enzyme responsible for the CO_2 fixation in the Calvin cycle [Sydney *et al.*(2013)].

The cycle can be divided into three phases. First, in the carboxylation phase, CO_2 is added to five carbon sugar molecule ribulose-1,5-biphosphate (RuBP) to form two molecules of 3-phosphoglycerate (3-PGA). This reaction is catalyzed by the Rubisco enzyme. In phase 2, reduction, 3-PGA is transformed into phosphoglyceraldehyde. This is achieved in two steps which are the phosphorylation of 3PGA via the catalysis by ATP of the enzyme phosphoglycerate kinase to form diphosphoglycerate (Glycerate-bis-P). The latter is then reduced by the enzyme glyceraldehyde 3-phosphate dehydrogenase to phosphoglyceraldehyde (G3P) by NADPH. The molecule G3P is a sugar consisting of 3 carbon atoms and it is the building block of fatty acids, amino acids, and carbohydrates. In phase 3, regeneration, RuBP is regenerated in several stages using ATP. For each cycle, a sixth of the G3P formed are exported to the cytoplasm of the cell, where they serve as the basic building blocks for the synthesis of carbohydrates, fatty acids, and amino acids. The remaining five-sixths are regenerated and used in the next cycle [Ke(2001)].

Rubsico is also known to display oxygenase activity where an oxygen molecule reacts with RuBP to form 3-PGA and phosphoglycolate. These two molecules are then oxidatively metabolized by photorespiration thus producing CO_2. This phenomenon is called photorespiration and it can be attributed to the low affinity of the enzyme Rubisco for CO_2. Photorespiration can be inhibited in the presence of a large amount of CO_2 [Sydney *et al.*(2013)].

1.1.3 Respiration

Respiration by microalgae takes place in the mitochondria. It is the process in which the cells catabolize their carbohydrates, lipids, and proteins and the energy released by oxidation is used to form ATP that can be used for metabolism [Sydney *et al.*(2013)]. In contrast to photosynthesis, respiration utilizes oxygen and releases CO_2. The first step of respiration is

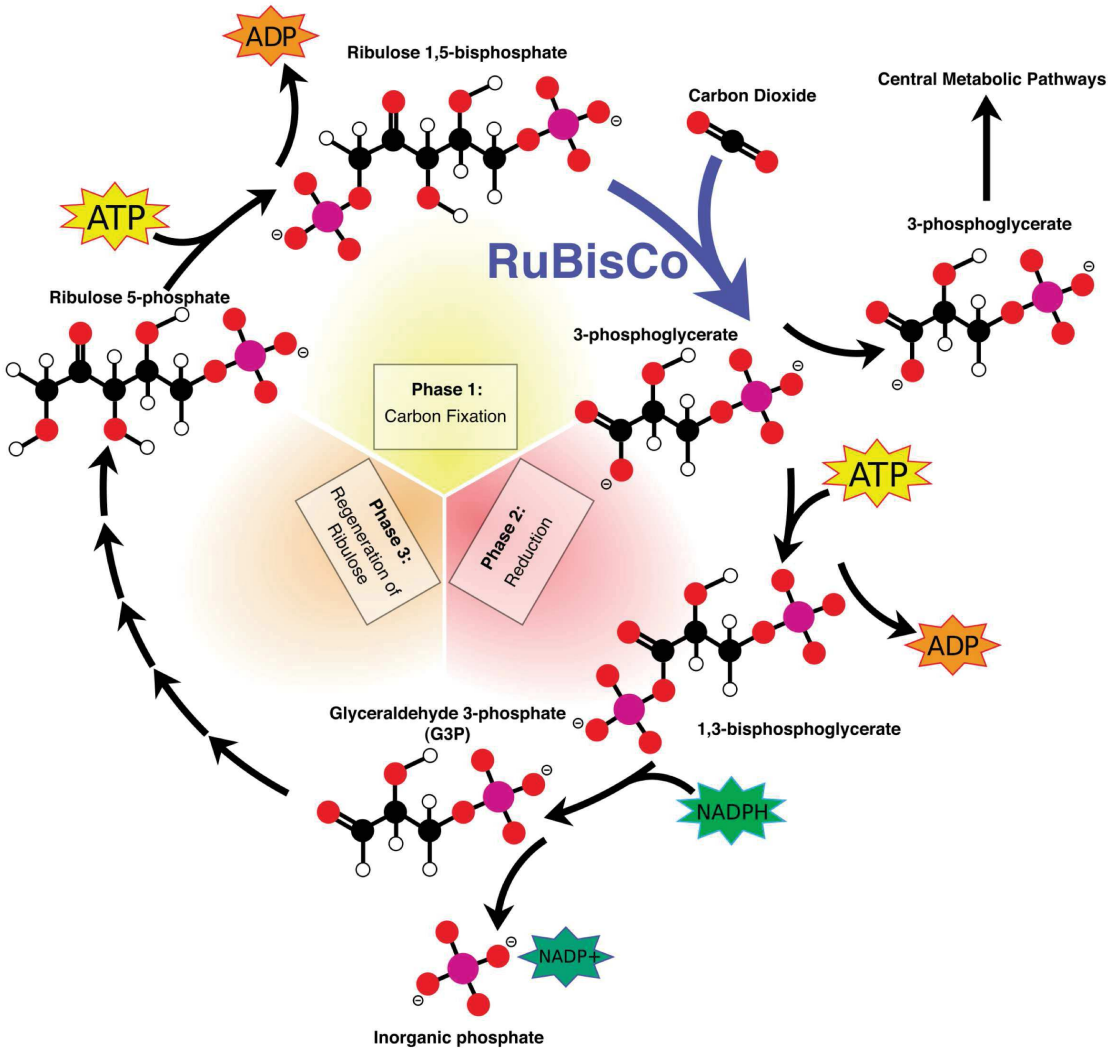

Figure 1.3: Overview of the Calvin cycle [Jones(2010)].

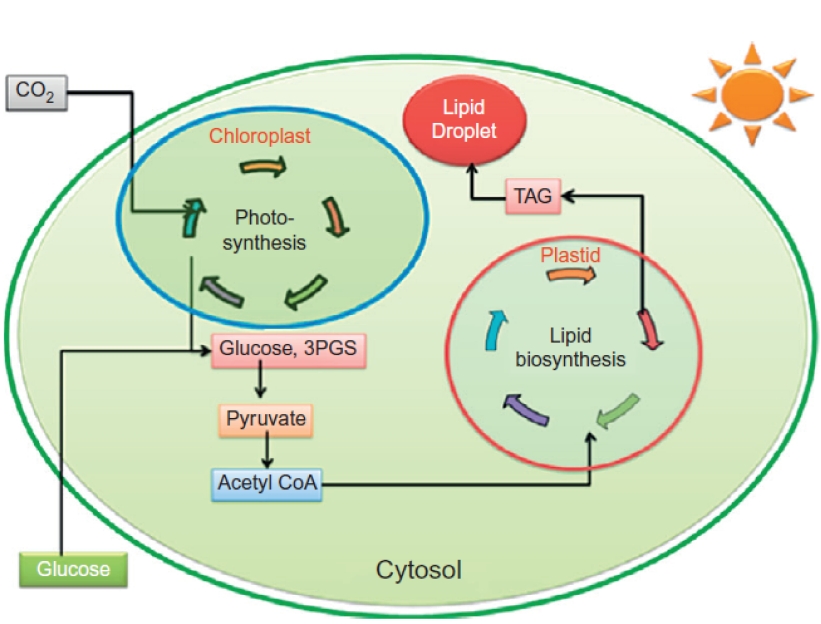

Figure 1.4: Schematic of the lipid synthesis pathway in microalgae and the localization of each component [Mohan *et al.*(2013)].

glycolysis which takes place in the cytosol. Here, two pyruvate molecules are produced in addition to two ATPs and 2 NADPH. Then, the pyruvate molecule is oxidized to produce an Acetyl-CoA, an important molecule in cell metabolism. Next, the citric acid cycle oxidizes two molecules of acetyl-CoA into CO_2. It uses 8 enzymes and per cycle produces a guanosine triphosphate (GTP), 3 reduced nicotinamide adenine dinucleotide (NADH), and single reduced flavin adenine dinucleotide ($FADH_2$). These are later used in the electron transport chain to produce ATPs. In the electron transport chain, each NADH is oxidized to produce 3 ATPs and each $FADH_2$ produces 2 ATPs in a process called oxidative phosphorylation.

1.2 Lipids

Lipids are a diverse group of compounds that can be found in microalgal cells. They are classified based on their structure and polarity into two groups : polar lipids and neutral lipids [Hu *et al.*(2008)]. In general, the polar lipids consist primarily of phospholipids and

glycolipids that are structural and functional components of cell membranes and the membranes of intracellular organelles [Mohan *et al.*(2013)]. By contrast, neutral lipids contain no hydrophilic portion. They are mainly intracellular lipids and in general consist of triglycerides [Fang(2013)]. The latter do not fulfill a structural role but are used primarily for the storage of energy and carbon by the cells [Hu *et al.*(2008),Merchant *et al.*(2012),Fang(2013)]. In contrast to higher plants, lipid metabolism and the biosynthetic pathways of triglycerides in microalgae have not been fully characterized in detail [Hu *et al.*(2008),Merchant *et al.*(2012)]. However, it is generally accepted that the basics of fatty acids and triglyceride biosynthesis in microalgae are very similar to those identified in higher plants [Khozin-Goldberg and Cohen(2011), Merchant *et al.*(2012)].

1.2.1 Fatty acid formation

The cell produces fatty acids to meet its needs to synthesize structural or reserve lipids. Figure 1.4 illustrates a schematic of the pathway a cell uses to synthesis Acetyl CoA, the basic building block of the fatty acid biosynthesis. Their biosynthesis occurs in the thalakoyd and stromal regions of the chloroplast and is catalyzed by acetyl-CoA carboxylaze (ACCase) and the type-2 fatty acid synthase [Fang(2013)]. Acetyl CoA is then converted to malonyl CoA by ACCase and then transferred to a small acyl carrier protein (ACP) to form malonyl-ACP [Hu *et al.*(2008)]. Then through series of reactions, two methylene carbons are cyclically incorporated into the growing acyl chain [Mohan *et al.*(2013)]. The chain is elongated until it is 16 or 18 carbon molecules long. Finally, it is converted to acyl-CoA by the acyl-CoA synthetase [Fang(2013)].

1.2.2 TAG metabolism

Figure 1.6 illustrates the pathway a microalgae cell uses to synthesize TAG lipids. It can materialize via two methods the *de novo* synthesis of TAG (acyl CoA-dependent pathway) or by recycling the membrane lipids (acyl CoA-independent pathway) [Fang(2013)]. In the *de*

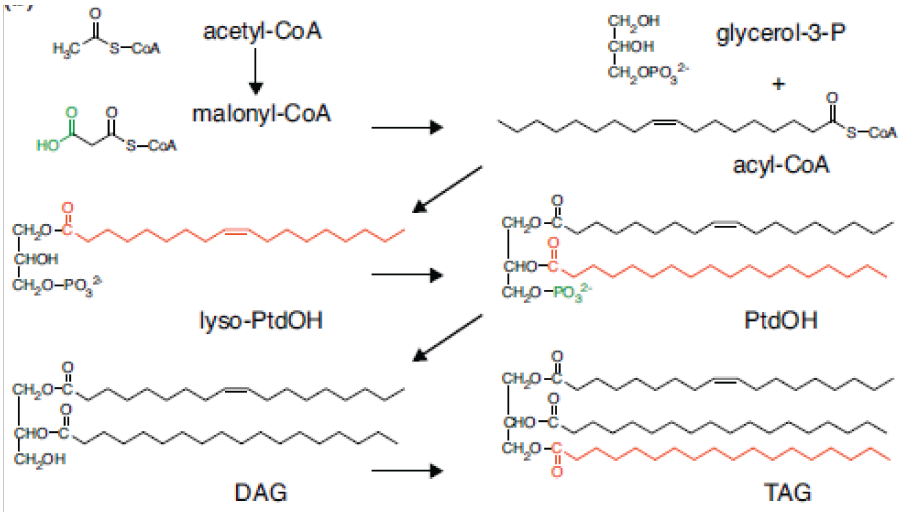

Figure 1.5: The structure of the compounds synthesized during the *de novo* TAG synthesis [Merchant *et al.*(2012)].

novo pathway, the acyl-CoA are transferred to positions 1 and 2 of a G3P (Figure 1.5), formed during glycolysis, resulting in the formation of phosphatidic acid [Merchant *et al.*(2012)]. The latter is converted to diacylglycerol (DAG) by dephosphorylation. Finally, a third acyl-CoA is transferred to position 3 of the DAG catalyzed by diacylglycerol acyltransferases [Liu *et al.*(2013a)]. The *de novo* TAG synthesis pathway also has the role of protecting the cell by acting as an electron sink during photo-oxydative stress [Hu *et al.*(2008)]. Reactive oxygen species (ROSs) are produced under intense illumination due to the accumulation of excess electrons in the photosynthetic electron transport chain. These ROSs cause inhibition of photosynthesis as well as damage to proteins, carbohydrates and lipids. In order to quench the accumulated excess electrons, the cells synthesize fatty acids which consume significantly more NADPH to synthesize than carbohydrates or proteins of the same mass [Hu *et al.*(2008)].

In terms of carbon partitioning in cells under stress conditions, the storage carbohydrates of the cells are directed into the glycolysis pathway in order to generate acetyl-CoA that can be used for fatty acid and TAG synthesis [Jia *et al.*(2015)]. Another strategy that cells use during stress conditions such as nitrogen starvation is recycling membrane lipids in order to

synthesis TAG using the acyl CoA-independent pathway. Then, the membrane lipids can be used as acyl donors for TAG synthesis catalyzed by the enzyme phospholipid :diacylglycerol acyltransferase (PDAT) [Hu *et al.*(2008)]. In *C. reinhardtii* and *Nannochloropsis oceanica* overexpression of the PDAT enzyme has been observed during the early stages of nitrogen starvation [Yoon *et al.*(2012), Jia *et al.*(2015)].

The TAGs assembly can occur in both the chloroplast and the endoplasmic reticulum where they are concentrated into structures called lipid droplets. These droplets are filled with neutral lipids and surrounded by a single-layer of lipid membrane.

1.3 Microalgae cultivation systems

1.3.1 Parameters affecting microalgae growth and lipid accumulation

Microalgae are photosynthetic single cell organisms that need a light source, an inorganic carbon source, and minerals to grow. In addition, for optimal growth, pH and temperature must be controlled. Most species typically grow suspended in the growth medium but they can also grow in biofilms. The suspension must be mixed to maintain the cells in suspension and maintain homogenous growth conditions (pH, nutrient concentration, temperature) thorough the cultivation vessel. The optimized production of microalgae ultimately requires good management of all these operating parameters.

The microalgae growth medium must include inorganic carbon as well as the major macro-nutrients nitrogen, sulfur, and phosphate and the micro-nutrients such as potassium, magnesium, calcium, manganese, copper, and iron. Moreover, the carbon source must be dissolved in the culture medium in the form of bicarbonates either by dissolving bicarbonate salts or by injecting gaseous CO_2 in the medium. On of the most important elements in cell growth and metabolism is nitrogen. It plays an important role in the synthesis of proteins, chlorophyll, and various enzymes. It is a constituent of the chlorophyll molecule which is responsible for light absorption. Nitrogen is assimilated by cells in the form of ammonium NH_4^+, nitrates NH_3^-, or nitrites NH_2^{-2}.

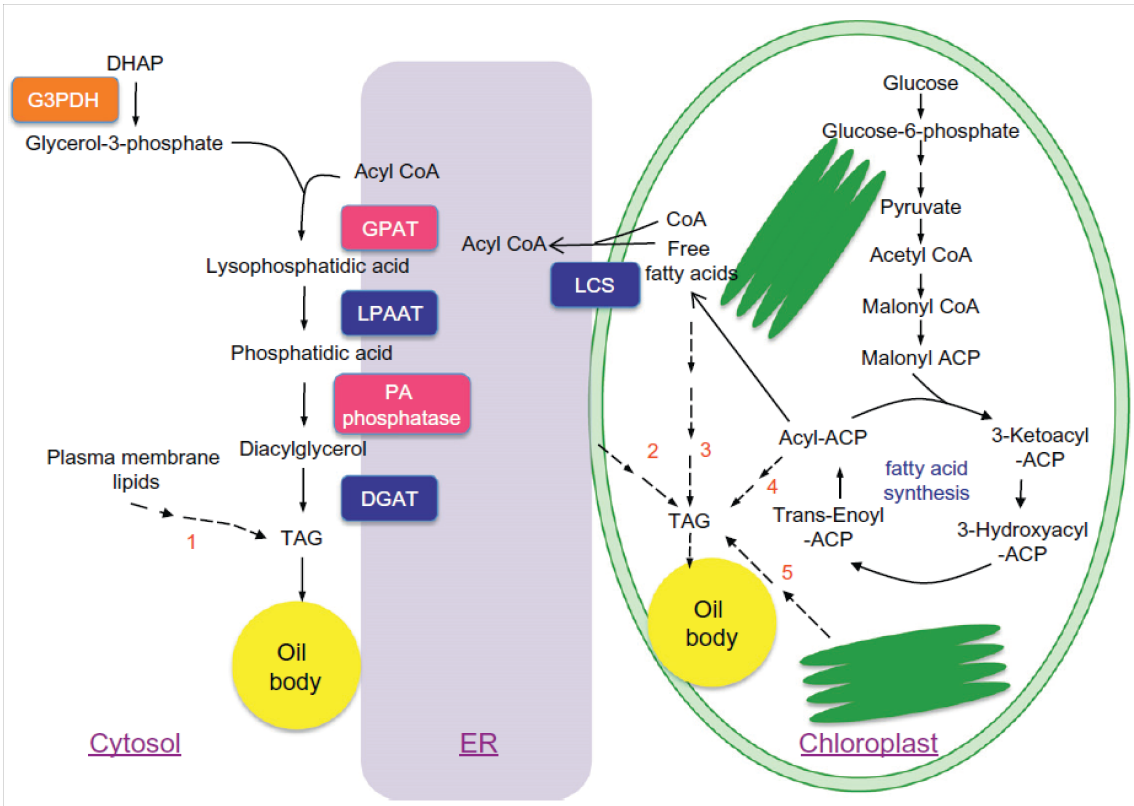

Figure 1.6: Schematic representation of the pathways and lipid and TAG synthesis in microalgae. Legend : TAG synthesis pathways are shown in black arrow and unknown TAG synthesis pathways are shown in dashed lines. Acyl group are derived from 1) plasma membrane lipids, 2) chloroplast envelope membrane, 3) fatty acid synthesized in the chloroplast, 4) acyl-ACP synthesized in chloroplast, and 5) thylakoid membranes. [Fang(2013)]

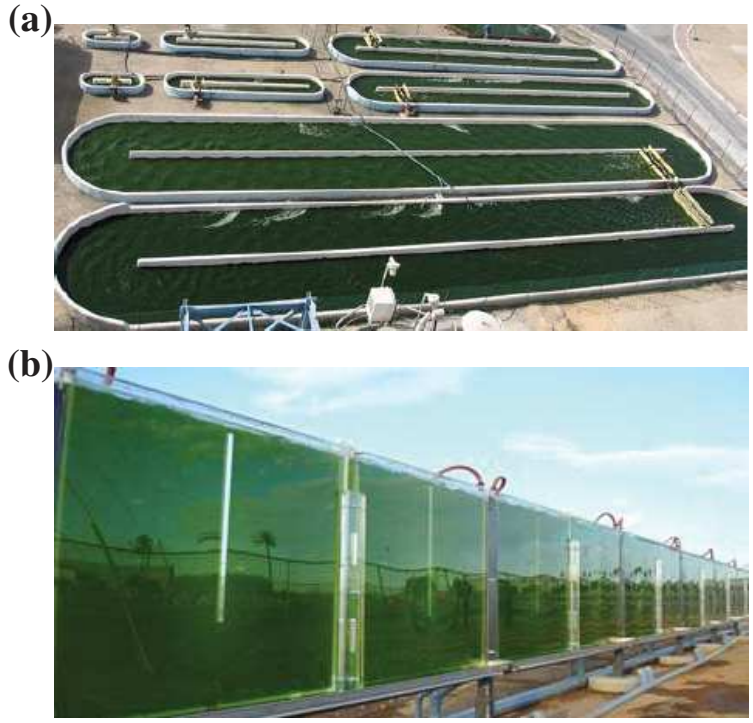

Figure 1.7: Field demonstration of (a) open-pond PBRs [Seambiotic Ltd.(2014)] and (b) vertical flat-plate closed PBRs [ASU(2014)].

1.3.2 Types of photobioreactors and cultivation modes

Photosynthetic microalgae are typically cultivated in open-ponds or enclosed photobioreactors (PBRs) [Chisti(2007), Pilon *et al.*(2011)]. Each has its own advantages and disadvantages. However, feasibility of profitable large-scale outdoor production has not yet been fully demonstrated [Moody *et al.*(2014)]. Figure 1.7 shows examples of open-pond and closed PBRs.

In outdoor cultures, the open-pond systems such as raceways and open basins are the most inexpensive and can be easily scaled-up for large scale production of biomass. However, they suffer from several limitations that inhibit the productivity of these systems [Chisti(2012)]. For example, due to the direct contact of the culture with its surrounding environment it is prone to contamination by bacteria, viruses, paramecium that may graze on the microalgae or

it may lead to contamination by local photosynthetic microorganisms that may outcompete the strain being cultivated. In addition, since the culture is open to the environment, the culture medium enriched in gaseous CO_2 transfers large amounts of the carbon dioxide to the atmosphere due to the relative small concentration of CO_2 in air. Moreover, large amount of water evaporates at the surface of the culture which necessitates the addition of fresh water to the cultures adding to the expense and the environmental impact of the culture system. Due to these limitations and poor mixing of the culture broth, open-pond systems enjoy productivity much smaller than the maximum obtained in fully-controlled cultures.

On the other hand, a closed photobioreactor (PBR) is an enclosure that hold microalgae cultures and is exposed to a source of photosynthetically active radiation. It has the advantage of being able to maintain sterile conditions and the ability to prevent contamination. The nutrient concentration, temperature, pH, mixing can be fully controlled in PBRs. They have much larger biomass productivity compared to open-ponds. However, they require significantly larger capital investment compared to open-pond systems and they have a higher cost of operation. Figure 1.8 shows examples of lab-scale (a) torus and (b)-(c) airlift PBRs used in this study for microalgae cultivation.

Micorlagae can be cultivated in continuous or batch modes. In continuous cultures, the PBR is continuously injected with fresh medium at the same rate as biomass is withdrawn from the culture. Continuous processes can be achieved by two methods. In chemostat mode, the flow rate of fresh medium is kept constant. On the other hand, in turbidostat mode, the turbidity of the culture is maintained at a set value by diluting the culture when the turbidity exceeds the set value. For large scale biomass or biodiesel production, continuous processes are more advantageous as they can be less labor intensive and they can produce a consistent quality of biomass [Croughan *et al.*(2015)]. Continuous cultures are also of interest in laboratory scale studies since the culture reaches a steady-state and physical conditions in the PBR remain constant. This enables the study of the changes in the biochemical composition of cells in response to the limitation of one or more of the substrates such as light or nutrients.

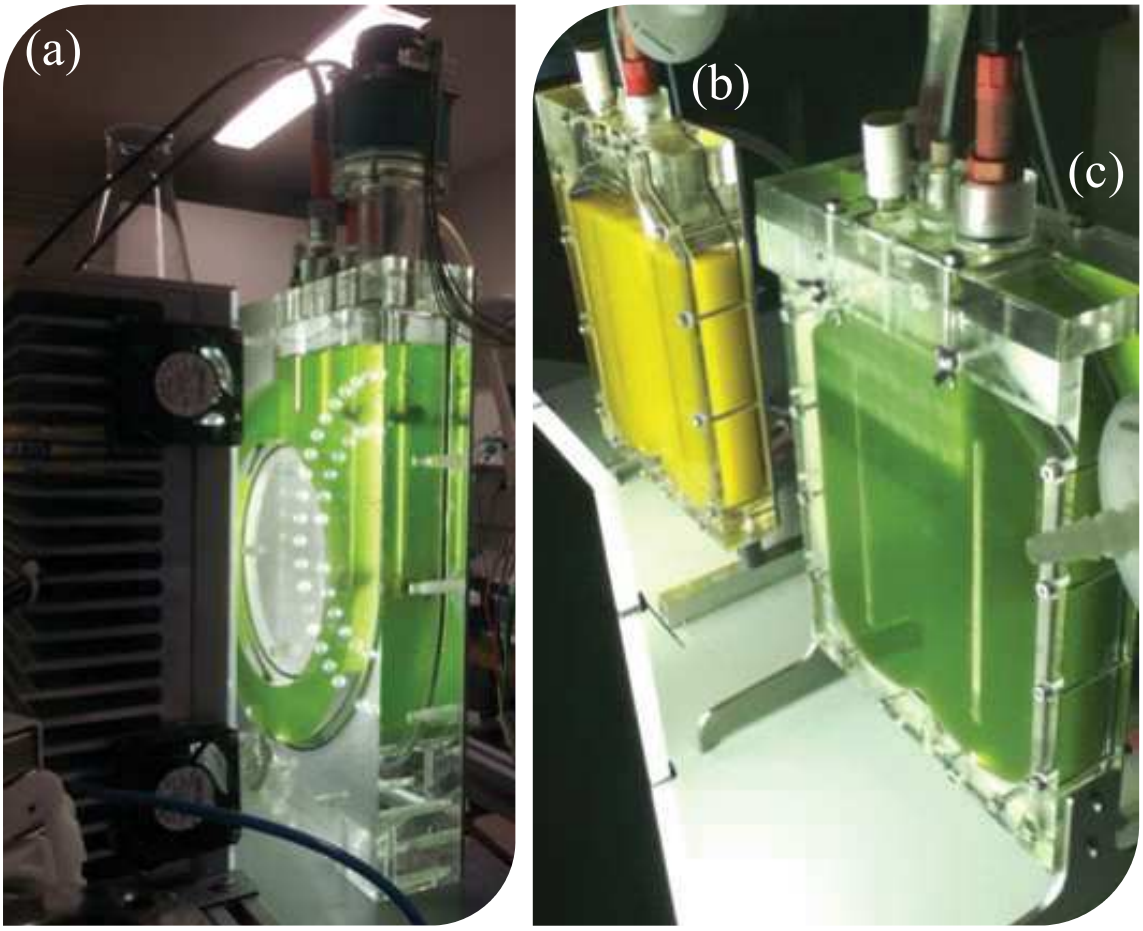

Figure 1.8: Laboratory scale (a) 1.5 L torus PBR containing the micralgae *C. reinhardtii* grown in optimal conditions, and 1 L air-lift flat plate PBR containing *N. oculata* cultures (b) subjected to nitrogen starvation and (c) grown in nutrient replete conditions.

In batch processes, all the nutrients are added to the PBR before inoculation. This is the most common mode in the cultivation of microalgae, due to its ease and simplicity [Croughan *et al.*(2015)]. After inoculation, the biomass concentration increases with the assimilation of nutrients, until the stationary phase is reached. This is due to limitation by one or more of the growth substrates. In the case of microalgae, the stationary phase can be reached after consuming nutrients such as nitrates and/or when the fluence rate in the PBR does not support net positive growth.

In the semi-continuous cultivation mode, the culture in the PBR is harvested periodically and fresh medium is added. This method of cultivation represents a compromise between the continuous and batch modes. It is a common cultivation method in the industry where the culture is harvested at the end of each day and the batch culture restarted the following morning.

1.3.3 Microalgae species of interest for TAG production

The microalgae studied in this thesis are the green fresh-water algae *Chlorella vulgaris* and *Parachlorella kessleri* and the marine eustigmatophyceae *Nannochloropsis oculata*. They were chosen for their large biomass productivity or their ability to accumulate large amounts of TAG lipids.

1.3.4 Chlorella vulgaris

Chlorella vulgaris is a unicellular microalgae with spherical shape and 1-6 μm in diameter. This particular species of green microalgae has garnered special attention for its large areal biomass productivity reaching up to 16 g/m^2 per day and its relatively short cell doubling time of 16 hours [Griffiths and Harrison(2009)]. In addition, it has been identified as a potential source of protein for human and animal feed [Tokuşoglu and Ünal(2003)]. It is also an important source for the commercial production of carotenoids and various biopharmaceuticals [Mendes *et al.*(2003)]. It can also produce lipids to be converted into biodiesel [Brennan

and Owende(2013)]. Finally, this freshwater species can be cultivated in wastewater for simultaneous wastewater treatment and production of value-added products [Feng *et al.*(2011)].

1.3.5 Parachlorella kessleri

Parachlorella kessleri is a fresh water microalgae spherical in shape and physiologically very similar to *C. vulgaris*. They can contain lipids in quantities up to 10 dry wt.% when grown in nutrient replete conditions and up to 60 dry wt.% when cultivated under nutrient limited conditions [Li *et al.*(2013)].

1.3.6 Nannochloropsis oculata

Nannochloropsis oculata are marine eustigmatophyceae containing up to 30-70% lipid by dry weight [Hodgson *et al.*(1991), Rodolfi *et al.*(2009)]. Majority of these lipids produced during nitrogen starvation are in the form of TAGs which are ideal for biodiesel production [Van Vooren *et al.*(2012)]. Additionally, *Nannochloropsis oculata* has a high biomass productivity reaching up to 3 g/L·day resulting in large lipid productivity [Chisti(2007), Briassoulis *et al.*(2010), Chen *et al.*(2011), Van Vooren *et al.*(2012)]. Moreover, it can be cultivated in seawater, thus eliminating competition with freshwater used for human consumption.

1.3.7 Strategies for increased TAG accumulation

TAG are the main feedstock for lipid to biodiesel conversion through transesterification reaction with methanol to produce methyl esters of fatty acids that are essentially biodiesel [Chisti(2007)]. Several strategies can be used to enhance TAG and lipid productivity [Williams and Laurens(2010)]. For example, nitrogen starvation triggers large amounts of lipid accumulation [Hu *et al.*(2008), Van Vooren *et al.*(2012)]. The stressful conditions of nitrogen starvation lead cells to synthesize neutral lipids mainly in the form of triglyceride fatty acids (TAG) [Van Vooren *et al.*(2012)]. They are believed to serve as carbon and energy storage compound for the cells [Hu *et al.*(2008)]. The accumulation of TAG during nitro-

gen starvation has been observed in numerous microalgal species including *Nannochloropsis oculata* [Van Vooren *et al.*(2012)], *Nannochloropsis* sp. [Pal *et al.*(2011)], *Neochloris oleoabundans* [Pruvost *et al.*(2009)], *Scenedesmus obliquus* [Breuer *et al.*(2013)], *Chlorella sp.*, and many others [Adams *et al.*(2013)]. Typically, 40-50 dry wt.% is the maximum concentration of TAG reported in microalgae cells [Hu *et al.*(2008)].

Batch nitrogen starvation of *N. oculata* cultures can be achieved by two methods. *Sudden starvation* consists of two steps : first, the microalgae are grown in nitrogen replete conditions. Then, they are transferred into a nitrogen-free medium. *Progressive starvation* consists of initially adding a small amount of nitrogen to the culture medium in the form of nitrate, for example. After inoculating the PBR, the microalgae grow and multiply until they consume all the nitrates in the medium and the culture medium becomes deprived of nitrogen. Cells subjected to progressive nitrogen starvation have a slightly different behavior than those in sudden starvation [Van Vooren *et al.*(2012)]. Indeed, the culture goes through a nitrogen replete phase followed by nitrogen limitation phase and finally a nitrogen starvation phase. By contrast, in sudden starvation, the cells go from a nitrogen replete phase directly to a nitrogen starvation phase. Nitrogen limitation results in a decrease in pigment concentrations. Therefore, cells undergoing progressive starvation enter the nitrogen starvation phase with significantly lower pigment concentrations than those subjected to sudden starvation. This modifies the light availability in the PBR in a non-obvious way. Finally, both methods can lead to appreciable amount of TAG accumulation [Van Vooren *et al.*(2012)]. However, in practice, progressive starvation is preferable for mass production as it requires only one production stage and does not require the costly biomass filteration/separation from growth medium and re-suspension in a nitrogen-free medium [Van Vooren *et al.*(2012), Oeschger and Posten(2012)]. Unfortunately, in batch cultures the unfavorable conditions of nitrogen starvation causes pigment and photosystem degradation leading to eventual cell death. An alternative, less common, method for producing TAG lipids is by nitrogen limitation of cells in continuous cultures [Hoffmann *et al.*(2010), Klok *et al.*(2013)]. Here, a small amount of nitrate is continuously added to the PBR operated as a chemostat or a turbidostat. The goal

of this process is to achieve simultaneous cell division and TAG accumulation.

One of the consequences of nitrogen starvation is the reduction in the total pigment concentration in the cells as well as the increase in carotenoid to chlorophyll *a* (chl*a*) concentration ratio [Heath *et al.*(1990)]. Pruvost *et al.* [Pruvost *et al.*(2009)] observed a ten fold decrease in total pigment concentration in *Neochloris oleoabundans* cells during nitrogen starvation. In addition, changes in chl*a* to carotenoid ratio greatly modifies the color and light absorption of microorganisms thus affecting their ability to perform photosynthesis and accumulate TAG [Van Vooren *et al.*(2012)].

The radiation characteristics and optical properties of *N. oculata* in batch grown cultures over the photosynthetically active radiation (PAR) region were reported by Kandilian *et al.* [Kandilian *et al.*(2013)]. A significant decrease in the absorption cross-section of the cells at wavelengths between 400 and 750 nm was observed during nitrogen limitation compared with cells grown in nitrogen replete media [Kandilian *et al.*(2013)]. Furthermore, Flynn *et al.* [Flynn *et al.*(1993)] demonstrated that nitrogen deprived *N. oculata* cells can undergo two cell divisions after the onset of NH_4^+ deprivation. To do so, each cell divides its nitrogen content between the daughter cells [Flynn *et al.*(1993)]. In fact, the authors reported that nitrogen replete *N. oculata* cells had a carbon to nitrogen ratio (C/N) of 6 while NH_4^+ deprived cells featured C/N ratio of nearly 26 [Flynn *et al.*(1993)].

1.3.8 Effect of light stress on TAG productivity

Subjecting the cells to intense light during nitrogen starvation has been shown to be essential in TAG synthesis [Hu *et al.*(2008), Van Vooren *et al.*(2012)]. This is in contrast to the synthesis and accumulation of polar lipids under light limited growth conditions [Hu *et al.*(2008)]. Van Vooren *et al.* [Van Vooren *et al.*(2012)] demonstrated that greater light availability in flat-plate PBRs used to cultivate *N. oculata* in nitrogen starvation resulted in larger lipid productivity. Indeed, peak areal TAG productivity was 3.6 $g/m^2 \cdot day$ for sudden starvation of batch culture with initial biomass concentration of 0.41 kg/m^3 exposed to

250 $\mu mol_{h\nu}/m^2 \cdot s$ compared with 1.4 $g/m^2 \cdot day$ for the same illumination conditions when the initial biomass concentration was 0.76 kg/m^3. The larger initial biomass concentration resulted in stronger light attenuation and lower light availability in the PBR. Similarly, *N. oculata* cultivated in a 5 cm flat-plate PBR had 50% lower TAG productivity than those cultivated in 3 cm flat-plate PBR under the same conditions. Pal *et al.* [Pal *et al.*(2011)] also showed that nitrogen starved *Nannochloropsis sp.* grown in cylindrical PBR 6 cm in diameter and exposed to 750 $\mu mol_{h\nu}/m^2 \cdot s$ of white light contained 35% total lipids by dry weight compared with 22% for cells grown exposed to 170 $\mu mol_{h\nu}/m^2 \cdot s$.

In addition, in the absence of mineral limitation, light is also the substrate that limits growth in microalgae cultivation. However, in contrast to other factors affecting growth such as temperature, minerals, and CO_2, light cannot be mixed in the culture and is therefore always heterogeneously distributed due to absorption and scattering of light by the microorganisms. In order to design and optimize biomass and lipid productivity by microalgae cultures grown in PBRs, radiation transfer analysis must be performed.

1.4 Radiation transfer in photobioreactors

As previously stated, the light utilization efficiency of these PBRs is perhaps the most important parameter affecting the overall efficiency of the biofuel production process. Careful light transfer analysis must be conducted to design, optimize light transport, and operate efficient PBRs for converting solar energy into biofuels using microorganisms [Pilon *et al.*(2011)]. To do so, the spectral radiation characteristics of microalgae are necessary.

Figure 1.9 shows a schematic of different phenomena that takes place when light is incident upon the culture in a PBR. Light transfer within absorbing, scattering, and non-emitting microalgal suspension in photobioreactors is governed by the radiative transport equation (RTE) expressed on a spectral basis as [Modest(2003)]

$$\hat{s} \cdot \nabla I_\lambda = -\kappa_\lambda I_\lambda (\hat{r}, \hat{s}) - \sigma_{s,\lambda} I_\lambda (\hat{r}, \hat{s}) + \frac{\sigma_{s,\lambda}}{4\pi} \int_{4\pi} I_\lambda (\hat{r}, \hat{s}_i) \, \Phi_{T,\lambda} (\hat{s}_i, \hat{s}) \, d\Omega_i \tag{1.3}$$

where $I_\lambda(\hat{r}, \hat{s})$ is the spectral radiation intensity in direction $\hat{s}$ at location $\hat{r}$ (in $W/m^2 \cdot nm \cdot sr$)

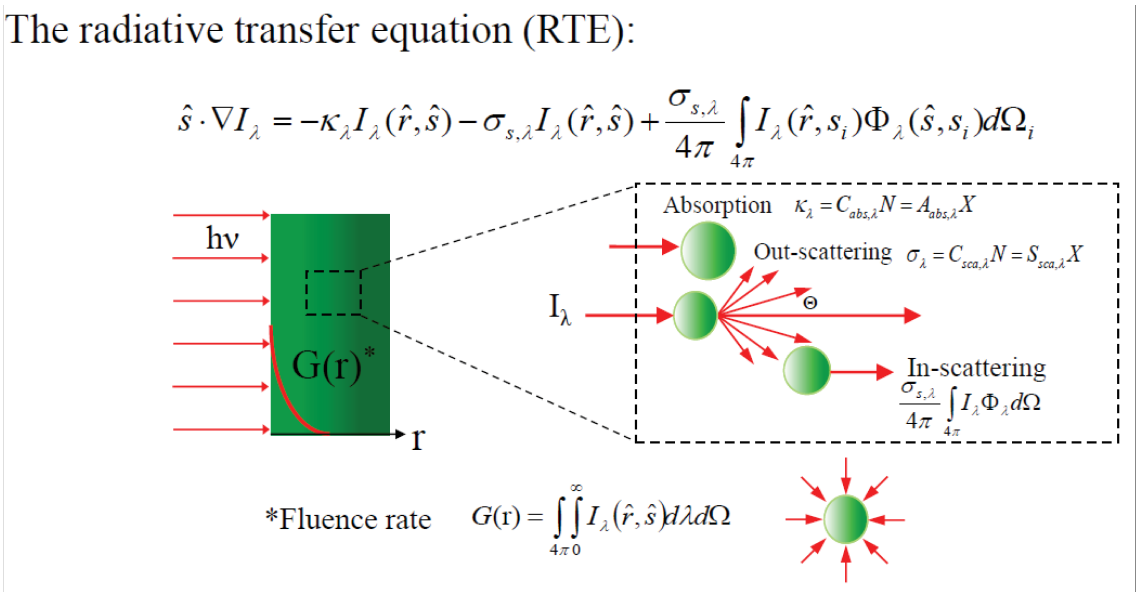

Figure 1.9: Graphic representation of the phenomena that occur when light is incident on microalgae cultures.

while κ_λ and $\sigma_{s,\lambda}$ are the effective absorption and scattering coefficients of the suspension (in 1/m). The total scattering phase function of the suspension $\Phi_{T,\lambda}(\hat{s}_i,\hat{s})$ represents the probability that radiation traveling in the solid angle $d\Omega_i$ around direction $\hat{s}_i$ is scattered into the solid angle $d\Omega$ around the direction $\hat{s}$ and is normalized such that

$$\frac{1}{4\pi}\int_{4\pi}\Phi_{T,\lambda}(\hat{s}_i,\hat{s})\,d\Omega_i = 1. \tag{1.4}$$

The backward scattering ratio, denoted by b_λ, and the asymmetry factor, denoted by g_λ, for an axisymmetric phase function are defined as [Pilon *et al.*(2011)]

$$b_\lambda = \frac{1}{2}\int_{\pi/2}^{\pi}\Phi_{T,\lambda}(\Theta)\sin\Theta\mathrm{d}\Theta \quad \text{and} \quad g_\lambda = \frac{1}{2}\int_0^{\pi}\Phi_{T,\lambda}(\Theta)\cos\Theta\sin\Theta\mathrm{d}\Theta \tag{1.5}$$

where Θ is the scattering angle between directions $\hat{s}_i$ and $\hat{s}$. The effective absorption coefficient κ_λ of a polydisperse microorganism suspension is related to the average absorption cross-sections, denoted by $\bar{C}_{abs,\lambda}$, as [Pilon *et al.*(2011)]

$$\kappa_\lambda = \int_0^\infty C_{abs,\lambda}(d_s)p(d_s)\mathrm{d}d_s = \bar{C}_{abs,\lambda}N_T \tag{1.6}$$

where $p(d_s)$ is the number of cells per unit volume of suspension having diameter between d_s and $d_s + \mathrm{d}d_s$ and $C_{abs,\lambda}(d_s)$ is the absorption cross-section of a single spherical scatterer of diameter d_s. Here, N_T is the cell density defined as the total number of cells per m^3 of suspension. Similarly, the effective scattering coefficient can be written as

$$\sigma_{s,\lambda} = \int_0^\infty C_{sca,\lambda}(d_s) p(d_s) \mathrm{d}d_s = \bar{C}_{sca,\lambda} N_T \tag{1.7}$$

where $C_{sca,\lambda}(d_s)$ is the scattering cross-section of a single spherical scatterer of diameter d_s and $\bar{C}_{sca,\lambda}$ is the size averaged scattering cross-section. Alternatively, the absorption and scattering coefficients can be expressed as the product of the average specific (or mass) absorption and scattering cross-sections $\bar{A}_{abs,\lambda}$ and $\bar{S}_{sca,\lambda}$ (in m^2/kg) and the microorganism mass concentration X (in kg/m^3) so that $\kappa_\lambda = \bar{A}_{abs,\lambda} X$ and $\sigma_{s,\lambda} = \bar{S}_{sca,\lambda} X$. Finally, the extinction coefficient β_λ (in $1/\mathrm{m}$) is given by

$$\beta_\lambda = \kappa_\lambda + \sigma_{s,\lambda}. \tag{1.8}$$

The total scattering phase function of polydisperse microalgae cells $\Phi_{T,\lambda}(\Theta)$ can be estimated by averaging the scattering phase function of individual cells of diameter d_s, $\Phi_\lambda(d_s, \Theta)$ according to [Modest(2003)]

$$\Phi_{T,\lambda}(\Theta) = \frac{\int_0^\infty C_{sca,\lambda}(d_s) \Phi_\lambda(d_s, \Theta) p(d_s) \mathrm{d}d_s}{\int_0^\infty C_{sca,\lambda}(d_s) p(d_s) \mathrm{d}d_s} \tag{1.9}$$

1.4.1 Light transfer modeling in PBRs

In the case of absorbing and scattering media such as microalgal culture, the local spectral fluence rate $G_\lambda(z)$ can be obtained by solving the radiative transfer equation [Jonasz and Fournier(2007)]. Several methods of solution exist [Pilon *et al.*(2011), Dauchet *et al.*(2013), Lee *et al.*(2014)]. However, for one-dimensional flat-plate PBRs with transparent front window containing strongly forward scattering microalgae, the two-flux approximation

yields satisfactory results [Pottier *et al.*(2005), Lee *et al.*(2014)]. In the case of normally incident radiation $G_{\lambda,0}$, the local fluence rate $G_\lambda(z)$ at depth z can be expressed as

$$\frac{G_\lambda(z)}{G_{\lambda,0}} = 2\frac{[\rho_\lambda(1+\alpha_\lambda)e^{-\delta_\lambda L} - (1-\alpha_\lambda)e^{-\delta_\lambda L}]e^{\delta_\lambda z} + [(1+\alpha_\lambda)e^{\delta_\lambda L} - \rho_\lambda(1-\alpha_\lambda)e^{\delta_\lambda L}]e^{-\delta_\lambda z}}{(1+\alpha_\lambda)^2 e^{\delta_\lambda L} - (1-\alpha_\lambda)^2 e^{-\delta_\lambda L} - \rho_\lambda(1-\alpha_\lambda^2)e^{\delta_\lambda L} + \rho_\lambda(1-\alpha_\lambda^2)e^{-\delta_\lambda L}} \tag{1.10}$$

where ρ_λ is the diffuse reflectance of the PBR's back wall while the coefficients α_λ and δ_λ are expressed as [Pottier *et al.*(2005)]

$$\alpha_\lambda = \sqrt{\frac{\bar{A}_{abs,\lambda}}{\bar{A}_{abs,\lambda} + 2b_\lambda \bar{S}_{sca,\lambda}}} \quad \text{and} \quad \delta_\lambda = X\sqrt{\bar{A}_{abs,\lambda}\left(\bar{A}_{abs,\lambda} + 2b_\lambda \bar{S}_{sca,\lambda}\right)} \tag{1.11}$$

The backward scattering ratio is approximately constant over the PAR region and was recently measured to be 0.002 for *N. oculata* [Kandilian *et al.*(2013)]. The PAR-averaged fluence rate $G_{PAR}(z)$ can be expressed as

$$G_{PAR}(z) = \int_{400}^{700} G_\lambda(z)\mathrm{d}z. \tag{1.12}$$

Note that in batch cultivation, absorption and scattering cross-sections of the microalgae as well as the biomass concentration are all time-dependent.

1.4.2 Simplified one-dimensional radiative transfer equation

Figure 1.10 shows a schematic of a microalgae suspension of thickness ℓ illuminated with collimated, unpolarized, and normally incident light along with the associated coordinate system. Light transfer through such absorbing, anisotropically scattering, and non-emitting suspension can be treated as one-dimensional (1D) along the z-direction taken as the direction of the incident light.

Note that in cases when the suspension scatters strongly in the forward direction, then b_λ tends to zero, α_λ approaches unity, and $\delta_\lambda = A_{abs,\lambda}X = \kappa_\lambda$. Then, the above expression for $G_\lambda(z)$ simplifies to [Lee *et al.*(2014)]

$$G_\lambda(z) = G_{in,\lambda}e^{-A_{abs,\lambda}Xz} + \rho_\lambda G_{in,\lambda}e^{-A_{abs,\lambda}X(2L-z)}. \tag{1.13}$$

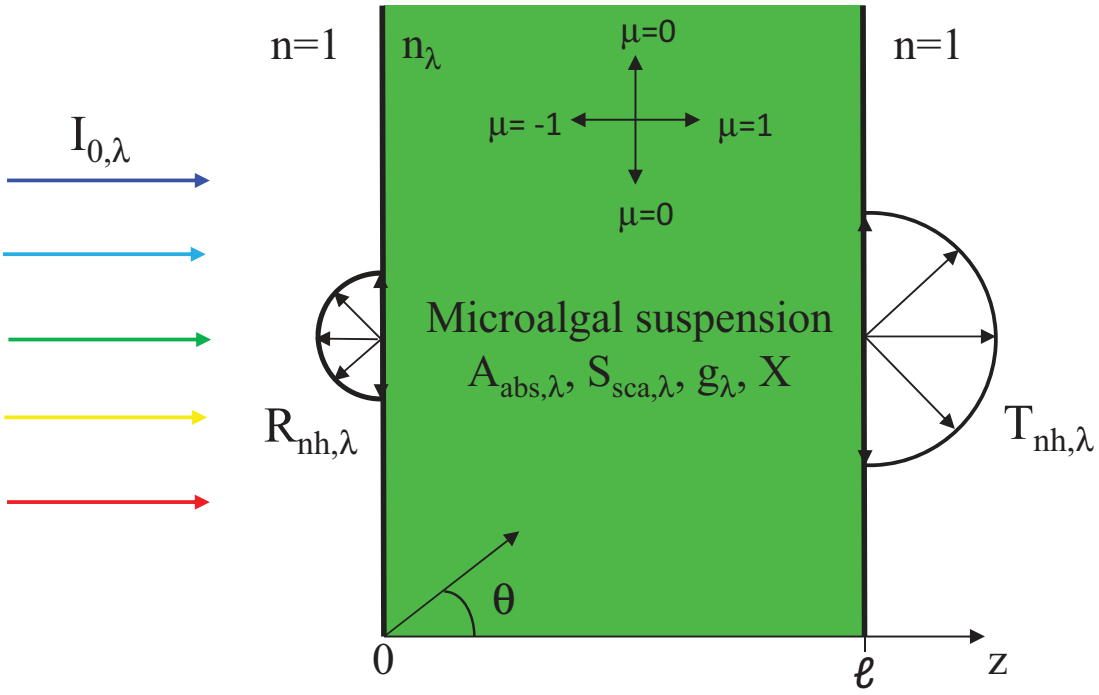

Figure 1.10: Schematic of one-dimensional light transfer in a refracting, absorbing, and scattering microalgae suspension illuminated with collimated and normally incident light.

The first term represents the remaining of the incident irradiance after it has travel a distance z while the second term accounts for the incident irradiance that has traveled once through the suspension, got reflected by the back wall, and traveled a distance (L-z) in the suspension. This simplified expression has been validated against predictions by Equation (1.10) and by the numerical solutions of the 3D RTE using the discontinuous Galerkin method combined with the discrete-ordinate method for outdoor open ponds and flat plate PBRs [Lee *et al.*(2014)]. Note that Equation (1.13) differs from Beer-Lambert's law in that (i) it depends only on the absorption coefficient $\kappa_\lambda = A_{abs,\lambda}X$ and not on the extinction coefficient $\beta_\lambda = (A_{abs,\lambda} + S_{sca,\lambda})X$ and (ii) it accounts for reflection within the PBR. More importantly, the simplified expression for the fluence rate $G_\lambda(z)$ given by Equation (1.13) depends only on the mass absorption cross-section $A_{abs,\lambda}$ of the suspension.

1.4.3 Normal-hemispherical transmission and reflectance

In cases when scatterers are much larger than the radiation wavelength, scattering is mainly forward and the scattering phase function can be estimated based on the transport approximation as [Kellar and Box(1981)]

$$p_\lambda(\mu_0) = 1 - g_\lambda + 2g_\lambda\delta(1-\mu_0). \tag{1.14}$$

Here, $\delta(\mu)$ is the Dirac delta function and g_λ is the asymmetry factor at wavelength λ defined as

$$g_\lambda = \frac{1}{2}\int_{-1}^{1} p_\lambda(\mu_0)\mu_0 \mathrm{d}\mu_0. \tag{1.15}$$

Then, the RTE can be expressed as

$$\mu\frac{\partial I_\lambda}{\partial \tau_{tr,\lambda}} = -I_\lambda + \frac{\omega_{tr,\lambda}}{2}\int_0^{\pi} I_\lambda(\mu', z)\mathrm{d}\mu' \tag{1.16}$$

where $\tau_{tr,\lambda} = \beta_{tr,\lambda} z$ is the transport optical thickness (dimensionless) with $\beta_{tr,\lambda} = \kappa_\lambda + (1 - g_\lambda)\sigma_{s,\lambda}$ is the transport extinction coefficient while $\omega_{tr,\lambda} = (1-g_\lambda)\sigma_{s,\lambda}/\beta_{tr,\lambda}$ is the transport single scattering albedo.

Let us now consider a homogenous absorbing, scattering, but non-emitting microalgae suspension exposed to collimated and normally incident radiation. Radiation transfer in this case can be assumed to be one dimensional [Berberoğlu *et al.*(2007), Lee *et al.*(2014)]. The suspension was assumed to be reflecting and refracting and the incident radiation was subject to internal reflection. Then solving the RTE based on the modified two-flux approximation leads to an analytical expression for the spectral normal-hemispherical transmittance $T_{nh,\lambda}$ given by [Dombrovsky *et al.*(2005)]

$$T_{nh,\lambda,pred} = T^0_{nh,\lambda} + \frac{D_\lambda}{2}[(1+\rho_{1,\lambda})e^{-\tau_{tr,\lambda,\ell}} + A_\lambda/\beta_\lambda] \tag{1.17}$$

where $\tau_{tr,\lambda,\ell}$ is the transport optical thickness defined as $\tau_{tr,\lambda,\ell} = \beta_{tr,\lambda}\ell = [\bar{A}_{abs,\lambda} + (1 - g_\lambda)\bar{S}_{sca,\lambda}]X\ell$. Here, $T^0_{nh,\lambda}$ is the spectral normal-hemispherical transmittance of an absorbing and single scattering suspension expressed as [Modest(2013)]

$$T^0_{nh,\lambda} = \frac{(1-\rho_{1,\lambda})^2}{1-\rho_{1,\lambda}C_{tr,\lambda}}e^{-\tau_{tr,\lambda,\ell}} \tag{1.18}$$

where $\rho_{1,\lambda}$ is the normal-normal reflectivity of the suspension/air interface given by Fresnel's equations. For an optically smooth surface with normally incident radiation and assuming that the complex index of refraction of the suspension can be approximated as that of the PBS medium, i.e., $m_{PBS,\lambda} = n_{PBS,\lambda}$ in the PAR region, then

$$\rho_{1,\lambda} = \frac{(n_{PBS,\lambda} - 1)^2}{(n_{PBS,\lambda} + 1)^2}. \tag{1.19}$$

The parameters A_λ, B_λ, $C_{tr,\lambda}$, and D_λ are defined as [Dombrovsky *et al.*(2005)]

$$A_\lambda = \frac{(\gamma_{1,\lambda} - \gamma_{2,\lambda}\rho_{1,\lambda})(\varphi_\lambda s_\lambda + c_\lambda)e^{-\tau_{tr,\lambda,L}} - (\gamma_{2,\lambda} - \gamma_{1,\lambda}C_{tr,\lambda})}{(1+\varphi_\lambda^2)s_\lambda + 2\varphi_\lambda c_\lambda} \tag{1.20}$$

$$B_\lambda = \frac{(\gamma_{1,\lambda} - \gamma_{2,\lambda}\rho_{1,\lambda})e^{-\tau_{tr,L}} - (\gamma_{2,\lambda} - \gamma_{1,\lambda}C_{tr,\lambda})(\varphi_\lambda s_\lambda + c_\lambda)}{(1+\varphi_\lambda^2)s_\lambda + 2\varphi_\lambda c_\lambda} \tag{1.21}$$

$$C_{tr,\lambda} = \rho_{1,\lambda}e^{-2\tau_{tr,\lambda,\ell}} \tag{1.22}$$

$$D_\lambda = \frac{\gamma_\lambda(1-\mu_{c,\lambda}^2)\chi_\lambda\zeta_\lambda^2}{\zeta_\lambda^2 - 1}. \tag{1.23}$$

Here, the parameters γ_λ, $\mu_{c,\lambda}$, $\bar{\gamma}_\lambda$, $\gamma_{1,\lambda}$, $\gamma_{2,\lambda}$, χ_λ, φ_λ, β_λ, s_λ, and c_λ are given by [Dombrovsky *et al.*(2005)]

$$\begin{gathered}
\gamma_\lambda = \frac{1-\rho_{1,\lambda}}{1+\rho_{1,\lambda}},\ \mu_{c,\lambda} = \frac{(n_\lambda^2-1)^{1/2}}{n_\lambda},\ \bar{\gamma}_\lambda = \frac{\gamma_\lambda}{1+\mu_{c,\lambda}},\ \gamma_{1,\lambda} = 1-2\bar{\gamma}_\lambda, \gamma_{2,\lambda} = 1+2\bar{\gamma}_\lambda, \\
\chi_\lambda = \frac{\omega_{tr,\lambda}}{1-\omega_{tr,\lambda}}\frac{1-\rho_{1,\lambda}}{1-\rho_{1,\lambda}C_{tr,\lambda}},\ \varphi_\lambda = 2\bar{\gamma}_\lambda/\zeta_\lambda,\ \zeta_\lambda^2 = \frac{4}{(1+\mu_{c,\lambda})^2}\frac{1-\omega_{tr,\lambda}}{1-\omega_{tr,\lambda}\mu_{c,\lambda}}, \\
s_\lambda = \sinh(\zeta_\lambda\tau_{tr,\lambda,\ell}),\ \text{and}\quad c_\lambda = \cosh(\zeta_\lambda\tau_{tr,\lambda,\ell})
\end{gathered} \tag{1.24}$$

In order to predict the normal-hemispherical transmittance $T_{nh,\lambda}$ using Equations (1.17) to (1.24), one needs to know (i) the thickness ℓ of the suspension, (ii) the index of refraction of the medium $n_{PBS,\lambda}$, (iii) the absorption coefficient of the suspension κ_λ, and (iv) the transport scattering coefficient $\sigma_{s,tr,\lambda} = \sigma_{s,\lambda}(1-g_\lambda)$. Here, the thickness ℓ of the cuvette was 10 mm. The spectral refraction index of PBS was given by the Cauchy dispersion relation [Zhernovaya *et al.*(2011)]

$$n_{PBS,\lambda} = 1.32711 + \frac{0.0026}{\lambda^2} + \frac{0.00005}{\lambda^4} \tag{1.25}$$

where the wavelength λ is expressed in μm. On the other hand, in the visible part of the spectrum, PBS can be treated as non-absorbing, i.e., $k_{PBS,\lambda} \approx 0$ [Zhernovaya *et al.*(2011)].

This corresponded to μ_c around 0.66 or to a critical angle θ_c of about 48^o while the reflectivity $\rho_{1,\lambda}$ was about 2%.

1.4.4 Mean rate of photon absorption

In photochemical reactions, the reaction kinetics are proportional to the absorbed useful energy or the local rate of photon absorption, $\mathscr{A}$ expressed in $\mu\text{mol}_{h\nu}/\text{g}\cdot\text{s}$ [Aiba(1982),Cornet *et al.*(1992a), Cassano *et al.*(1995)]. In the context of photobioreactors, it represents the amount of photons absorbed per unit time and per unit weight of biomass. In the case of photosynthetic microalgae, the useful energy is contained in the PAR region defined by the spectral region between 400 and 700 nm. The local rate of photon absorption depends on the absorption cross-section of the species and on the radiation field inside the PBR in the PAR region. The volumetric rate of photon absorption (VRPA) $\mathscr{A}_\mathscr{V}$ (in $\mu\text{mol}_{h\nu}\text{m}^3\cdot\text{s}$) can be expressed as

$$\mathscr{A}_\mathscr{V} = \int_{400}^{700} \bar{A}_{abs,\lambda} G_\lambda(z) X d\lambda = \int_{400}^{700} \bar{C}_{abs,\lambda} G_\lambda(z) N_T d\lambda \tag{1.26}$$

The mean volumetric rate of photon absorption (MVRPA) $\langle \mathscr{A}_\mathscr{V} \rangle$ in the PBR can be expressed as [Pruvost and Cornet(2012)]

$$\langle \mathscr{A}_\mathscr{V} \rangle = \frac{1}{L} \int_0^L \mathscr{A}_\mathscr{V} dz \tag{1.27}$$

where L is the thickness of the PBR (in m). Similarly, the mean rate of photon absorption (MRPA) $\langle \mathscr{A} \rangle$ (in μmol/kg·s) can be expressed as

$$\langle \mathscr{A} \rangle = \frac{\langle \mathscr{A}_\mathscr{V} \rangle}{X} \tag{1.28}$$

The MRPA $\langle \mathscr{A} \rangle$ accounts for the cumulative effects of (i) biomass concentration, (ii) absorption cross-section of the microalgae, and (iii) the fluence rate inside the PBR. Note that all these parameters vary during the course of nitrogen starvation experiments. Therefore, $\langle \mathscr{A} \rangle$ is more indicative of the amount of light absorbed by the microalgae than the fluence rate in the PBR or the absorption cross-section of the cells considered separately. Aiba [Aiba(1982)] demonstrated that the specific growth rate of the purple bacteria

rhodopseudomonas sphaeroides depended linearly on the mean rate of photon absorption (in μmol/kg·s) in batch grown cultures. Similarly, Lehana [Lehana(1990)] and Yun and Park [Yun and Park(2003)] observed a linear relation between the mean rate of photon absorption $\mathscr{A}$ and the specific growth rate of the microalgae *Chlorella vulgaris* grown in unlimited nutrient conditions.

Moreover, Pruvost *et al.* [Pruvost *et al.*(2006)] performed an energy balance on the radiant energy in a 1 dimensional PBR to demonstrate that the rate of photon absorbed by the culture was related to the total radiative flux input and output on the external surfaces of the reactor. In the case where the incident irradiance is fully absorbed in the PBR this expression can be expressed as [Pruvost *et al.*(2006)]

$$\langle \mathscr{A} \rangle = \frac{1}{XL} G_{in} \tag{1.29}$$

1.4.5 Microalgae growth modeling

The time rate of change of the microorganism mass concentration $X(t)$ can be predicted by the exponential growth equation

$$\frac{dX}{dt} = \langle r_x \rangle - D \cdot X. \tag{1.30}$$

where D (in 1/h) corresponds to the dilution rate of the culture and $\langle r_x \rangle$ (in kg/m^3·h) corresponds to the volume averaged productivity in the PBR. The latter can be expressed as [Takache *et al.*(2012)]

$$\langle r_x \rangle = \frac{\langle J_{O_2} \rangle X M_x}{\nu_{O_2-X}}. \tag{1.31}$$

Here, M_x is the C-molar mass of the biomass and ν_{O_2-X} the stoichiometric coefficient of the oxygen production. The volume averaged oxygen production $\langle J_{O_2} \rangle$ (in mol$_{O_2}$/kg$_X$·s) can be obtained by integrating the local oxygen production rate $J_{O_2}(z)$ as

$$\langle J_{O_2} \rangle = \frac{1}{L} \int_0^L J_{O_2}(z) dz \tag{1.32}$$

Table 1.1: Kinetic model parameters used for predicting biomass productivity of *C. vulgaris* [Pruvost *et al.*(2016)]

Parameter	Value	Units
M_x	0.024	Kg/mol
J_{NADH_2}	2.80×10^{-3}	mol_{NADH_2}/kg·s
ν_{O_2-X}	1.13	$\text{mol}_{O_2}/\text{mol}_X$
ρ_M	0.8	
ϕ'_{O_2}	1.10×10^{-7}	$\text{mol}_{O_2}/\mu\text{mol}_{h\nu}$
$\nu_{NADH_2-O_2}$	2	$\text{mol}_{NADH_2}/\text{mol}_{O_2}$
K	4.0×10^{4}	$\mu\text{mol}_{h\nu}$/kg·s
K_r	557	$\mu\text{mol}_{h\nu}$/kg·s

Finally, the local oxygen production rate $J_{O_2}(z)$ can be determined using an equation proposed by Takache et al. [Takache *et al.*(2012)]

$$J_{O_2}(z) = \rho_M \frac{K}{K + \mathscr{A}(z)} \phi'_{O_2} \mathscr{A}(z) - \frac{J_{NADH_2}}{\nu_{NADH_2-O_2}} \frac{K_r}{K_r + \mathscr{A}(z)} \tag{1.33}$$

where ρ_M is the maximum energy yield for photon conversion, ϕ'_{O_2} is the quantum yield of O_2 (in mol_{O_2}/μ $\text{mol}_{h\nu}$) for the Z scheme of photosynthesis, and K and K_r (in $\mu\text{mol}_{h\nu}/\text{kg}_X$·s) are, respectively, the half-saturation constant for photosynthesis and the saturation constant describing the inhibition of respiration in light. Similarly, J_{NADH_2} is the specific rate of cofactor regeneration on the respiratory chain and $\nu_{NADH_2-O_2}$ is the stoichiometric coefficient of cofactor regeneration on the respiratory chain. Table 1.1 presents the parameters used in predicting the growth kinetics of *C. vulgaris* using Equation (1.33).

Pruvost and Cornet [Pruvost and Cornet(2012)] developed a model predicting the maximum biomass productivity of both microalgae [Takache *et al.*(2010)] and cyanobacteria [Cornet and Dussap(2009)] in various PBRs as a function of PFD. The authors used the concept of MVRPA to obtain an analytic expression for the maximum biomass productivity $r_{x_{max}}$

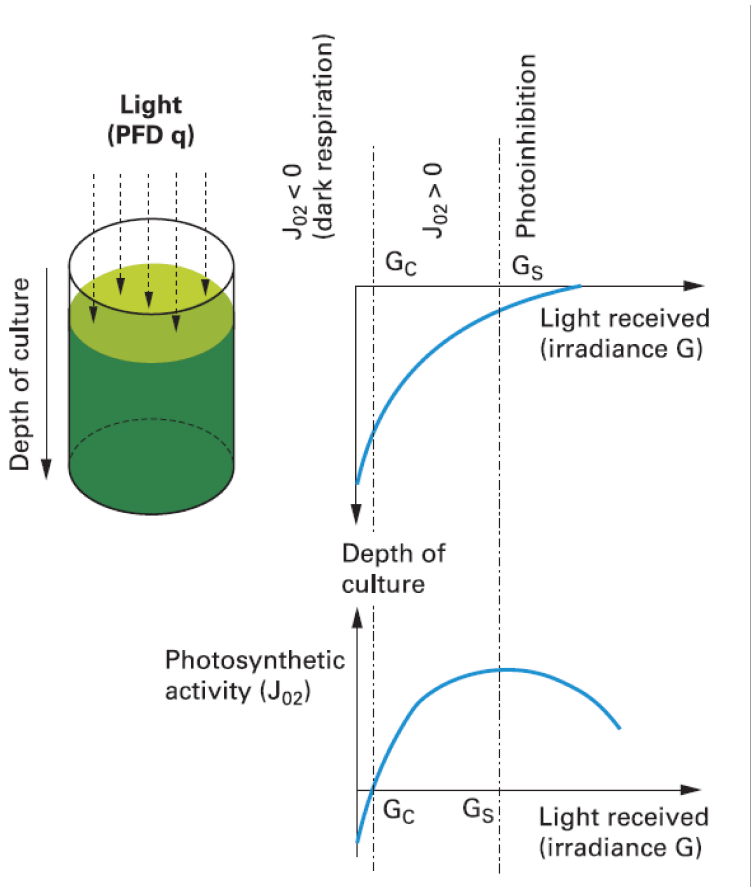

Figure 1.11: Schematic representation of light attenuation profile in PBRs [Pruvost and Cornet(2012)].

(in kg/m^2.day) given by [Cornet and Dussap(2009)]

$$\langle r_{x_{max}} \rangle = \bar{\phi} \rho_m \frac{K_S}{G_{in}} \ln \left(1 + \frac{G_{in}}{K_S} \right) \langle \mathscr{A}_\mathscr{V} \rangle_{max} \tag{1.34}$$

where $\bar{\phi}$ and K_S are properties of the photosynthetic and metabolic activities of the microorganisms. Specifically, $\bar{\phi}$ is the time-averaged mass quantum yield for the Z-scheme of photosynthesis (in kg of biomass/$\mu mol_{h\nu}$) and K_S (in μmol$_{h\nu}$/m^2·s) is the average photosynthesis half saturation constant.

1.4.6 Light-limited microalgae growth and the working illuminated volume

To optimize the fluence rate and light absorption rate in the microalgae cultures and maximize biomass productivity, radiation transfer analysis in the photobioreactors (PBRs) must be performed. Cornet and co-workers [Cornet *et al.*(1992a), Cornet and Dussap(2009), Takache *et al.*(2010)] introduced the concept of illuminated volume fraction γ as a simple tool to determine the biomass productivity of the culture (Figure 1.12). It is a dimensionless quantity that can be used to estimate the mean specific growth rate $\langle\mu\rangle$ in the PBR [Cornet *et al.*(1992a)]. In a flat-plate PBR it is expressed as

$$\gamma = \frac{z(A_c)}{L} \tag{1.35}$$

where $z(A_c)$ is the depth at which the LRPA in the PBR is equal to the photosynthetic compensation point $\mathscr{A}_c$ of the species. The latter corresponds to the minimum amount of energy that is necessary to balance cell respiration or cell maintenance. An illumination fraction $\gamma = 1$ corresponds to the case where the cells at the back wall of the PBR receive adequate amount of energy to maintain their metabolism. This is the most energetically efficient state of the PBR where the mean growth rate and productivity of the culture is at its maximum [Pruvost and Cornet(2012)]. On the other hand, $\gamma < 1$ indicates the appearance of the so called "dark zone" in the PBR where $\mathscr{A}(z) < \mathscr{A}_c$ and the growth rate is negative. Moreover, $\gamma > 1$ corresponds to the hypothetical case where the photosynthesis compensation point is situated outside the PBR boundary. This case is associated with suboptimum mean growth rate and loss in productivity of the culture due to the under utilization of the incident radiation which is lost by light transmission. Takache *et al.* [Takache *et al.*(2012), Dauchet(2012)] reported $A_c = 1800$ $\mu\text{mol}_{h\nu}$/kg·s for *C. reinhardtii* and Soulies [Soulies(2014)] reported $A_c = 1200$ $\mu\text{mol}_{h\nu}$/kg·s for *C. vulgaris*.

1.4.7 Photosynthesis curve

Figure 1.13 shows a typical response of microorganisms to the level of incident light also called a PI curve. The PI curve can be divided into three segments, the photolimited,

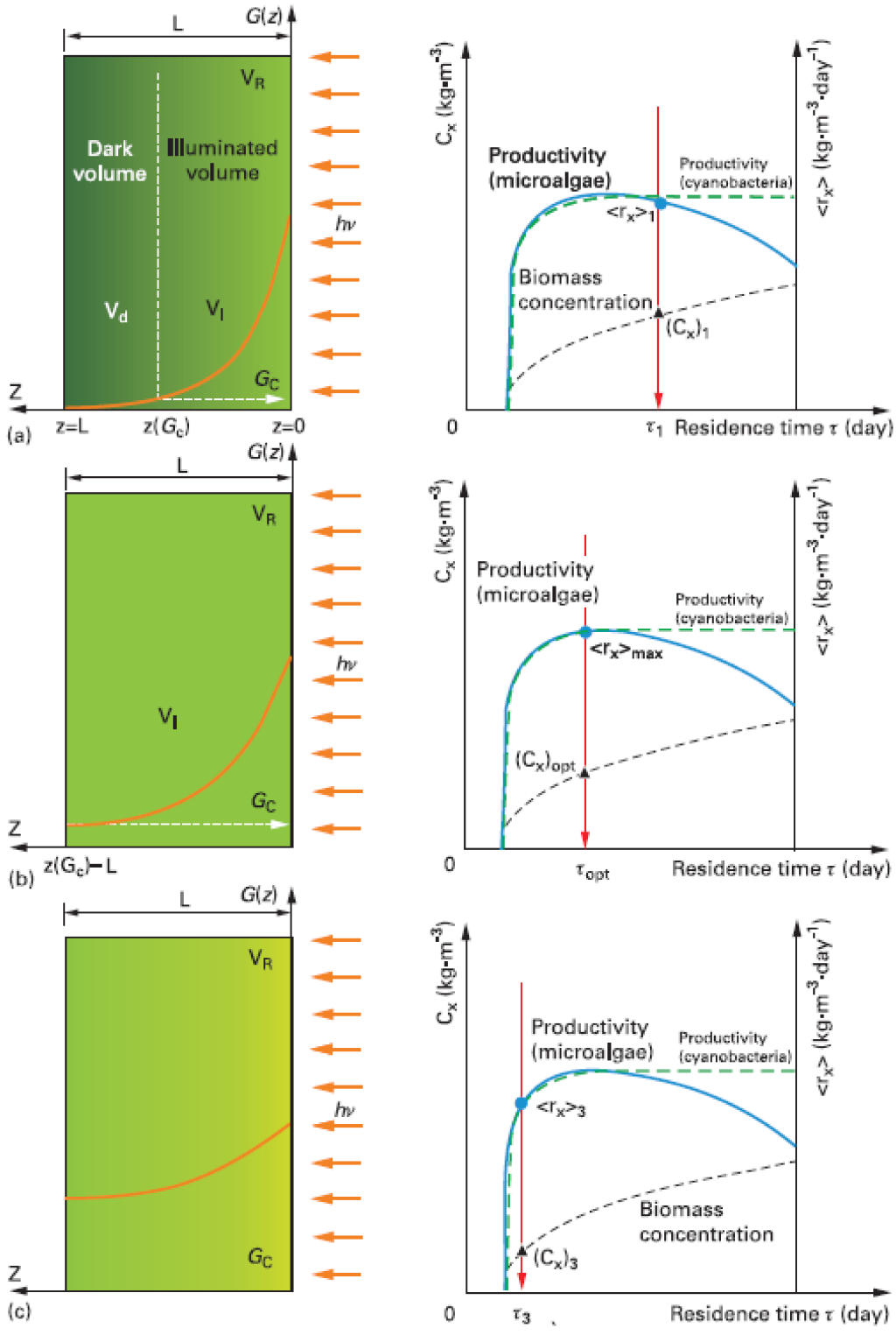

Figure 1.12: Schematic of the three regimes of illumination in microalgae cultures as a function of microalgae residence time τ [Pruvost and Cornet(2012)].

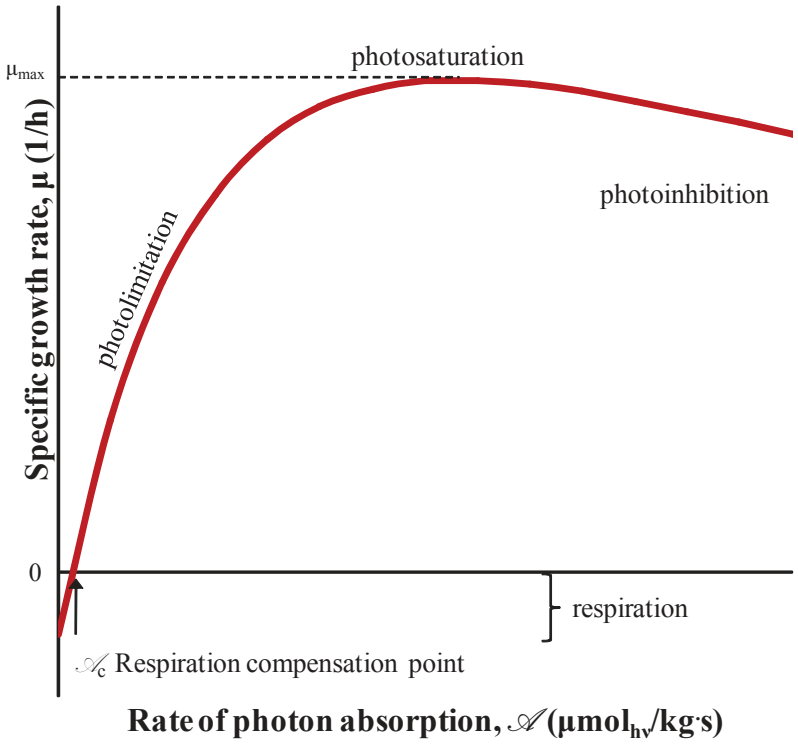

Figure 1.13: Typical response of microorganisms to the level of incident light.

the saturation, and the photinhibition regions. When the light received by cells is smaller than the so called "respiration compensation point" A_c, the growth rate is negative. This corresponds to the minimum energy needed to be generated by photosynthesis to allow for cell respiration.In the photolimited region, the specific growth rate (or oxygen evolution) is linearly dependent on the fluence rate. When the fluence rate is larger than the so called saturation point K_s, the growth rate is "saturated" and thus independent of fluence rate. For fluence rate larger than the photoinhibition point K_I, the growth rate decreases due to photoinhibition as previously discussed.

1.5 Determination of radiation characteristics

The absorption cross-sections of microorganisms varies significantly among species [Berberoğlu *et al.*(2007), Berberoğlu *et al.*(2008), Heng *et al.*(2014b)] or during the biomass growth, in particular during nitrogen starvation [Heng *et al.*(2014b),Heng *et al.*(2014a),Kandilian *et al.*(2014b)]. It can be directly measured experimentally along with the scattering phase function and scattering cross-section for dilute suspension [Pilon *et al.*(2011)]. However, such experimental measurements require expensive equipment and can be time consuming [Berberoğlu *et al.*(2008)]. Alternatively, the absorption cross-section can be estimated theoretically using electromagnetic wave theory and solutions of Maxwell's equations such as the Lorenz-Mie theory. However, such theoretical predictions assume that the microorganisms have simple shape (e.g., spherical) [Pottier *et al.*(2005)] and require the effective refraction and absorption indices of the cells. The latter can be estimated based on additional simplifying assumptions [Pottier *et al.*(2005)].

1.5.1 Experimental determination

The spectral mass absorption and scattering cross-sections $\bar{A}_{abs,\lambda}$ and $\bar{S}_{sca,\lambda}$ of microalgae cultures can be experimentally measured according to the method outlined and reviewed by Pilon *et al.* [Pilon *et al.*(2011)]. In this method, the normal-normal and normal-hemispherical

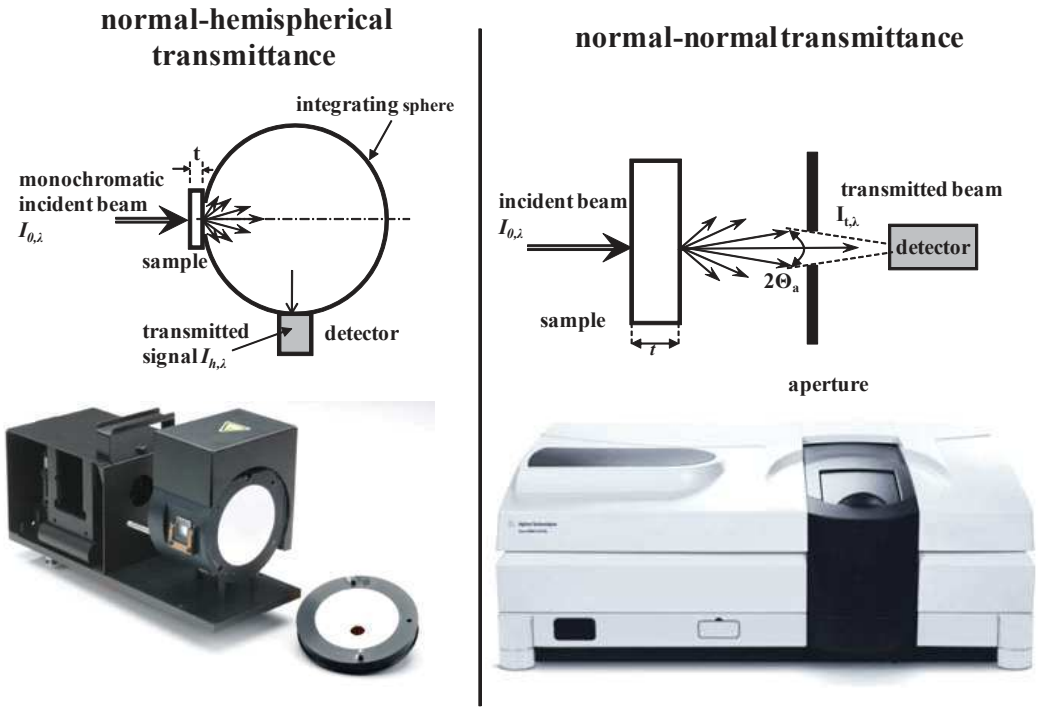

Figure 1.14: Schematic and the instruments used for normal-normal and normal-hemispherical transmission measurements.

transmissions of several dilute microalgae suspensions with different known concentrations are measured using a spectrometer equipped with an integrating sphere shown in Figure 1.14.

The size-average spectral mass absorption and scattering cross-sections $\bar{A}_{abs,\lambda}$ and $\bar{S}_{sca,\lambda}$ of dilute suspensions of randomly oriented microorganisms can be experimentally measured according to a method outlined and reviewed by Pilon et al. [Pilon *et al.*(2011)]. First, the apparent extinction coefficient β^*_λ can be obtained from normal-normal transmittance $T_{nn,\lambda,X}$ measurements of dilute microalgae suspensions with different known concentrations placed in a cuvette, of pathlength t [Pilon *et al.*(2011)]

$$\beta^*_\lambda = -\frac{1}{t} ln \left(\frac{T_{nn,\lambda,X}}{T_{nn,\lambda,ref}} \right) \tag{1.36}$$

where $T_{nn,\lambda,ref}$ is the normal-normal transmittance of the medium alone in the cuvette. Similarly, the apparent absorption coefficient $\kappa^*_{nh,\lambda}$ can be defined from the normal-hemispherical

transmittance $T_{nh,\lambda}$ measured using an integrating sphere as [Pilon *et al.*(2011)]

$$\kappa_\lambda^* = -\frac{1}{t} ln \left(\frac{T_{nh,\lambda,X}}{T_{nh,\lambda,ref}} \right) \tag{1.37}$$

The apparent extinction coefficient β_λ^* can be expressed as a function of the actual absorption κ_λ and scattering $\sigma_{s,\lambda}$ coefficients as [Pilon *et al.*(2011)]

$$\beta_\lambda^* = \kappa_\lambda + (1 - \epsilon_n)\sigma_{s,\lambda}. \tag{1.38}$$

Here, ϵ_n represents the fraction of light scattered in the forward direction and detected by the spectrometer. Ideally, ϵ_n is equal to zero so that $\beta_\lambda^* = \beta_\lambda = \kappa_\lambda + \sigma_{s,\lambda}$. However, due to the finite size of the acceptance angle of the detector, ϵ_n is larger than zero and is assumed to be constant over the PAR region. It can be estimated from the suspension scattering phase function $\Phi_{T,\lambda}(\Theta)$ according to [Pilon *et al.*(2011)]

$$\epsilon_n = \frac{1}{2} \int_0^{\Theta_a} \Phi_{T,\lambda}(\Theta) sin(\Theta) d\Theta \tag{1.39}$$

where Θ_a is the half acceptance angle of the detector. The actual extinction coefficient $\beta_\lambda = \kappa_\lambda + \sigma_{s,\lambda}$ can then be determined according to [Pilon *et al.*(2011)]

$$\beta_\lambda = \frac{\beta_\lambda^* - \epsilon_n \kappa_\lambda}{1 - \epsilon_n}. \tag{1.40}$$

Similarly, the apparent absorption coefficient κ_λ^* is related to the actual absorption κ_λ and scattering $\sigma_{s,\lambda}$ coefficients as [Pilon *et al.*(2011)]

$$\kappa_\lambda^* = \kappa_\lambda + (1 - \epsilon_h)\sigma_{s,\lambda} \tag{1.41}$$

Here, ϵ_h is the fraction of the scattered light detected by the detector. Ideally, when all the scattered light is accounted for, ϵ_h is equal to unity and $\kappa_\lambda^* = \kappa_\lambda$. Moreover, at $\lambda = 750$ nm green microalgae are assumed to be non-absorbing, i.e., $\kappa_{750} = 0$ m^{-1}. Then, Equations (1.38) and (1.41) simplify to

$$\kappa_{750}^* = (1 - \epsilon_h)\sigma_{s,750} \quad \text{and} \quad \beta_{750}^* = (1 - \epsilon_n)\sigma_{s,750} \tag{1.42}$$

Combining Equations (1.40) to (1.42) yields

$$\kappa_\lambda = \kappa^*_\lambda - \kappa^*_{750}\left(\frac{\beta^*_\lambda - \kappa^*_\lambda}{\beta^*_{750} - \kappa^*_{750}}\right) \quad \text{and} \quad \sigma_{s,\lambda} = \frac{\beta^*_\lambda - \epsilon_n\kappa_\lambda}{1-\epsilon_n} - \kappa_\lambda \tag{1.43}$$

Finally, the size-averaged spectral mass absorption $\bar{A}_{abs,\lambda}$ and scattering $\bar{S}_{sca,\lambda}$ cross-sections (in m^{-1}) of the microalgae suspension of dry mass concentration X (in $\mathrm{kg/m}^3$) are defined as [Pilon *et al.*(2011)]

$$\bar{A}_{abs,\lambda} = \kappa_\lambda / X \quad \text{and} \quad \bar{S}_{sca,\lambda} = \sigma_{s,\lambda}/X \tag{1.44}$$

In this method, the pathlength and concentration of the samples are to be chosen such that single scattering prevails, i.e., photons undergo at most one scattering event as they travel through the suspension. In practice, cuvette pathlength must be smaller than the photon mean-free path. Then, $\bar{A}_{abs,\lambda}$ and $\bar{S}_{sca,\lambda}$ should be independent of concentration X. This can be verified experimentally by repeating the measurements for suspensions with different concentrations. This experimental procedure has been validated with polystyrene microspheres 2-20 μm in diameter and long glass fibers 15-20 μm in diameter [Pilon and Kandilian(2015)].

The total scattering phase function was measured at 633 nm by a polar nephelometer shown in Figure 1.15. The experimental setup and data analysis have previously been reported in detail by Berberoğlu *et al.* [Berberoğlu *et al.*(2008), Pilon *et al.*(2011)].

Bellini *et al.* [Bellini *et al.*(2014)] developed an experimental method to determine the absorption $A_{abs,\lambda}$ and the transport scattering $(1-g_\lambda)S_{sca,\lambda}$ cross-sections of microalgae. The authors measured the total reflectance (diffuse plus specular reflectance) and the normal-hemispherical transmittance of microalgae suspensions using a double integrating sphere spectrometer and retrieved $A_{abs,\lambda}$ and $(1-g)S_{sca,\lambda}$ using the inverse-adding-doubling (IAD) method [Prahl *et al.*(1993)]. The microalgae suspensions each featured a concentration between 1.1×10^{13} and 2.4×10^{13} cells/m^3. This method was not able to estimate the absorption and the transport scattering cross-section accurately especially for samples with low absorption coefficient. Indeed, the authors stated in the article that "in samples with low absorption and high scattering coefficients, the unwanted light losses may be interpreted by

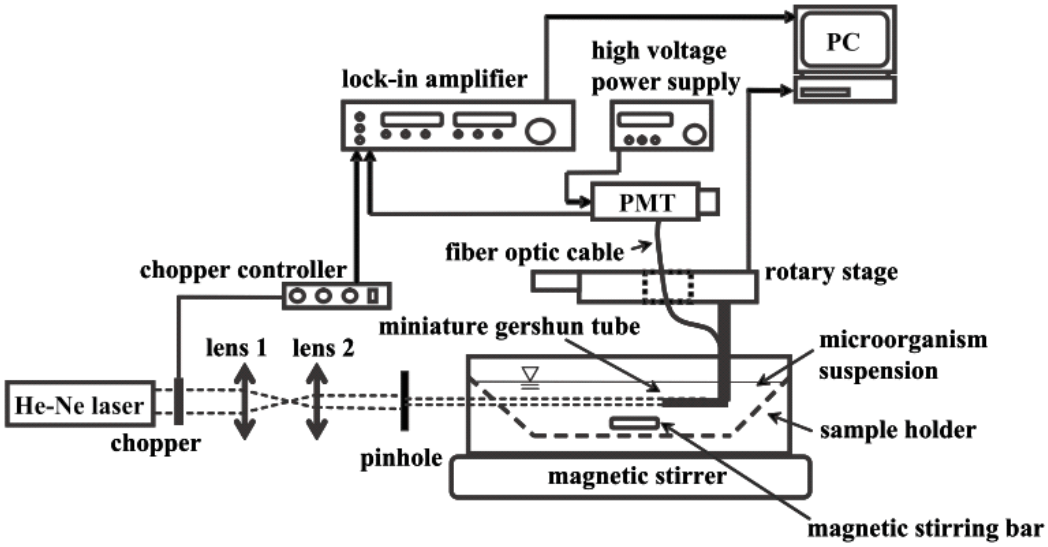

Figure 1.15: The schematic of the nephelometer used for measuring the scattering phase function of the microalgae suspensions.

the IAD algorithm as absorption phenomena inside the sample rather than losses in the outside world, leading to an overestimation of the absorption coefficient" [Bellini *et al.*(2014)]. They recommended for this method to be only used for qualitative analysis of microalgae cultures.

1.5.2 Theoretical predictions

Theoretical predictions of $\bar{A}_{abs,\lambda}$ and $\bar{S}_{sca,\lambda}$ can be obtained by Lorenz-Mie theory, for both homogeneous or coated spheres, based on the cell size distribution and the effective complex index of refraction m_λ of the microalgae [Pottier *et al.*(2005), Berberoğlu *et al.*(2007), Jonasz and Fournier(2007)]. The Lorenz-Mie theory predicts the absorption $C_{abs,\lambda}$ and scattering $C_{sca,\lambda}$ cross-sections (m^2) of a homogeneous spherical cell of complex index of refraction $m_\lambda = n_\lambda + ik_\lambda$ and radius r_{eq}. Microalgae cells are polydisperse with size distribution $f(r_{eq})$. Then, the size-averaged absorption $\bar{C}_{abs,\lambda}$ and scattering $\bar{C}_{sca,\lambda}$ cross-sections of polydisperse

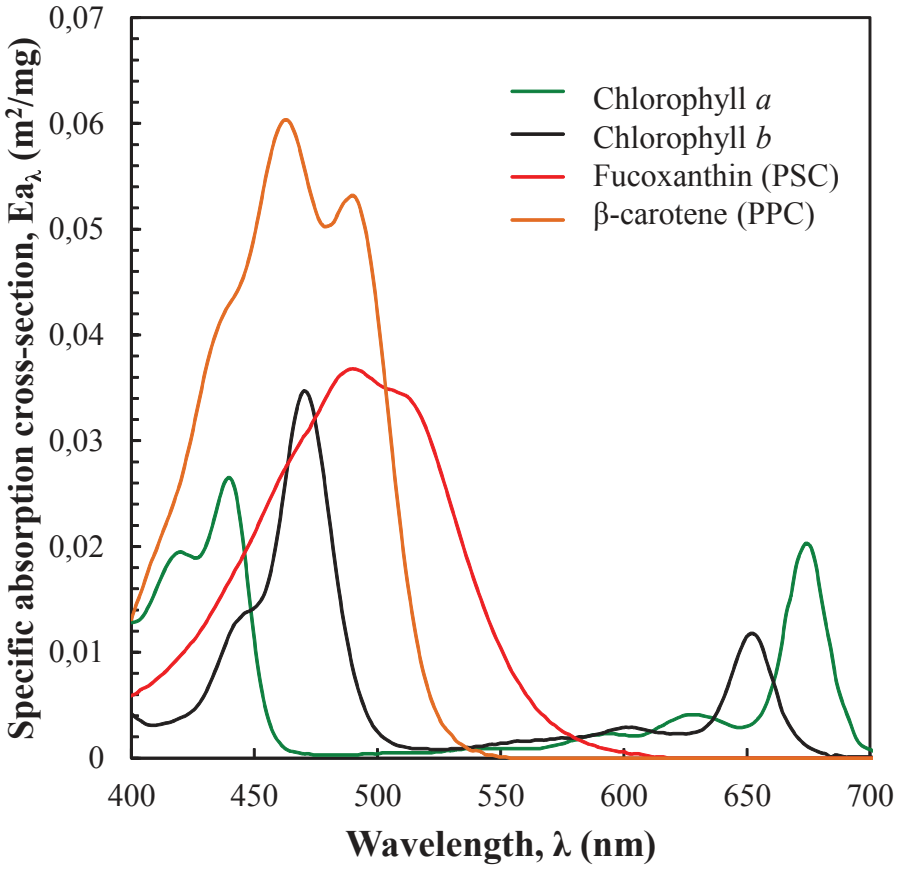

Figure 1.16: Specific absorption cross-sections Ea_λ of pigments Chlorophyll$a$, chlorophyll$b$, fucoxanthin (PSC), and β-carotene (PPC) [Bidigare *et al.*(1990)].

microalgae of a known size distribution $f(r_{eq})$ can be estimated as [Pilon *et al.*(2011)]

$$\bar{C}_{abs,\lambda} = \int_0^\infty C_{abs,\lambda}(r_{eq}) f(r_{eq}) \mathrm{d}r_{eq} \quad \text{and} \quad \bar{C}_{sca,\lambda} = \int_0^\infty C_{sca,\lambda}(r_{eq}) f(r_{eq}) \mathrm{d}r_{eq} \tag{1.45}$$

It is often more useful to express cross-sections in size-averaged mass absorption $\bar{A}_{abs,\lambda}$ and mass scattering $\bar{S}_{sca,\lambda}$ cross-sections (in m^2/kg) [Cornet *et al.*(1992a), Takache *et al.*(2010), Takache *et al.*(2012), Kandilian *et al.*(2014b), Kandilian *et al.*(2014a)]. The latter are related to the absorption $\bar{C}_{abs,\lambda}$ and scattering $\bar{C}_{sca,\lambda}$ cross-sections by [Pottier *et al.*(2005)]

$$\bar{A}_{abs,\lambda} = \frac{\bar{C}_{abs,\lambda}}{V_{32}\rho_{dry}(1-x_w)} \quad \text{and} \quad \bar{S}_{sca,\lambda} = \frac{\bar{C}_{sca,\lambda}}{V_{32}\rho_{dry}(1-x_w)} \tag{1.46}$$

where V_{32} (in m^3) is the Sauter mean diameter of the cell, ρ_{dry} is the density of the dry biomass (in kg/m^3), x_w is the average water fraction in the cells.

In addition, the total scattering phase function $\Phi_{T,\lambda}(\Theta)$ of the polydisperse microorganisms is given by [Modest(2013)]

$$\Phi_{T,\lambda}(\Theta) = \frac{\int_0^\infty C_{sca,\lambda}(r_{eq}) \Phi(r_{eq}, \Theta) f(r_{eq}) \mathrm{d}r_{eq}}{\int_0^\infty C_{sca,\lambda} f(r_{eq}) \mathrm{d}r_{eq}} \tag{1.47}$$

The backward scattering ratio b_λ is defined as the fraction of the radiation scattered backwards and is estimated from the suspension's scattering phase function [Pottier *et al.*(2005)]

$$b_\lambda = \frac{1}{2} \int_{\pi/2}^{\pi} \Phi_{T,\lambda}(\Theta) sin\Theta d\Theta. \tag{1.48}$$

The absorption index k_λ and the refraction index n_λ must be known in order to obtain the size-averaged spectral mass absorption $\bar{A}_{abs,\lambda}$ and scattering $\bar{S}_{sca,\lambda}$ cross-sections of the microorganisms. Pottier et al. [Pottier *et al.*(2005)] proposed the following expression for the absorption index k_λ

$$k_\lambda = \frac{\lambda}{4\pi} \sum_j C_j E a_j = \frac{\lambda}{4\pi} \rho_{dry}(1-x_w) \sum_j w_j E a_j \tag{1.49}$$

Here, C_j (in kg/m^3) is the concentration of pigment "j" in the cell while and $w_j = C_j/X$ is the pigment concentration on dry mass basis. Moreover, Ea_j (in m^2/kg) is the specific absorption cross-section of individual pigments chlorophyll a (chl$a$), chlorophyll b (chl$b$), photoprotective carotenoids (PPC), and photosynthetic carotenoids (PSC) as reported by Bidigare et al. [Bidigare *et al.*(1990)].

Pottier et al. [Pottier *et al.*(2005)] predicted the radiation characteristics of *Chlamydomonas reinhardtii* using the Lorenz-Mie theory assuming that (i) the cells were spherical, (ii) the absorption index k_λ was given by Equation (1.49), and (iii) the refraction index n_λ was constant over the PAR and equal to 1.55. Recently, Dauchet et al. [Dauchet *et al.*(2015)] relaxed the latter assumption and developed a method to predict the spectral refraction index n_λ of microalgae cells using the subtractive Kramers-Kronig relation based on the spectral absorption index k_λ given by Equation (1.49). Then, the real index of refraction can be estimated using an equation relating the refraction and absorption indices of the cells [Dauchet *et al.*(2015)]

$$n_\nu = n_{\nu_p} + 2\frac{(\nu^2 - \nu_p^2)}{\pi} P \int_{\nu_{min}}^{\nu_{max}} \frac{\nu' k_{\nu'}}{(\nu'^2 - \nu^2)(\nu'^2 - \nu_p^2)} d\nu'. \tag{1.50}$$

Here, $\nu = c/\lambda$ is the frequency of radiation, c is the speed of light in vacuum, and P is the Cauchy principal value. The anchor frequency denoted by ν_p was chosen such that the cells did not absorb at that frequency, i.e., $k_{\nu_p} = 0$. On the other hand, the value for n_{ν_p} must be known or retrieved experimentally. For example, Dauchet et al. [Dauchet *et al.*(2015)] chose the anchor wavelength λ_p as 820 nm for *C. reinhardtii* as green microalgae do not absorb at $\lambda \geq 750$ nm [Dauchet *et al.*(2015)]. Dauchet et al. [Dauchet *et al.*(2015)] retrieved a value of 1.44 for *C. reinhardtii* using an inverse method that minimized the difference between the measured and the predicted normal-hemispherical transmittance at 820 nm. The latter was estimated by solving the RTE using the Monte-Carlo approach and the predicted radiation characteristics of the microorganisms. Finally, Dauchet et al. [Dauchet *et al.*(2015)] measured the spectral normal-hemispherical transmittance $T_{nh,\lambda}$, over the PAR, of dense microalgae cultures and compared it with predictions by the Monte-Carlo method solving the RTE using the radiation characteristics estimated using the theoretical method. The authors assumed

that an agreement between the measured and predictions transmittance $T_{nh,\lambda}$ would validate the accuracy of the theoretically predicted radiation characteristics.

Moreover, Lee et al. [Lee *et al.*(2013)] retrieved the complex index of refraction of *C. reinhardtii* using an inverse method combining the Lorenz-Mie theory, the measured size-averaged spectral mass absorption $\bar{A}_{abs,\lambda}$ and scattering $\bar{S}_{sca,\lambda}$ cross-sections, and the measured surface area equivalent cell radius distribution $f(r_{eq})$. The authors reported a refraction index n_λ over the PAR region ranging from 1.35-1.37 and an absorption index k_λ ranging from 0 to 7 $\times 10^{-3}$.

Finally, Quirantes and Bernard [Quirantes and Bernard(2006)] modeled *Aureococcus anophagefferens* cells as coated spheres with a shell volume fraction of 15%. The inner core and outer coating corresponded to the cell cytoplasm and to the chloroplast, respectively and they featured complex index of refraction equal to 1.36 and $1.4+i0.005$, respectively. The authors compared theoretical predictions of algal bloom reflectance to measurements by a tethered surface radiometer. They found better agreement between measurements and prediction when the cells were modeled as coated spheres compared to when they were modeled as homogeneous spheres. This was attributed to the larger backscattering ratio of the coated spheres compared with homogeneous spheres of the same outer radius and effective volume averaged index of refraction.

CHAPTER 2

Comparison of experimentally and theoretically determined radiation characteristics of photosynthetic microorganisms

Abstract

This chapter aims to experimentally validate a theoretical method to predict the radiation characteristics of photosynthetic microorganisms. Such predictions would facilitate light transfer analysis in photobioreactors to optimize and control their operation so as to maximize the production of biofuel and other high-value products. However, the predictive method relies on various assumptions and simplifications whose validation and impact on the predictions need to be assessed. This study presents a comparison between experimentally measured and theoretically predicted mass absorption and scattering cross-sections and the scattering phase function of *Chlamydomonas reinhardtii* grown under nitrogen-replete and nitrogen-limited conditions and of *Chlorella vulgaris* grown under nitrogen-replete conditions. First, good agreement was found between the two methods for determining the radiation characteristics of both nitrogen-replete and nitrogen-limited *C. reinhardtii* microalgae treated as volume-equivalent homogeneous spheres. However, the theoretical predictions significantly overestimated the absorption cross-section of *C. vulgaris* cells. The latter was then modeled as coated spheres with a non-absorbing 130 nm coating accounting for the presence of a rigid cell wall made of sporopollenin leading to better agreement with the experimental data. Measurements of normal-hemispherical transmittance of high concentration samples were compared with predictions by the modified two-flux approximation. The

normal-hemispherical transmittance predictions were found to be strongly dependent on the absorption cross-section of the cells but only weakly on their scattering cross-section.

2.1 Introduction

Numerous kinetic models have been developed for coupling microalgae biomass or lipid productivity to light transfer in the PBR [Cornet *et al.*(1992b),Cornet and Dussap(2009),Takache *et al.*(2010), Takache *et al.*(2012), Béchet *et al.*(2013)]. Such predictive models are crucial for optimizing and for scaling-up bioprocesses to industrial scales as well as for performing economic and life cycle analysis. They require the knowledge of the local fluence rate in the PBR and therefore the solution to the radiative transfer equation (RTE) [Cornet *et al.*(1992a)]. The latter depends on the radiation characteristics of the microorganisms including their absorption and scattering cross-sections and the scattering phase function [Pilon *et al.*(2011)]. They can be obtained experimentally [Pilon *et al.*(2011)] or predicted theoretically based on electromagnetic wave theory [Pottier *et al.*(2005), Dauchet *et al.*(2015)].

The experimental method applies to absorbing and scattering particles or cells of any arbitrary shape. It assumes that they are (i) dilute to ensure that single scattering prevails, (ii) randomly oriented such that the suspension average scattering phase function has azimuthal symmetry, and (iii) scattering is mainly in the forward direction, as satisfied by cells whose diameter is larger than the wavelength of the incident light. The validity of these assumptions can be verified experimentally [Pilon *et al.*(2011)]. However, the experimental setup can be costly and the experimental procedure time consuming. Thus, it may be difficult to implement in actual production systems. In addition, measurements are valid only for specific growth conditions and need to be repeated each time conditions change including pH, temperature, illumination, and medium composition. This is particularly true under nitrogen-limited conditions when pigment concentrations decreases dramatically [Kandilian *et al.*(2014b), Heng and Pilon(2014)].

On the other hand, the theoretical method is based on Lorenz-Mie theory [Hulst(1957)]. It assumes that (1) the microalgae cells can be approximated as equivalent spheres of identical volume and that (2) the cells are homogeneous, i.e., the effects of the cell organelles and any other heterogeneities within the cells can be accounted for through an effective complex index of refraction $m_\lambda = n_\lambda + ik_\lambda$ where n_λ and k_λ are the cells' effective refraction and absorption

indices, respectively. The main challenge of the theoretical approach resides in modeling these effective optical properties as a function of wavelength and of the cell's biochemical composition including water content and pigments, for example. The theoretical method is relatively fast and could be used for simulating microalgae growth under various operating conditions affecting cell size and/or pigment concentrations. It can also be employed for the design and model-based control of PBRs, and for, ultimately, maximizing their productivity. However, the theoretical model has only been validated indirectly by considering the normal-hemispherical transmittance measurements of *Chlamydomonas reinhardtii* suspension grown under optimal conditions [Pottier *et al.*(2005), Dauchet *et al.*(2015)].

The present chapter aims to directly compare, for the first time, the theoretical and experimental methods of determining the radiation characteristics of microalgae suspensions. It considered two different green microalgae species namely *Chlamydomonas reinhardtii* and *Chlorella vulgaris* grown under not only optimal but also nitrogen-limited conditions characterized by low cell pigment concentrations [Pruvost *et al.*(2009), Van Vooren *et al.*(2012), Kandilian *et al.*(2013), Kandilian *et al.*(2014b)].

2.2 Materials and Methods

2.2.1 Species and culture medium

A wild type of *Chlamydomonas reinhardti* (137 AH) was supplied by Commissariat à l'Energie Atomique (CEA) Cadarache, France while the *C. vulgaris* (211/19) strain was obtained from the culture collection of protozoa and microalgae (CCAP) in Scotland, UK. Both species were cultivated in a modified Suoeka medium with the following composition (in mM) : NH_4Cl 2.71, $MgSO_4{\cdot}7H_2O$ 1.14, $CaCl_2{\cdot}2H_2O$ 0.34, KH_2PO_4 4.48, $NaHCO_3$ 20, and 1 mL of Hutner's trace elements solution. The medium was sterilized by autoclaving it at 121^{o}C for 25 minutes.

C. reinhardtii culture was grown in optimal conditions in a 1.5 L torus type PBR with a depth of 4 cm in chemostat mode with a culture dilution rate of 0.01 1/h. It was exposed to

110 $\mu\text{mol}_{h\nu}/\text{m}^2\cdot\text{s}$ of white LED light. A detailed description of the PBR was given by Takache et al. [Takache *et al.*(2010)] and need not be repeated. The nitrogen-limited *C. reinhardtii* culture was grown in a modified Suoeka medium containing 1 mM of NH_4 instead of 2.71 mM and exposed to 400 $\mu\text{mol}_{h\nu}/\text{m}^2\cdot\text{s}$ white LED light. Finally, *C. vulgaris* cells were grown in a 3 cm thick flat plate airlift PBR, described in Ref. [Pruvost *et al.*(2009)], and exposed to 500 $\mu\text{mol}_{h\nu}/\text{m}^2\cdot\text{s}$ white LEDs. The PBR was operated in chemostat mode with a dilution rate of 0.01 1/h.

2.2.2 Biomass concentration

Microorganisms dry biomass concentration X was estimated gravimetrically by filtering 5 mL of culture through a pre-dried and pre-weighed 0.45 μm pore size glass-microfiber filter (Whatman GF/F). The filters were dried for a minimum of 24 hours in an oven at 105^{o}C and weighed after being cooled in a desiccator for 30 minutes. Each sample was analyzed in triplicates and the mean value of the biomass concentration was reported.

2.2.3 Pigment concentration

Pigments were extracted in pure methanol and quantified spectrophotometrically. A volume of 0.5 mL of culture was first centrifuged at 13,400 rpm for 10 minutes. The medium was discarded and the cells were resuspended in 1 mL of pure methanol and sonicated for 20 seconds. The samples were left for 1 hour in an oven at 45^{o}C and the extract was then centrifuged. The optical density OD_λ of the supernatant was measured at wavelengths 750, 665, 652, and 480 nm using a UV-VIS spectrophotometer (Jasco V-730 Easton, Maryland). All extractions were performed in triplicates. Chlorophyll *a* and Chlorophyll *b* concentrations, respectively denoted by C_{chla} and C_{chlb}, were estimated according to the correlations [Ritchie(2006)]

$$\begin{aligned} C_{chla}[mg/L] &= -8.0962(OD_{652} - OD_{750}) + 16.5169(OD_{665} - OD_{750}) \\ C_{chlb}[mg/L] &= 27.4405(OD_{652} - OD_{750}) - 12.1688(OD_{665} - OD_{750}). \end{aligned} \tag{2.1}$$

Similarly, total carotenoid concentration, consisting of both photoprotective and photosynthetic caroteniods, $C_{PPC+PSC}$ was estimated according to [Strickland and Parsons(1968b)]

$$C_{PPC+PSC}[mg/L] = 4(OD_{480} - OD_{750}). \tag{2.2}$$

The ratio of PPC to PSC concentrations was assumed to be 6 [Dubinsky and Stambler(2000)].

2.2.4 Determination of size distribution

The cell size distribution was measured using 2D microscope images captured using a Zeiss microscope connected to a CCD camera. The image analysis software imageJ was used to manually measure the major a and minor b Ferret diameters of individual cells. Then spheroid aspect ratio was defined as $\epsilon = a/b$. The volume equivalent radius r_{eq} was determined as [Dauchet *et al.*(2015)]

$$r_{eq} = a\left(\frac{3}{2\epsilon}\right)^{1/3} \tag{2.3}$$

Then, the frequency distribution of the volume equivalent radius $f(r_{eq})$ was estimated according to

$$f(r_{eq}) = \frac{N(r_{eq})}{\int_0^\infty N(r_{eq})\mathrm{d}r_{eq}} = \frac{N(r_{eq})}{N_T} \tag{2.4}$$

where $N(r_{eq})$ is the number of cells per unit volume of suspension with a volume equivalent radius between r_{eq} and r_{eq}+dr_{eq}. N_T is total cell concentration in suspension (in cells/m^3). A minimum of 500 cells were measured from each culture.

2.2.5 Transmission measurements

The normal-normal transmission measurements were performed using a UV-vis-NIR spectrophotometer (Agilent Cary 5000, Santa Clara, CA). The normal-hemispherical transmission measurements were performed using an integrating sphere attachment (Agilent Cary DRA-2500, Santa Clara, CA) to the same spectrophotometer. The microalgae were centrifuged at 13,400 rpm for 10 min and washed with phosphate buffer saline (PBS) solution and resuspended in PBS to avoid absorption and scattering by the growth medium. The

measurements were performed in 1 cm pathlength quartz cuvettes (110-10-40 Hellma Analytics, Müllheim, Germany) in the wavelength range from 350 to 750 nm. The microalgae suspensions were diluted to ensure that single scattering prevailed. The average mass absorption and mass scattering cross-sections of microalgae suspensions were measured for three biomass concentrations between 0.01 and 0.15 kg/m^3 to ensure that they were independent of microalgae concentration X. The cross-sections reported correspond to the mean of the three measurements.

2.2.6 Theoretical predictions for the coated sphere cell model

The radiation characteristics of microalgae were predicted theoretically based on the method developed by Dauchet et al. [Dauchet *et al.*(2015)]. The microorganisms were modeled as homogeneous spheres with an effective complex index of refraction $m_\lambda = n_\lambda + ik_\lambda$ where k_λ and n_λ were predicted by Equations (1.49) and (1.50), respectively. The anchor refraction index n_{820} used in Equation (1.50) was taken as either $n_{820} = 1.44$ or $n_{820} = 1.37$. The former was recommended for *C. reinhardtii* by Dauchet et al. [Dauchet *et al.*(2015)] and the latter corresponded to the refraction index at 750 nm reported by Lee et al. [Lee *et al.*(2013)] for *C. reinhardtii*. These anchor refraction indices were also used for *C. vulgaris* since they are both green microalgae and due to the lack of information available in the literature. The dry biomass density ρ_{dry} and the water fraction x_w of the cells were taken as 1400 kg/m^3 and 0.78 $\pm$0.02, respectively.

In addition, the *C. vulgaris* cells were modeled as coated spheres with an absorbing core of refraction and absorption indices $n_{c,\lambda}$ and $k_{c,\lambda}$ and a non-absorbing coating with refraction index $n_{coat,\lambda}$. Note that in order to conserve the mass of pigments in the cell while maintaining the same overall cell volume, the effective absorption index of the core must be adjusted when the cell pigments are packaged into the smaller volume of the coated sphere core. Then, the effective absorption index $k_{c,\lambda}$ of the core can be expressed as [Pottier *et al.*(2005)]

$$k_{c,\lambda} = \frac{\lambda}{4\pi} a_{cm,\lambda} \tag{2.5}$$

where $a_{cm,\lambda}$ is the effective absorption coefficient (in 1/m) of the substance contained within the cell walls of the microalgae expressed as

$$a_{cm,\lambda} = \sum_j E a_{j,\lambda} C_{j,c} \tag{2.6}$$

Here, $C_{j,c}$ is the pigment concentration in the core in kg of pigment per m^3. It can be expressed as $C_{j,c} = m_j / V_{core}$ where m_j is the average mass of pigment per cell (in kg/cell). The latter can be estimated by $m_j = C_j / N_T$ where C_j is the measured concentration of pigment j in the culture (in kg/m^3) and N_T is the cell number density in the culture (in cells/m^3). The latter can be related to the measured biomass concentration by [Pottier *et al.*(2005)]

$$N_T = \frac{X}{\rho_{dry}(1 - x_w) V_{cell}} \tag{2.7}$$

Thus, taking into account the fact that $w_j = C_j / X$, the core absorption index $k_{c,\lambda}$ can be expressed as

$$k_{c,\lambda} = \frac{\lambda}{4\pi} \sum_j E a_{j,\lambda} w_j \rho_{dry} (1 - x_w) \frac{V_{cell}}{V_{core}} = k_\lambda \frac{V_{cell}}{V_{core}} \tag{2.8}$$

Therefore, the absorption index k_λ of the homogeneous equivalent sphere must be scaled by the ratio of cell to core volumes in order to determine the absorption index $k_{c,\lambda}$ of the coated sphere core. Similarly, the refraction index $n_{c,\lambda}$ of the core was determined using Equation (1.50) by replacing k_λ with $k_{c,\lambda}$.

Geken et al. [Geken *et al.*(2013)] recently measured the cell wall thickness t_w of *C. vulgaris* to be 130 ± 20 nm. Moreover, Atkinson et al. [Atkinson *et al.*(1972)] reported that the cell wall of *C. vulgaris* is typically composed of sporopollenin whose refraction index is constant over the PAR region and equal to 1.48 [Traverse(2007)]. The Lorenz-Mie theory for coated spheres was used to predict the absorption $C_{abs,\lambda}$ and scattering $C_{sca,\lambda}$ cross-sections of the coated sphere based on its inner r_i and outer r_o radii, the core complex index of refraction $m_{c,\lambda} = n_{c,\lambda} + i k_{c,\lambda}$, and the shell refraction index n_{coat}. Finally, the size-averaged spectral mass absorption $\bar{A}_{abs,\lambda}$ and scattering $\bar{S}_{sca,\lambda}$ cross-sections of a suspension of a polydisperse microorganisms were estimated using Equations (1.45) and (1.46 by replacing r_{eq} with r_o. Here, the outer radius distribution of the coated sphere was assumed to be equal

to the volume-equivalent radius of the homogeneous sphere r_{eq}. Then, the inner radius was estimated as $r_i = r_{eq}(1 - t_w/\bar{r}_{eq})$ where the mean equivalent radius $\bar{r}_{eq}$ of *C. vulgaris* was reported as 1.89 μm [Souliés *et al.*(2013)]. Note that dry biomass density ρ_{dry} of the coated spheres was assumed to be identical to that of the homogeneous cell and equal to 1400 kg/m^3.

The theoretical predictions of the radiation characteristics of homogeneous or coated sphere microorganisms were implemented in Matlab® and the code was validated against results reported in Ref. [Dauchet *et al.*(2015)] for *C. reinhardtii* treated as homogeneous volume-equivalent spheres.

2.3 Results and Discussion

2.3.1 Size distribution and pigment concentrations

Table 2.1 summarizes the mean equivalent radius $\bar{r}_{eq}$ of the cells and the associated standard deviation, the Chl *a*, Chl *b*, PPC, and PSC concentrations of *C. reinhardtii* grown under optimal or nitrogen-limited conditions and of *C. vulgaris* grown under optimal conditions. These values were used to predict the radiation characteristics of the microalgae for each growth condition. Moreover, *C. reinhardtii* featured significantly smaller pigment concentrations when they were grown in nitrogen-limited conditions than in optimal conditions. This observation has been made previously for various microorganisms and was attributed to reduction in photosynthetic antenna size as a protection mechanism against oxidative light stress [Pruvost *et al.*(2009), Kandilian *et al.*(2013), Kandilian *et al.*(2014b)]. Lastly, *C. vulgaris* grown under optimal conditions featured the largest pigment concentration of the three cultures examined.

Figures 2.1a to 2.1c show histograms of the volume-equivalent radius frequency distribution $f(r_{eq})$ of *C. reinhardtii* grown in optimal and in nitrogen-limited conditions and *C. vulgaris* grown in optimal conditions. Furthermore, Figure 2.1d shows the histogram of the inner r_i and outer r_o radii of *C. vulgaris* modeled as coated spheres to represent their rigid cell wall.

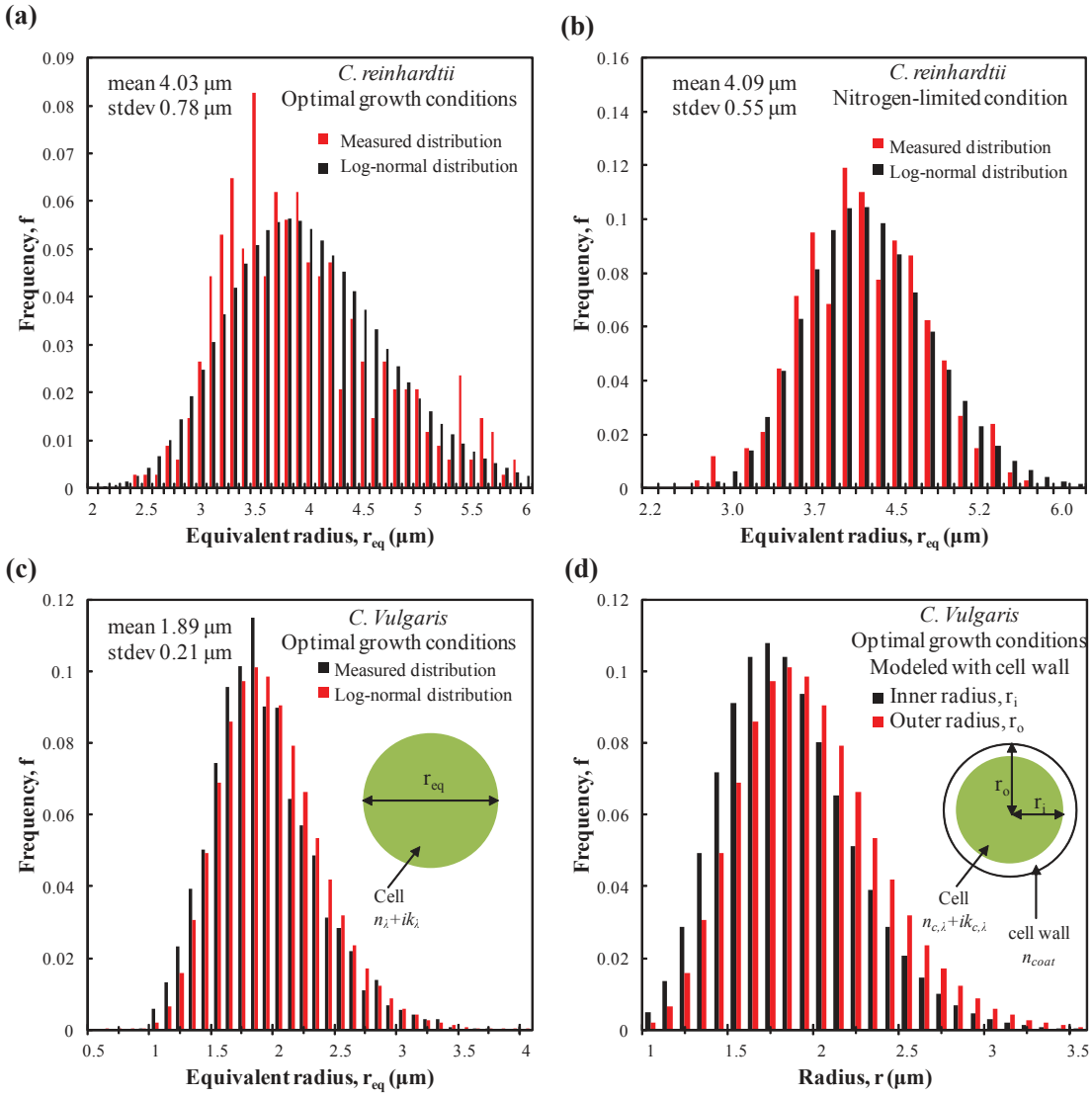

Figure 2.1: Measured volume-equivalent radius distribution $f(r_{eq})$ of (a) *C. reinhardtii* grown in optimal conditions, (b) *C. reinhardtii* grown in nitrogen-limited conditions, (c) *C. vulgaris* modeled as homogeneous spheres, and (d) the inner r_i and outer r_o radius distribution of *C. vulgaris* modeled as coated spheres.

Table 2.1: The mean equivalent radius $\bar{r}_{eq}$ of the cells, and the chl *a*, chl *b*, PPC, and PSC concentrations used to predict the radiation characteristics of *C. reinhardtii* grown under optimal or nitrogen-limited conditions and *C. vulgaris* grown under optimal conditions.

Species	Growth conditions	$\bar{r}_{eq}$ (μm)	Chl *a* (wt.%)	Chl *b* (wt.%)	PPC (wt.%)	PSC (wt.%)
C. reinhardtii	optimal	4.03 ± 0.78	3.2 ±0.3	1.21 ±0.1	0.92 ±0.09	0.15 ±0.01
C. reinhardtii	N-limited	4.09 ± 0.55	0.17 ±0.01	0.07 ±0.003	0.12 ±0.005	0.02 ±0.001
C. vulgaris	optimal	1.89 ±0.21	3.82 ±0.06	1.14 ±0.03	0.85 ±0.02	0.14 ±0.003

The mean volume-equivalent radius r_{eq} of *C. reinhardtii* cells grown in optimal and nitrogen-limited conditions were nearly identical and measured as 4.03 μm and 4.09 μm, respectively. This is consistent with the volume-equivalent radius of 3.93 μm reported by Dauchet et al. [Dauchet *et al.*(2015)] for *C. reinhardtii* grown in optimal conditions. Similarly, Berberoğlu et al. [Berberoğlu *et al.*(2008)] reported the surface area equivalent radius of *C. reinhardtii* as 4.03 μm. The difference between these reported mean radii were smaller than 2.5% and may be due to small differences in the size of the microorganisms due to the cultivation conditions. It may also be due to experimental uncertainty and/or differences in the experimental and analytical tools used.

On the other hand, *C. vulgaris* cells had a mean equivalent radius of 1.89 μm. Finally, the coated sphere *C. vulgaris* featured outer radius r_o distribution equal to the volume-equivalent homogeneous sphere radius r_{eq} distribution.

2.3.2 Scattering phase function

Figures 2.2a to 2.2c compare the experimentally measured and theoretically predicted total scattering phase function $\Phi_{T,633}(\Theta)$ at 633 nm of (a) *C. reinhardtii* grown in optimal and (b) in nitrogen-limited conditions and of (c) *C. vulgaris* grown in optimal conditions. In all cases, scattering was mostly in the forward direction. This was expected as the cells

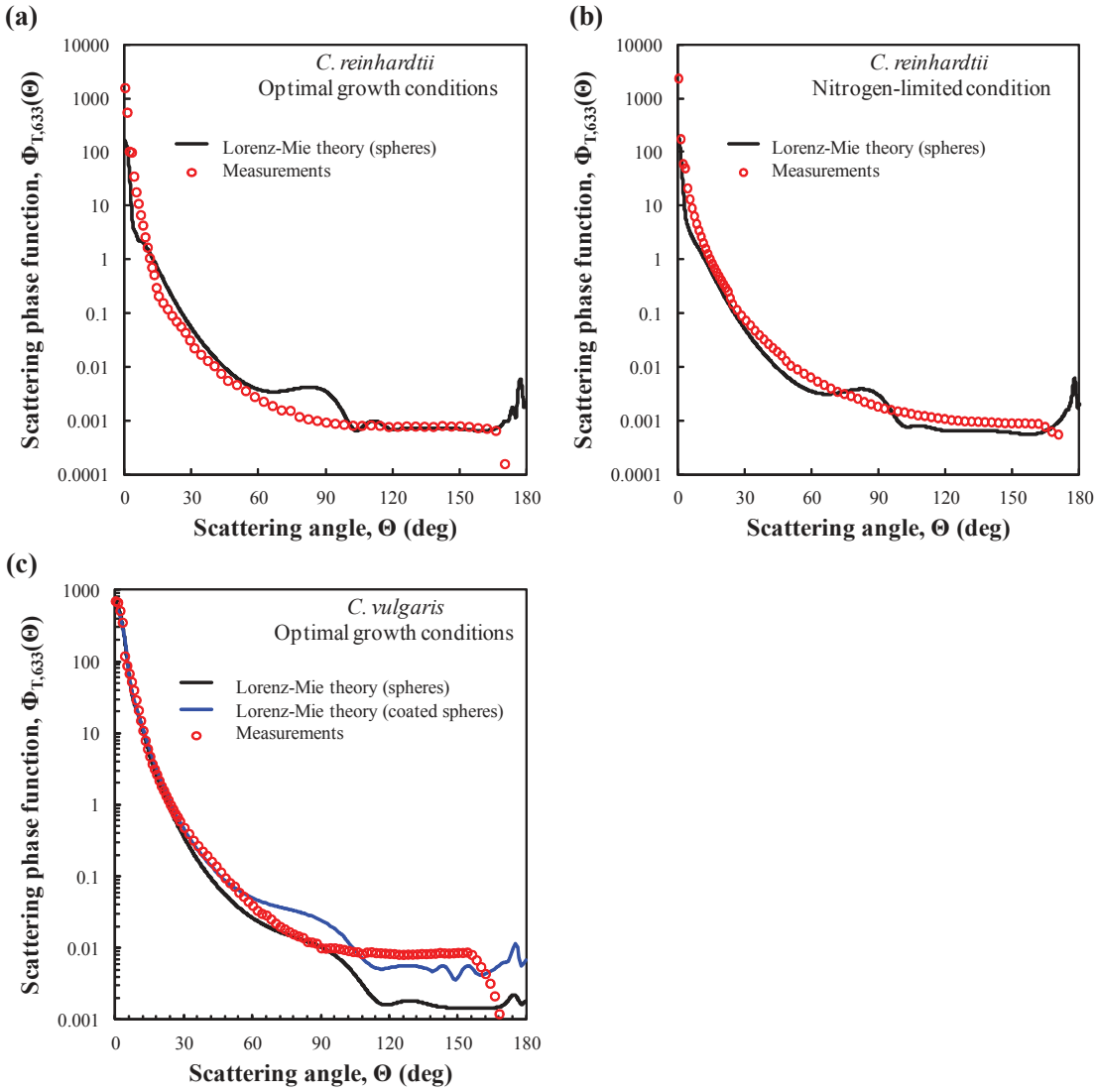

Figure 2.2: Measured and predicted total scattering phase function $\Phi_{T,633}(\Theta)$ at 633 nm for *C. reinhardtii* culture (a) grown in optimal conditions, (b) grown in nitrogen-limited conditions, and (c) *C. vulgaris* culture grown in optimal conditions.

were much larger than the wavelength of light in the PAR region. Indeed, the measured asymmetry factor g_{633} of *C. reinhardtii* grown in optimal or nitrogen-limited conditions was equal to 0.98 while that of *C. vulgaris* was 0.974. On the other hand, the theoretically predicted asymmetry factor g_{633} was estimated as 0.98, 0.962, and 0.982, respectively. The relatively good agreement between the measured and predicted asymmetry factors confirmed the accuracy of the measured size distribution of the microorganisms and their complex index of refraction. Similarly, the measured backward scattering ratio b_{633} of *C. reinhardtii* grown in optimal and nitrogen-limited conditions and *C. vulgaris* was 0.008, 0.008, and 0.004, respectively. The corresponding predicted backward scattering ratio b_{633} was 0.006, 0.007, and 0.002, respectively.

The scattering phase function predicted for *C. vulgaris*, modeled as a coated sphere, was similar to that for a solid sphere. However, it had a 13% smaller $\Phi_{T,633}(0)$ than its corresponding solid sphere and an asymmetry factor of 0.972. This may be due to an increase in backward scattering of the coated sphere compared to the solid sphere due to the mismatch in the refraction index between the medium, the coating and the core. Indeed, the predicted backward scattering ratio b_{633} of the coated sphere was two times larger than that of the homogeneous spherical cells and equal to the measured backward scattering ratio, i.e., b_{633}=0.004.

Finally, the correction factor ϵ_n used for correcting the measured scattering cross-section of the microorganisms was determined according to Equation (1.39) as 0.67 and 0.72 for *C. reinhardtii* grown in optimal conditions and in nitrogen-limited conditions, respectively, and 0.71 for *C. vulgaris* grown in optimal conditions.

2.3.3 Absorption and scattering cross-sections

2.3.3.1 *C. reinhardtii* grown in optimal conditions

Figures 2.3a and 2.3b compare the experimentally measured and the theoretically predicted size-averaged spectral mass absorption $\bar{A}_{abs,\lambda}$ and scattering $\bar{S}_{sca,\lambda}$ cross-sections and their

respective 95% confidence intervals for *C. reinhardtii* cultures grown in optimal conditions.

Estimations of the absorption cross-section by either method were in good agreement. In fact, the relative difference was well within the uncertainty range of either method. The error bars in the theoretical predictions of the absorption cross-section were due to uncertainties in the measurements of the culture pigment and biomass concentrations and of the cell water mass fraction. The relative difference in $\bar{A}_{abs,\lambda}$ between the two methods averaged over the PAR region was 8%. In addition, the relative difference between the two methods for $\bar{A}_{abs,440}$ and $\bar{A}_{abs,670}$, respectively corresponding to Chl *b* and Chl *a* absorption peaks, was smaller than 12%. Note that the choice of anchor refraction index did not have a large influence on the theoretical predictions of spectral absorption cross-section.

By contrast, the choice of anchor index of refraction n_{820} had a large impact on the magnitude and shape of the spectral mass scattering cross-section $\bar{S}_{sca,\lambda}$. Moreover, there was a significant difference in the average mass scattering cross-section predicted by the two methods. The PAR-averaged relative difference between the measured and predicted $\bar{S}_{sca,\lambda}$ was 33% when the anchor refraction index n_{820} was set to 1.44. However, it diminished to 13% when the anchor refraction index n_{820} was set to 1.37. Therefore, care must be taken to ensure that the proper anchor refraction index is used to predict the radiation characteristics of the microalgae. However, the lack of information in the literature about the refraction index of different microalgae species and strains may be a potential limitation of the theoretical method.

2.3.3.2 *C. reinhardtii* grown in nitrogen-limited conditions

Figures 2.4a and 2.4b plot the experimentally measured and the theoretically predicted size-averaged spectral mass absorption $\bar{A}_{abs,\lambda}$ and scattering $\bar{S}_{sca,\lambda}$ cross-sections and their respective 95% confidence intervals for *C. reinhardtii* cultures grown in nitrogen-limited conditions.

The average mass absorption cross-section $\bar{A}_{abs,\lambda}$ of the nitrogen-limited *C. reinhardtii*

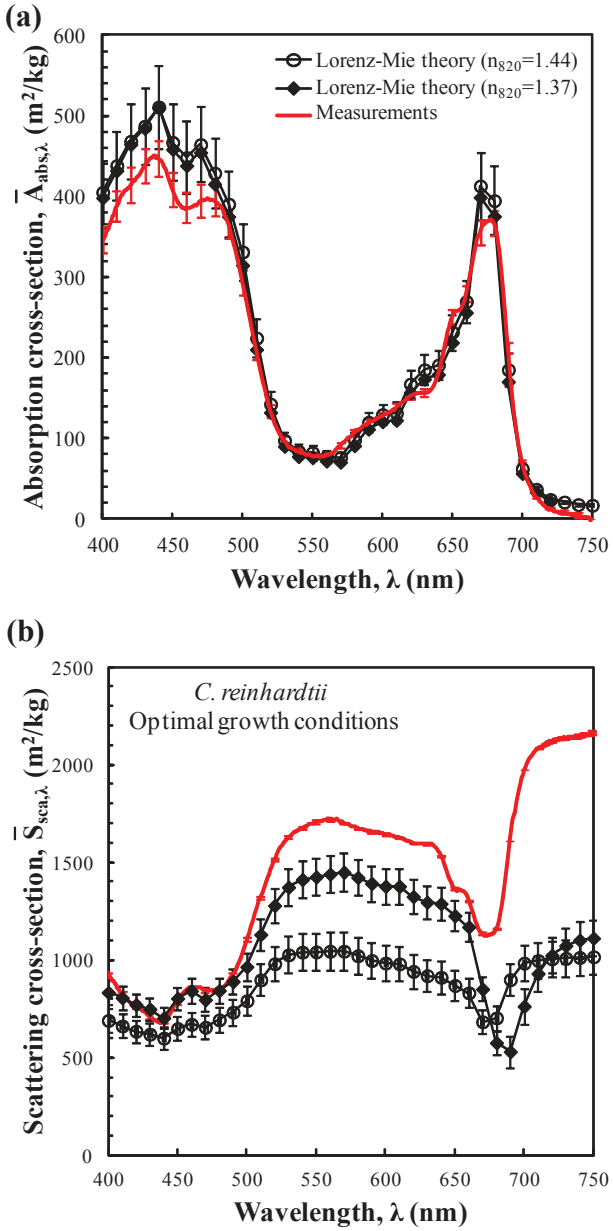

Figure 2.3: Comparison between measured and predicted size-averaged spectral mass (a) absorption $\bar{A}_{abs,\lambda}$ and (b) scattering $\bar{S}_{sca,\lambda}$ cross-sections of *C. reinhardtii* grown in optimal conditions.

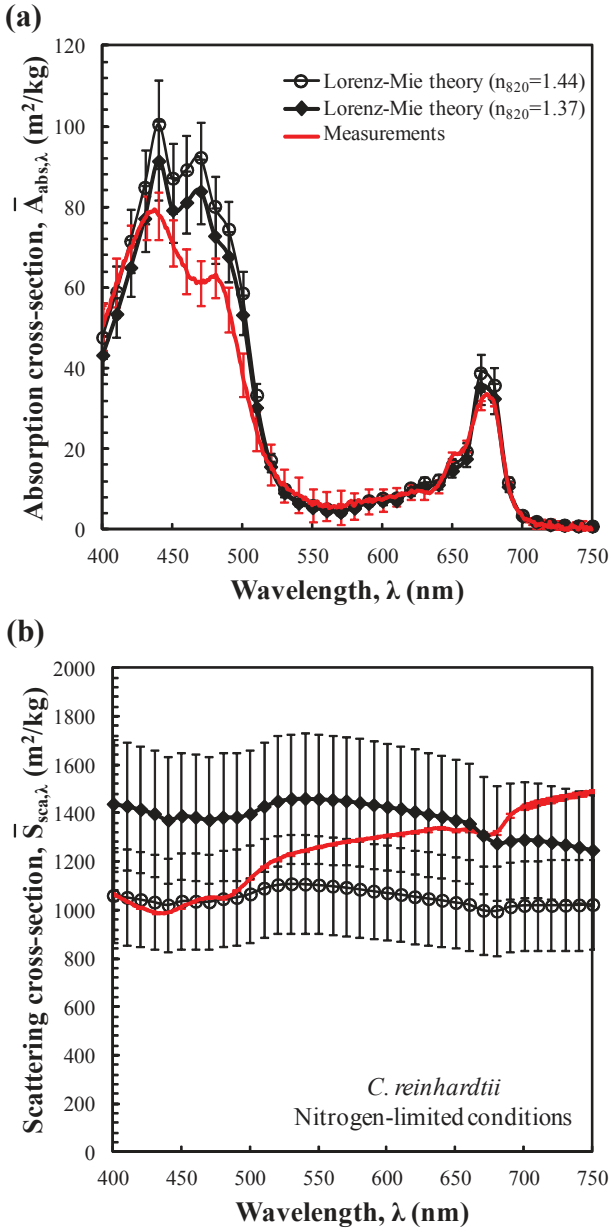

Figure 2.4: Comparison between measured and predicted size-averaged spectral mass (a) absorption $\bar{A}_{abs,\lambda}$ and (b) scattering $\bar{S}_{sca,\lambda}$ cross-sections of *C. reinhardtii* grown in nitrogen–limited conditions.

cells were much smaller than that for cells grown under optimal conditions (Figure 2.3a) due to their lower pigment concentrations (Table 2.1). The predicted size-averaged spectral mass absorption cross-section $\bar{A}_{abs,\lambda}$ agreed well with the measurements with a PAR-averaged relative difference of 16% and 15% when the anchor refraction index n_{820} was 1.44 and 1.37, respectively. However, the relative difference between the measured and predicted $\bar{A}_{abs,\lambda}$ reached up to 53% between 450 nm and 550 nm. Photosynthetic and photoprotective carotenoid pigments are responsible for absorption in this wavelength range. The differences in $\bar{A}_{abs,\lambda}$ between the two methods may be due to inaccuracies in the measured carotenoid pigment concentration and/or in the spectral specific absorption cross-sections Ea_{PPC} or Ea_{PSC} of the carotenoid pigments used to predict the cell effective absorption index [Equation (1.49)]. This phenomenon was more apparent in the nitrogen-limited *C. reinhardtii* culture as the cell carotenoid to chlorophyll ratio was nearly four times larger than in cells grown under optimal conditions. We speculate that the spectral specific absorption cross-sections of carotenoids, $Ea_{PPC,\lambda}$ and $Ea_{PSC,\lambda}$ may not be valid or general for all microorganisms. Indeed, the $Ea_{PPC,\lambda}$ and $Ea_{PSC,\lambda}$, used in the predictive method, correspond to β-carotene and fucoxanthin, respectively. However, Krinsky and Levine [Krinsky and Levine(1964)] reported the major carotenoids in *C. reinhardtii* as β-carotene, violaxnthin, lutein, and neoxanthin. These carotenoid pigments have different specific absorption cross-sections whose *in-vivo* values have not been measured or reported in the literature [Rodriguez-Amaya(2001)]. Moreover, the types of carotenoids in the cells change in response to nutrient limitation [Francis *et al.*(1975)]. Therefore, representing all of the photoprotective or photosynthetic carotenoids with a single absorption spectrum may be practical but may introduce inaccuracies in the predictions of cell absorption cross-sections $\bar{A}_{abs,\lambda}$, especially when the carotenoids become the dominant pigments in the cells such as in nitrogen-limited cultures.

The PAR-averaged relative difference between the measured and the predicted scattering cross-section $\bar{S}_{sca,\lambda}$ was 23% and 12% when the anchor refraction index n_{820} was set to 1.37 and 1.44, respectively. This indicates that for nitrogen-limited *C. reinhardtii* cells, the appropriate anchor refraction index may be 1.44 compared to 1.37 for *C. reinhardtii* grown

under optimal conditions. This suggests that the refraction index of the cells can vary with cultivation conditions as a result of changes in the biochemical composition of the cells. Therefore, the anchor refraction index must be known for each species as well as for every operating condition.

2.3.3.3 *C. vulgaris* grown in optimal conditions

Figures 2.5a and 2.5b show the experimentally measured and the theoretically predicted size-averaged spectral mass absorption $\bar{A}_{abs,\lambda}$ and scattering $S_{sca,\lambda}$ cross-sections and their respective 95% confidence intervals for *C. vulgaris* cultures grown in optimal conditions.

The measured size-averaged spectral mass absorption cross-section $\bar{A}_{abs,\lambda}$ of the *C. vulgaris* cells did not agree well with the Lorenz-Mie theory predictions when treating the cells as homogeneous spheres regardless of the anchor point selected. For example, the measured and predicted spectral mass absorption cross-sections of *C. vulgaris* at 430 nm, corresponding to one of Chl *a* peaks, were 580±15 m^2/kg and 840±100 m^2/kg, respectively. This 43% difference corresponded to the largest relative difference in $\bar{A}_{abs,\lambda}$ between the experimental and theoretical methods. In addition, the PAR-averaged relative difference in $\bar{A}_{abs,\lambda}$ was equal to 22%. Moreover, the relative difference in spectral mass scattering cross-section estimated by the two methods was 13% and 49% when the anchor index of refraction was 1.44 and 1.37, respectively. The relatively large deviation in both $\bar{A}_{abs,\lambda}$ and $\bar{S}_{sca,\lambda}$ could not be attributed to uncertainties in the pigment and biomass concentrations or in the cell water content x_w. However, the difference may be due to the presence of a rigid 130 nm thick sporolinelin wall surrounding the cells [Geken *et al.*(2013)] rendering the treatment of *C. vulgaris* as homogeneous spheres invalid.

Alternatively, *C. vulgaris* cells were modeled as coated spheres with an outer radius r_o identical to that of the homogeneous sphere r_{eq} (Figure 2.1d). As previously stated, the coating was assumed to be non-absorbing with a refraction index n_{coat} equal to 1.48 [Atkinson *et al.*(1972)]. Figure 2.5 indicates that both the predicted spectral mass absorption $\bar{A}_{abs,\lambda}$

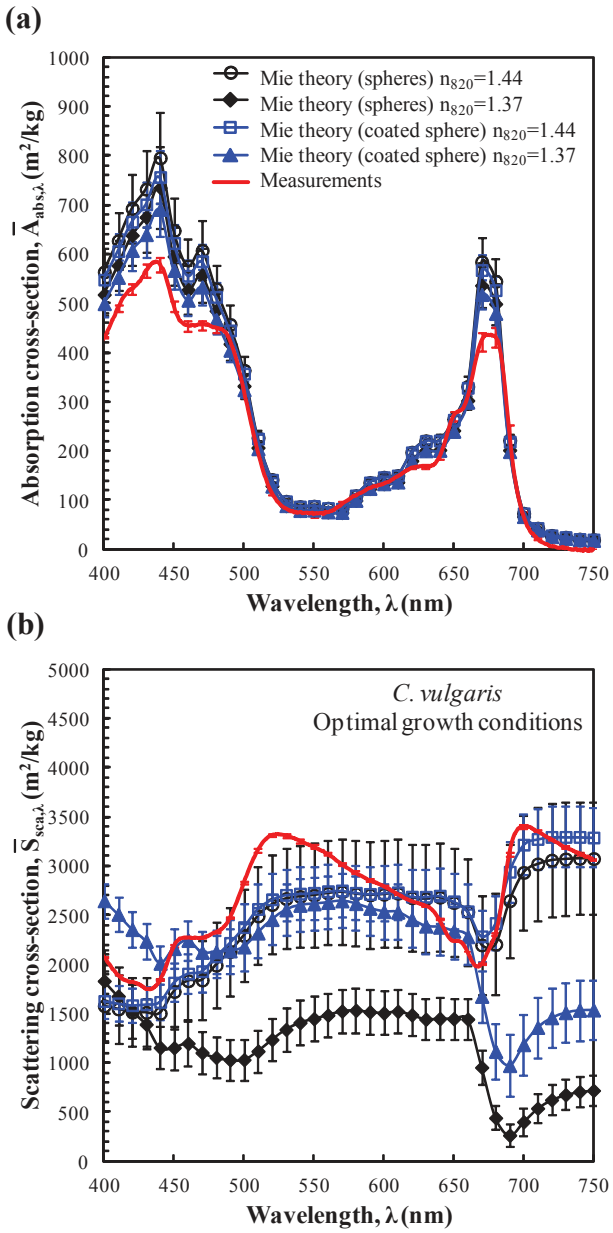

Figure 2.5: Comparison between the measured and predicted size-averaged spectral mass (a) absorption $\bar{A}_{abs,\lambda}$ and (b) scattering $\bar{S}_{sca,\lambda}$ cross-sections of *C. vulgaris* grown in optimal conditions.

and scattering $\bar{S}_{sca,\lambda}$ cross-sections considering *C. vulgaris* as coated spheres agreed well with experimental measurements. First, the PAR-averaged relative differences between the experimental and theoretical absorption cross-sections was 17% and 10% when the anchor refraction index was 1.44 and 1.37, respectively. It is interesting to note that $\bar{A}_{abs,\lambda}$ was smaller across the PAR region when treating the cells as coated spheres instead of homogeneous spheres for the same mass of pigments. This can be attributed to the package effect [Jonasz and Fournier(2007)].

Moreover, the PAR-averaged relative difference between the two methods was 11% and 19% when the anchor refraction index n_{820} was 1.44 and 1.37, respectively. Finally, the results illustrate that some microorganisms cannot be modeled as homogeneous spheres and their cell wall must be taken into account in predicting their radiation characteristics. Further studies should investigate the conditions under which microalgae cells can be treated as homogeneous spheres. In this context, determining the cell wall thickness and the cell optical properties is essential and currently lacking. Finally, it remains unclear if the chloroplast encasing the absorbing pigments needs to modeled as a separate entity inside the cell.

2.3.4 Normal-hemispherical transmittance

Figures 2.6a to 2.6b compare the measured and predicted normal-hemispherical transmittance $T_{nh,\lambda}$ spectra of *C. reinhardtii* grown in (a) optimal (X= 0.11 kg/m^3) and (b) nitrogen-limited (X=0.17 kg/m^3) conditions. Here, the cells were modeled as polydisperse homogeneous spheres with anchor refraction index $n_{820} = 1.44$ or 1.37. Similarly, Figure 2.6c and 2.6d compare the measured normal-hemispherical transmittance of *C. vulgaris* grown in optimal conditions (X=0.56 kg/m^3) and modeled as (c) homogeneous spheres and (d) coated spheres representing the rigid cell wall with anchor refraction index $n_{820} = 1.44$ or 1.37. The normal-hemispherical transmittance $T_{nh,\lambda}$ was predicted using the modified two-flux approximation [Equation (1.17)] employing either the experimentally measured or the theoretically predicted radiation characteristics. Similar comparison was performed by Dauchet et al. [Dauchet *et al.*(2015)] to validate the predictions of the radiation characteristics

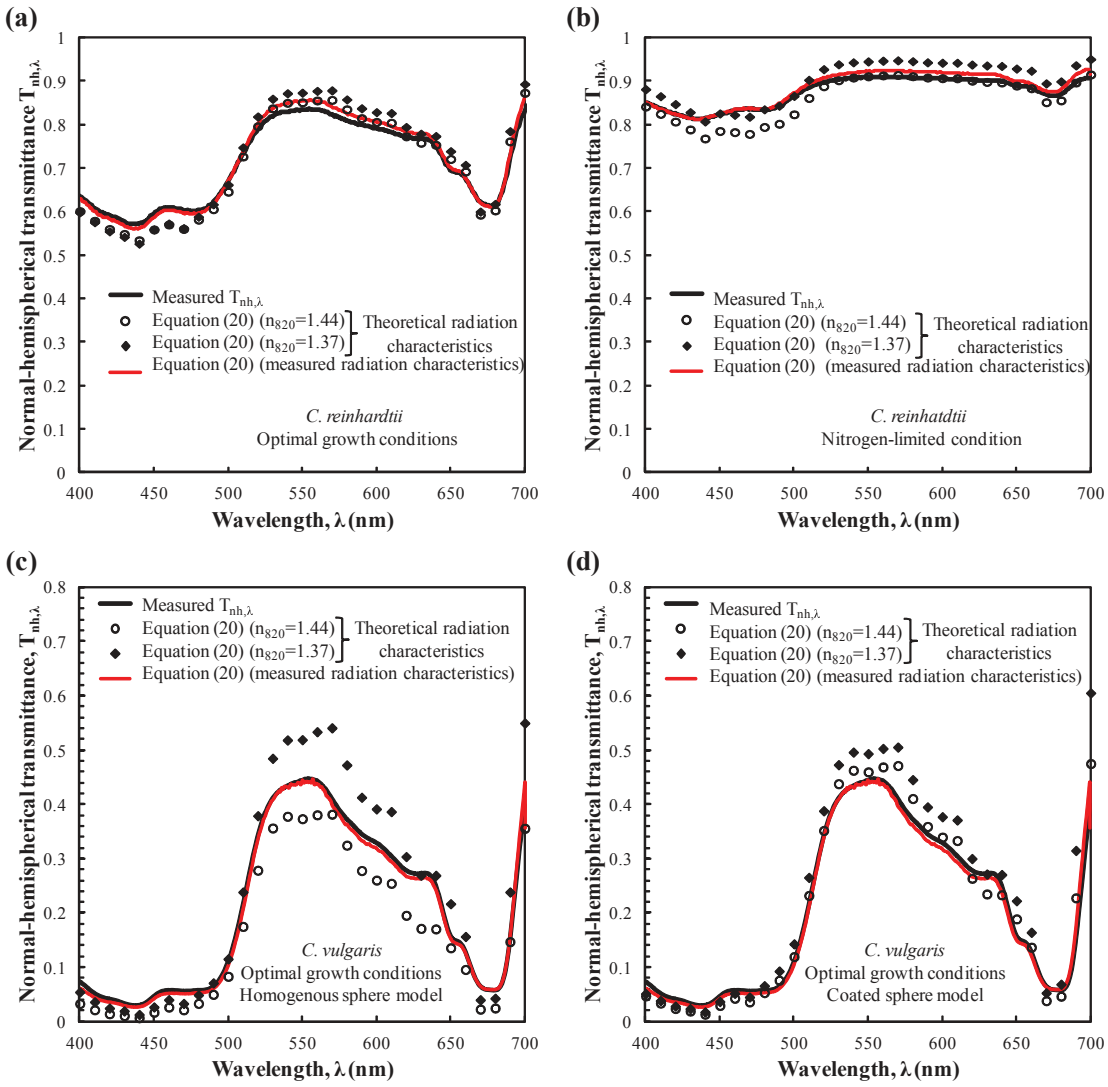

Figure 2.6: Comparison of the measured and predicted normal-hemispherical transmittance $T_{nh,\lambda}$ of concentrated samples of (a) *C. reinhardtii* grown in optimal conditions $X = 0.11$ kg/m^3, (b) *C. reinhardtii* grown in nitrogen-limited conditions $X = 0.17$ kg/m^3, and *C. vulgaris* grown in optimal conditions $X = 0.56$ kg/m^3 using predicted radiation characteristics for (c) homogeneous sphere and (d) coated sphere.

of *C. reinhardtii*.

For all three cultures, excellent agreement was found between the experimentally measured normal-hemispherical transmittance $T_{nh,\lambda}$ and the predictions using the measured radiation characteristics with a relative error, over the PAR region, smaller than 5%. This indicates that the modified two-flux approximation [Equation (1.17)] is an adequate model to predict the normal-hemispherical transmittance $T_{nh,\lambda}$ when paired with the measured radiation characteristics of the microalgae. Note that the measurements of $T_{nh,\lambda}$ shown in Figures 2.6a to 2.6d were not used for the determination of $\bar{A}_{abs,\lambda}$ or $\bar{S}_{sca,\lambda}$.

The PAR-averaged relative error between the measured and the predicted $T_{nh,\lambda}$ using the theoretical radiation characteristics of *C. reinhardtii* grown in optimal conditions or in nitrogen-limited conditions was less than 7.5%. The choice of anchor refraction index had no significant influence on the predictions of $T_{nh,\lambda}$. As previously discussed, the anchor refraction index had a significant impact on the prediction of the scattering cross-section $\bar{S}_{sca,\lambda}$ of the cells. However, the latter did not have a measurable impact on the normal-hemispherical transmittance of the sample. This was due to the fact that (i) the microorganisms had a large asymmetry factor such that $\bar{A}_{abs,\lambda} >> (1 - g_\lambda)\bar{S}_{sca,\lambda}$ and (ii) the scattered radiation was collected by the integrating sphere in measuring $T_{nh,\lambda}$. In fact, such measurements are used to estimate the absorption coefficient of the microalgae suspension κ_λ [Equation(1.37)]. As a consequence, the validation performed by Dauchet et al. [Dauchet *et al.*(2015)] and replicated here can only "validate" the cells' absorption cross-section but not their scattering cross-section.

Lastly, $T_{nh,\lambda}$ predicted by Equation (1.17) using the theoretical radiation characteristics predicted by the Lorenz-Mie theory for *C. vulgaris* treated as homogeneous spheres or as coated spheres featured relative error of 20% and 15%, respectively. The results indicate that the coated sphere is a better representation of the *C. vulgaris* cell compared to a homogeneous sphere. Here again, the anchor refraction index had a negligible effect on the PAR-averaged relative error in $T_{nh,\lambda}$.

2.3.5 Fluence rate and the local rate of photon absorption

Figures 2.7a to 2.7f show the PAR-averaged fluence rate $G_{PAR}(z)$ and local rate of photon absorption (LRPA) $\mathscr{A}(z)$ in the PBR, for all three cultures, estimated using Equations (1.10) and (1.26), respectively. Predictions were made using either the measured or the theoretical radiation characteristics using anchor refraction index n_{820} equal to 1.44 or 1.37.

The *C. reinhardtii* culture grown in optimal conditions achieved a steady-state biomass concentration X of 0.35 kg/m^3. At this concentration, the use of measured or theoretical radiation characteristics produced nearly identical predictions for fluence rate $G_{PAR}(z)$ and LRPA $\mathscr{A}(z)$ with a relative difference of less than 10% regardless of anchor refraction index. For practical purposes, this difference is negligible and both experimental and theoretical predictions are essentially equivalent.

Moreover, the *C. reinhardtii* culture grown in nitrogen-limited conditions had a steady-state biomass concentration X equal to 0.87 kg/m^3. For this concentration, the fluence rate $G_{PAR}(z)$ estimated with the measured or the theoretical radiation characteristics had a relative difference of less than 4% regardless of the anchor refraction index n_{820} used. On the other hand, the PAR-averaged relative difference in LRPA estimated using the measured and theoretical radiation characteristics was 16% or 23% when anchor point refraction index was 1.44 or 1.37, respectively. These large differences may be due to the overestimation in absorption cross-section between 450 nm and 500 nm, as previously discussed.

Finally, *C. vulgaris* cells grown in optimal conditions had a steady-state biomass concentration X equal to 2.11 kg/m^3. Here, $G_{PAR}(z)$ and the LRPA $\mathscr{A}(z)$ estimated using the measured radiation characteristics matched closely with those estimated using the predicted radiation characteristics for the coated spheres with anchor point refraction index $n_{820} = 1.44$.

2.4 Conclusion

This study compared a direct experimental method and a theoretical method for estimating the radiation characteristics of microalgae. The theoretical method was based on the

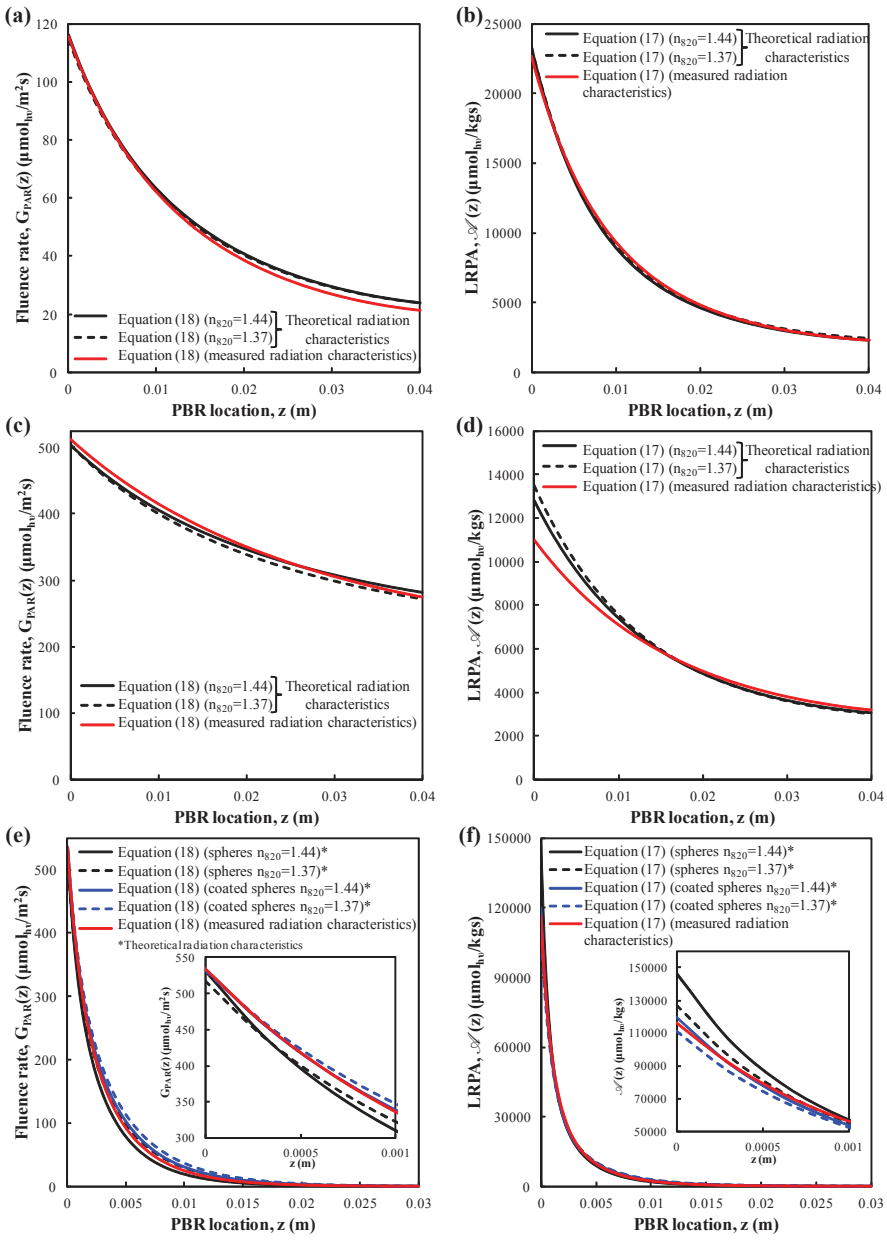

Figure 2.7: PAR-averaged fluence rate $G_{PAR}(z)$ and local rate of photon absorption LRPA $\mathscr{A}(z)$ in the PBRs predicted by Equations (1.10) and (1.26) for (a-b) *C. reinhardtii* in optimal conditions, (c-d) *C. reinhardtii* in nitrogen-limited conditions, and (e-f) *C. vulgaris* in optimal conditions using measured and theoretically predicted radiation characteristics.

Lorenz-Mie theory combined with a model for the effective complex index of refraction of the microalgae cells. Good agreement was found between the two methods for predicting the absorption and scattering cross-sections and the scattering phase function of *C. reinhardtii* grown in optimal or in nitrogen-limited conditions. The measured absorption cross-section of *C. vulgaris* grown in optimal conditions did not agree with theoretical predictions treating the cells as homogeneous spheres. In fact, these cells are known to have a thick wall made of sporolinelin [Geken *et al.*(2013)]. Modeling *C. vulgaris* cells as coated spheres with a non-absorbing outer shell, representing the cell wall, resulted in absorption and scattering cross-sections that fell within 15% of experimental measurements over the PAR region.

Measurements of normal-hemispherical transmittance of high concentration samples were compared to predictions by the modified two-flux approximation combined with experimentally measured or theoretically predicted radiation characteristics of *C. reinhardtii* modeled as homogeneous sphere, or *C. vulgaris* modeled as a coated sphere. The normal-hemispherical transmittance were found to be strongly dependent on the absorption cross-section of the cells and not on their scattering cross-section due to their large asymmetry factor.

Finally, the fluence rate and the local rate of photon absorption (LRPA) were estimated using the measured or the theoretical radiation characteristics. For practical purposes there was no difference in the fluence rate or the LRPA estimated using the radiation characteristics determined by either method.

CHAPTER 3

Simple Method to Measure the Spectral Absorption Cross-Section of Microalgae

abstract

The spectral absorption cross-section of microalgae is an essential parameter in modeling the microalgae metabolism and growth kinetics as well as in estimating the productivity and efficiency of photobioreactors. This chapter presents a simple experimental procedure for retrieving the average spectral absorption cross-section of concentrated microalgal suspensions featuring single or multiple scattering. The method combines experimental measurements of the normal-hemispherical transmittance and reflectance of the suspensions in conventional cuvettes with an inverse method based on genetic algorithm and analytical expressions obtained from the modified two-flux approximation. The method was validated with direct measurements of the scattering phase function and of the absorption and scattering cross-sections of freshwater microalgae *Chlorella vulgaris*. It was able to retrieve the absorption cross section with acceptable accuracy. The retrieved absorption cross-section was used to estimate successfully the fluence rate and the mean volumetric rate of photon absorption in flat plate PBRs.

3.1 Introduction

Physical modeling coupling light transfer to growth kinetics and metabolic activities can facilitate the optimum design, operation, and control of photobioreactors [Cornet *et al.*(1992a), Cornet *et al.*(1992b),Cornet *et al.*(1995),Cornet and Dussap(2009),Murphy and Berberoğlu(2011), Pilon *et al.*(2011), Takache *et al.*(2010), Takache *et al.*(2012), Pruvost and Cornet(2012), Wheaton and Krishnamoorthy(2012), Kandilian *et al.*(2014a), Kong and Vigil(2014)]. To do so, knowing the amount of light absorbed by the microalgae and driving the photosynthesis is essential. The goal of the study presented in this Chapter was to develop a simple yet accurate methodology for determining the spectral absorption cross-section of microalgae over the photosynthetically active radiation (PAR) region. *C. vulgaris* was used to illustrate the new method and for the wide range of applications.

3.2 Background

This Chapter presents a simple method for measuring the spectral absorption cross-section $C_{abs,\lambda}$ or $A_{abs,\lambda}$ from simple and rapid measurements of normal-hemispherical transmittance and reflectance of relatively concentrated suspensions in conventional cuvettes. In fact, we have argued that the absorption cross-section is sufficient to predict the local fluence rate $G_\lambda(z)$, the average growth rate $\langle\mu\rangle$, and the MRPA $\langle\mathscr{A}\rangle$.

3.3 Materials and Methods

3.3.1 Microalgae cultivation and sample preparation

The microalgae *Chlorella vulgaris* CCAP 221/19 were obtained from the culture collection of algae and protozoa (CCAP, Scotland, UK). The microorganisms were cultivated in a 4 cm thick, 1.4 L torus PBR constructed with transparent PMMA described in detail in Ref. [Pottier *et al.*(2005)]. The PBR was illuminated with 200 $\mu\text{mol}_{h\nu}/\text{m}^2\text{s}$ white LEDs incident on one side. It was operated in continuous mode by injection of fresh medium

at the dilution rate of 0.06 h^{-1} using a peristaltic pump. The microlgae were grown in modified Sueoka medium with the following composition (in mM) : NH_4Cl 27.1, $MgSO_4$-$7H_2O$ 1.14, $CaCl_2$ 0.45, KH_2PO_4 4.48, $NaHCO_3$ 20, $ZnSO_4$-$7H_2O$ 0.077, H_3BO_3 0.184, $MnCl_2$-$4H_2O$ 0.026, $CoCl_2$-$6H_2O$ 0.0067, $CuSO_4$-$5H_2O$ 0.0063, $FeSO_4$-$7H_2O$ 0.018, $(NH_4)_6Mo_7O_{24}$-$4H_2O$ 0.0009. KOH 0.89, Na_2EDTA 0.054. The culture temperature was maintained at 22^{o}C thanks to a liquid cooled heat exchanger attached to the stainless steel PBR back wall. The pH was continuously monitored using a pH sensor (Mettler Toledo SG 3253). It was maintained at 7.5 by injecting CO_2 gas when the culture medium pH exceeded 7.5. Agitation of the culture was achieved by mechanically mixing the culture using a marine propeller attached to an electric motor. The culture under steady-state continuous operation had dry biomass concentration X of 0.33 g/L. To obtain samples with larger biomass concentrations, a small volume of culture was harvested and centrifuged at 10,000g (ThermoScientific Sorvall RC 6 Plus, Massachusetts, USA) for 5 min at 4^{o}C and suspended in 3 ml of PBS. The volume of culture sampled was chosen based on the biomass concentration desired for optical measurements and ranged from 0.035 to 111.13 g/L.

3.3.2 Culture characterization

The cell size distribution of *Chlorella vulgaris* was measured using 165 microscope images captured using a digital camera (AxioCam MRc) mounted on an optical microscope (Zeiss Axio Scope A1). The diameters of 2873 cells, assumed to be spherical, were measured manually using an image processing software (Axio Vision Routine).

The culture dry biomass concentration X (in g/L) was determined gravimetrically by filtering 5 mL of culture through a pre-dried and pre-weighed 0.45 μm pore size glass-fiber filter (Whatman GF/F). The filters were dried overnight in an oven at 105^{o}C and weighed after being cooled in a desiccator for 10 min. The samples were analyzed in triplicates and the reported biomass concentration corresponded to the mean value. In addition, the cell density N_T (in $\#/m^3$) was counted using a 200 μm deep Malassez counting chamber.

The volume fraction of water in the cells x_w was estimated using the relation suggested by Pottier et al. [Pottier *et al.*(2005)] and given by

$$x_w = 1 - \frac{X}{N_T}\frac{1}{V_{32}\rho_{dm}} \tag{3.1}$$

where V_{32} is the cell volume corresponding to the Sauter mean diameter of the microorganism while ρ_{dm} corresponds to the density of dry biomass and was taken as 1350 kg/m^3 [Dauchet *et al.*(2015)].

The concentration of photosynthetic pigments in *Chlorella vulgaris* grown under the above mentioned conditions were estimated spectrometrically in terms of mass of pigments per unit volume of suspension (mg/m^3). A volume of 0.5 mL of culture was first centrifuged at 13,400 rpm (12,100g) for 10 min. The medium was discarded and the cells were resuspended in 1.25 mL pure methanol and sonnicated for 10 s. Pigments were extracted for 1 h at 45^{o}C and the extract was centrifuged. The optical density OD_λ of the supernatant was measured at wavelengths 750, 665, 652, and 480 nm using a UV-VIS-NIR spectrophotometer (Agilent Cary 5000, Santa Clara, CA). All extractions were performed in triplicates. Chlorophyll *a* and *b* concentrations, respectively denoted by C_{chla} and C_{chlb}, were estimated according to the correlations [Ritchie(2006)]

$$C_{chla} = \left[-8.0962(OD_{652} - OD_{750}) + 16.5169(OD_{665} - OD_{750})\right] V_2\ell^{-1}V_1^{-1} \tag{3.2}$$

$$\text{and } C_{chlb} = \left[27.4405(OD_{652} - OD_{750}) - 12.1688(OD_{665} - OD_{750})\right] V_2\ell^{-1}V_1^{-1} \tag{3.3}$$

where V_1 and V_2 are the volumes of the culture and of the solvent (methanol), respectively while ℓ is the thickness of the cuvette used to measure the optical density. Similarly, the total photoprotective (PPC) and photosynthetic (PSC) carotenoid concentration $C_{PPC+PSC}$ was estimated according to [Strickland and Parsons(1968a)]

$$C_{PPC+PSC} = 4(OD_{480} - OD_{750})V_2\ell^{-1}V_1^{-1}. \tag{3.4}$$

The corresponding mass fraction of pigment "i" per dry weight of biomass can be estimated as $w_i = C_i/X$.

3.3.3 Direct radiation characteristics measurements

3.3.3.1 Experiments

First, the total scattering phase function $p(\mu_0)$ of the microalgae suspension was measured at 632.8 nm using a polar nephelometer equipped with He-Ne laser. The experimental setup and data analysis were previously reported in details by Berberoğlu et al. [Berberoğlu *et al.*(2008)] and need not be repeated. Due to probe interference with the incident laser beam, it was only possible to collect measurements for scattering angles θ_0 up to 170^o. Then, the asymmetry factor g_{633} and the back-scattered fraction b_{633} at 632.8 nm were estimated according to Equation (1.5).

Second, the normal-normal transmittance of dilute suspensions of *C. vulgaris* in a cuvette, denoted by $T_{nn,\lambda}$, was measured using a UV-VIS-NIR spectrophotometer (Agilent Cary 5000, Santa Clara, CA). The normal-hemispherical transmittance $T_{nh,\lambda}$ of the same suspensions were measured using an integrating sphere attachment (Agilent Cary DRA-2500, Santa Clara, CA) to the spectrophotometer. These measurements were performed with 1 cm pathlength quartz cuvettes (110–10-40 Hellma Analytics, Müllheim, Germany) in the wavelength range from 350 to 750 nm with 1 nm spectral resolution. To avoid absorption and scattering by the growth medium, the microalgae were centrifuged at 13,400 rpm for 10 min and washed twice with phosphate buffer saline (PBS) solution and suspended in PBS. Two biomass concentrations were considered namely 0.035 and 0.049 dry mass g/L. Such dilute suspensions ensure that single scattering prevails so that measurements of $T_{nn,\lambda}$ and $T_{nh,\lambda}$ can be used in the direct measurements of the radiation cross-sections of *C. vulgaris*. Data analysis was carried out according to the method described in Chapter 1.

3.4 Inverse method

3.4.1 Experiments

The normal-hemispherical transmittance $T_{nh,\lambda}$ and reflectance $R_{nh,\lambda}$ of *C. vulgaris* suspensions, with mass concentration ranging from 0.1113 g/L to 111.3 g/L, were systematically measured using the above described spectrophotometer/integrating sphere assembly. Measurements for the different concentrations were performed within less than 1 hour. Therefore, the cell biomass, composition, and pigment concentrations and thus their radiation characteristics did not have time to change during the measurements. For the large concentrations considered, multiple scattering prevailed and the direct measurement method previously described in Chapter 1 and valid for single scattering could not be used. Instead, $T_{nh,\lambda}$ and $R_{nh,\lambda}$ experimentally measured were used as input parameters in the inverse method to retrieve the average spectral mass absorption and scattering cross-sections of *C. vulgaris*.

3.4.2 Inverse method optimization

Figure 3.1 shows a block diagram of the procedure used to simultaneously retrieve the spectral mass absorption $A_{abs,\lambda}$ and transport scattering $(1-g_\lambda)S_{sca,\lambda}$ cross-sections from the normal-hemispherical transmittance $T_{nh,\lambda}$ and reflectance $R_{nh,\lambda}$ measurements over the PAR region. The objective is to find the values of $A_{abs,\lambda}$ and $(1-g_\lambda)S_{sca,\lambda}$ that minimize the difference between the predicted and experimentally measured normal-hemispherical transmittance and reflectance of the microalgal suspension in the least-square sense. Various optimization algorithms can be used to minimize, for each wavelength, the objective function δ_λ defined as,

$$\delta_\lambda = \left(\frac{T_{nh,\lambda,pred} - T_{nh,\lambda}}{T_{nh,\lambda}}\right)^2 + \left(\frac{R_{nh,\lambda,pred} - R_{nh,\lambda}}{R_{nh,\lambda}}\right)^2 . \tag{3.5}$$

Genetic algorithm can find a global minimum of an objective function using the concept of evolution theory [Baeck(1996)]. A given set of input parameters [e.g., ($A_{abs,\lambda}$, $(1-g_\lambda)S_{sca,\lambda}$) or ($g_\lambda$, $A_{abs,\lambda}$, $S_{sca,\lambda}$)] is called an individual and each parameter is called a gene. The numerical

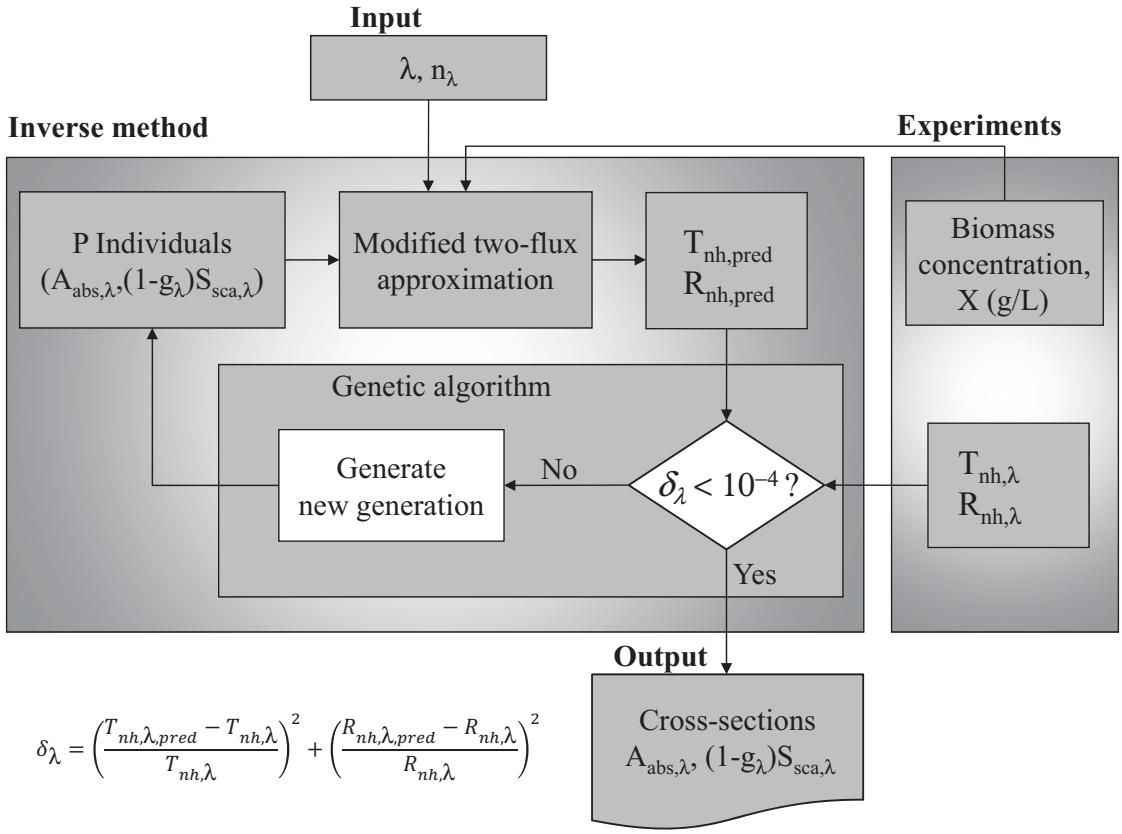

Figure 3.1: Block diagram of the procedure used to retrieve the average mass absorption and transport scattering cross-sections $A_{abs,\lambda}$ and $(1-g_\lambda)S_{sca,\lambda}$ of concentrated suspensions at a given wavelength λ from spectral normal-hemispherical transmittance and reflectance measurements. We used P=120 individuals per generation for a maximum of 50 generations.

procedure starts with a randomly generated population consisting of numerous individuals. The objective function (or fitness function) is calculated for each individual of the population and estimates some difference between experimental measurements and model predictions. Individuals with the largest value of the objective function are dismissed. Those with the smallest objective function are selected to form a new population. Breeding of the new generation consists of producing new individuals by recombination and random mutation of the genes of an arbitrary pair of individuals. The fitness function is evaluated for each individual and the procedure is repeated generation after generation until the objective

function falls below a given convergence criterion. This method tends to be slow but it is robust and eventually converges to the global minimum [Charbonneau(1995)].

In the present study, genetic algorithm was implemented using the general purpose function optimization code PIKAIA [Charbonneau and Knapp(1995),Charbonneau(2002a),Charbonneau(2002b)]. Here, the spectral mass absorption and transport scattering cross-sections $A_{abs,\lambda}$ and $(1-g_\lambda)S_{sca,\lambda}$ were retrieved and assumed to range from 0 to 1000 based on past experience and on the literature [Pilon *et al.*(2011)]. The genetic algorithm used a maximum of 50 generations with a population consisting of P=120 individuals. The convergence criteria was set as $\delta_\lambda < 10^{-4}$.

3.5 Results and Discussion

3.5.1 *Chlorella vulgaris* characterization

Figure 3.2 shows the measured size distribution of *C. vulgaris* obtained with 2873 cells. The cells featured a mean radius $\bar{r}_s$ of 1.98 μm with a standard deviation of 0.41 μm. The cell number density N_T was related to the dry biomass concentration X by $N_T = 1.17 \times 10^{14} X$. In addition, the mass fraction of water in the microorganisms was estimated as x_w = 82 wt.% based on Equation (3.1). The pigment concentrations were measured spectrophotometrically according to the procedure described earlier. The concentrations of Chl *a*, Chl *b*, and total carotenoids were such that C_{Chla} = 25.95 ± 0.82 mg/L, C_{Chlb} = 4.81 ± 0.36 mg/L, $C_{PPC+PSC}$ = 6.14 ± 0.29 mg/L. These results corresponded to the following weight percentage w_{chla}=4.41 ± 0.14 wt.%, w_{chlb}=0.82 ± 0.05 wt.%, and $w_{PPC+PSC}$=1.04 ± 0.06 wt.%.

3.5.2 Direct measurements

Figure 3.3 shows the azimuthally symmetric scattering phase function of *C. vulgaris* measured experimentally at 632.8 nm. It is evident that *C. vulgaris* scattered visible light

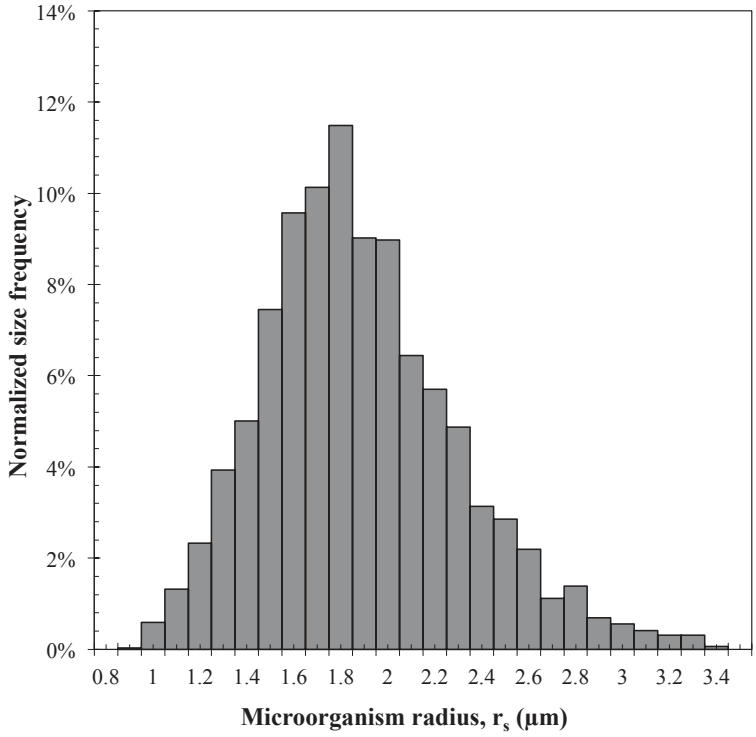

Figure 3.2: Experimentally measured size distribution of *Chlorella vulgaris* with mean radius $\bar{r}$=1.98 μm.

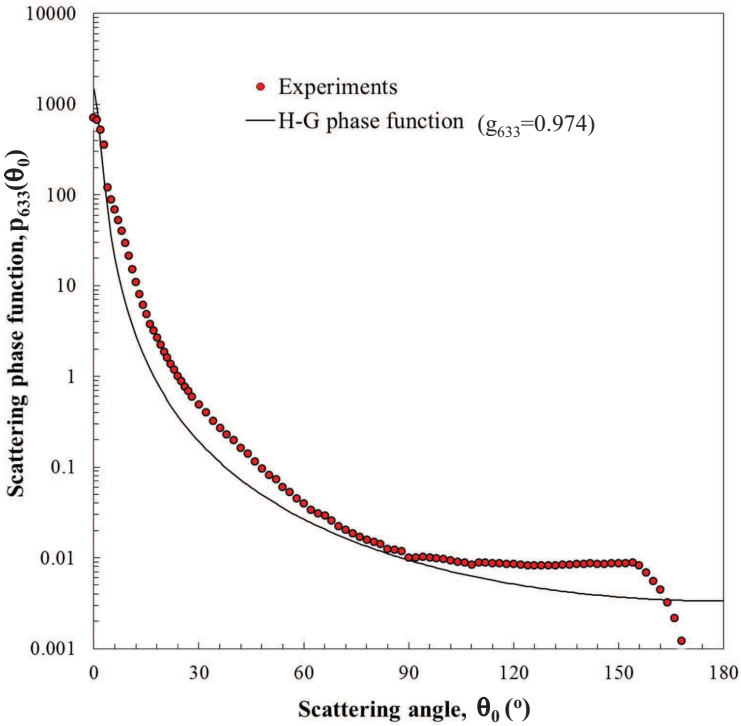

Figure 3.3: Experimentally measured phase function of *Chlorella vulgaris* at 632.8 nm along with the associated Henyey-Greenstein phase function for asymmetry factor $g_{633} = 0.974$.

strongly in the forward direction, as expected for such large scatterers with mean size parameter $\bar{\chi} = 2\pi\bar{r}_s/\lambda$=19.7. In fact, the corresponding asymmetry factor g_{633} and back-scattered fraction b_{633} were 0.974 and 0.0042, respectively. Figure 3.3 also plots the corresponding Henyey-Greenstein approximate phase function. In addition, the correction factors ϵ_n used in the direct measurements of the extinction cross-section was estimated to be ϵ_n=0.71.

Figures 3.4 plots the average mass absorption $A_{abs,\lambda}$ and scattering $S_{sca,\lambda}$ cross-sections (in m^2/kg) as functions of wavelength between 350 and 750 nm measured directly for small biomass concentrations of 0.035 and 0.049 g/L. First, the cross-sections measured for both concentrations collapse on the same curve confirming that single scattering conditions prevailed [Hulst(1957)]. Figures 3.4 also indicates that the scattering cross-section $S_{sca,\lambda}$ was much larger than the absorption cross-section $A_{abs,\lambda}$. Note, however, that the transport scattering cross-section $S_{sca,\lambda}(1-g_\lambda)$ was smaller than the absorption cross-section since g_λ approached unity. The absorption peaks of Chl *a* were apparent at 435, 630, and 676 nm, based on the absorption peaks of *in vivo* photosynthetic pigments reported by Bidigare et al. [Bidigare *et al.*(1990)]. The shoulder from 455 to 485 nm may be attributed to superposition of the absorption peaks of Chl *b* at 475 nm and of PPC around 462 and 490 nm. Another absorption peak of Chl *b* can be observed around 650 nm. These absorption and scattering cross-sections obtained from direct measurements will be treated as references in evaluating the performance of the inverse method.

3.5.3 Results from inverse method

Figure 3.5 shows the normal-hemispherical (a) transmittance $T_{nh,\lambda}$ and (b) reflectance $R_{nh,\lambda}$ as a function of wavelength between 350 and 750 nm for *C. vulgaris* concentration ranging from 0.1113 to 111.3 g/L. It indicates that the transmittance decreased sharply as the mass concentration increased. In fact, for concentration larger or equal to 5.565 g/L, the transmittance vanished over the PAR region. On the other hand, the reflectance remains relatively constant around 4%. Interestingly, it increased with increasing concentration beyond 700 nm due to the fact that the suspension absorption coefficient vanished and scattering,

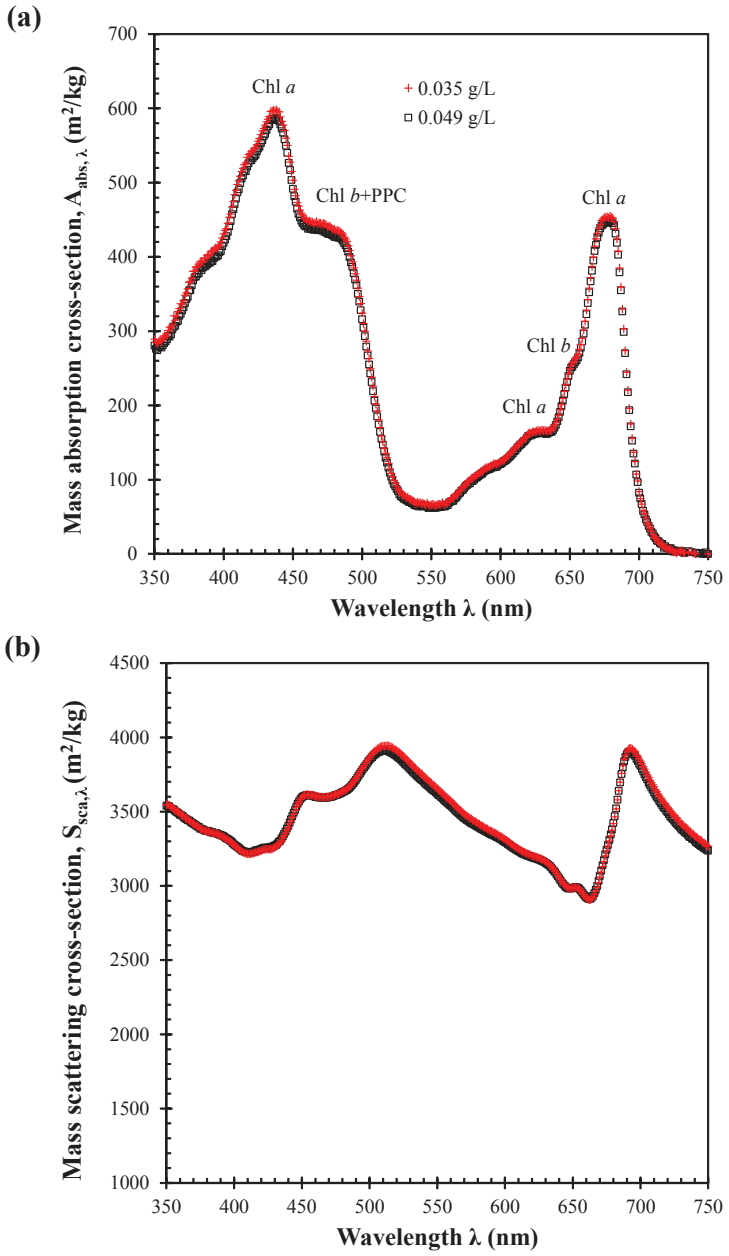

Figure 3.4: Directly measured spectral mass absorption $A_{abs,\lambda}$ and scattering $S_{sca,\lambda}$ cross–sections of *C. vulgaris* suspensions between 350 and 750 nm for biomass concentrations X of 0.035 and 0.049 g/L.

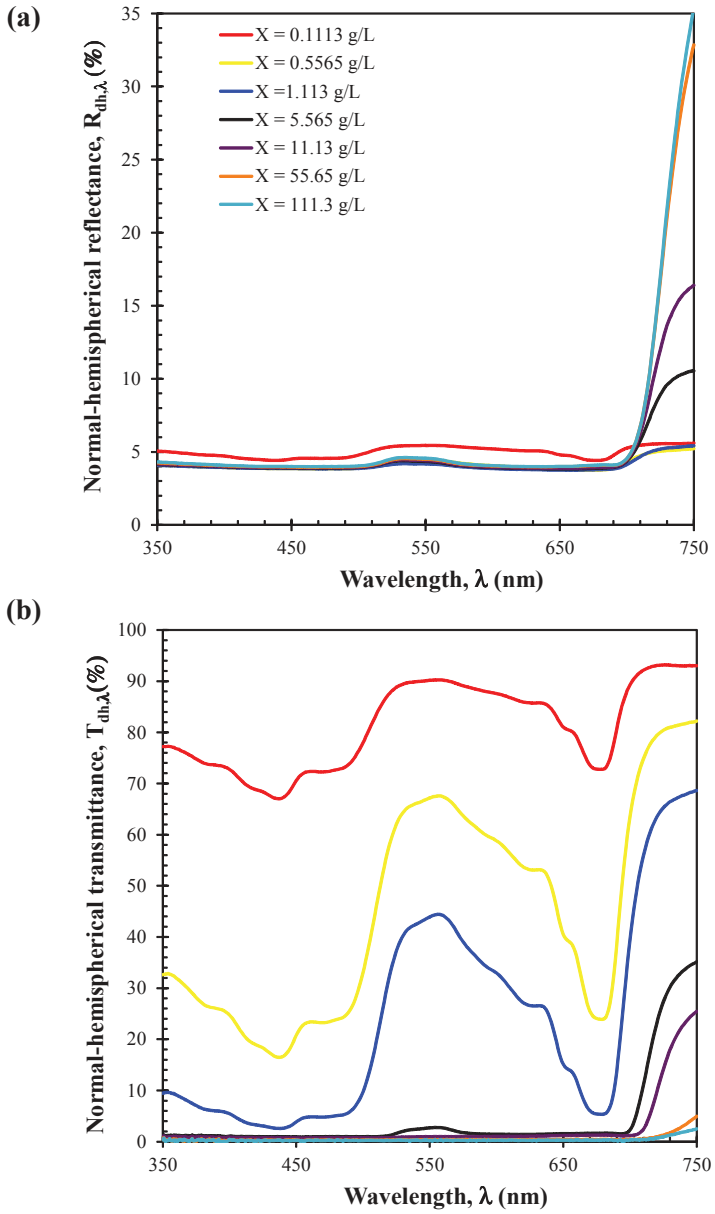

Figure 3.5: Experimentally measured normal-hemispherical transmittance $T_{nh,\lambda}$ and reflectance $R_{nh,\lambda}$ between 350 and 750 nm for *C. vulgaris* suspensions in quartz cuvettes with a path length of 1 cm with different values of biomass concentrations X ranging from 0.1113 to 111.3 g/L.

including back-scattering, increased. Overall, only normal-hemispherical transmittance and reflectance measurements for cell concentrations 0.1113, 0.5565, and 1.113 g/L had a large enough signal to noise ratio to be used in the inverse method. Data for larger concentrations led to very noisy and unrealistic retrieved values of both $A_{abs,\lambda}$ and $S_{sca,\lambda}(1-g_\lambda)$.

Figures 3.6 compares the average mass absorption $A_{abs,\lambda}$ and transport scattering $(1-g_\lambda)S_{sca,\lambda}$ cross-sections as functions of wavelength between 350 and 750 nm either measured directly or retrieved by the inverse method from measurements of $T_{nh,\lambda}$ and $R_{nh,\lambda}$ for three different concentrations. First, the retrieved spectral average mass absorption cross-section $A_{abs,\lambda}$ was similar for each biomass concentration, as expected from its definition. In addition, the values of $A_{abs,\lambda}$ retrieved by the inverse method was in relatively good agreement with that obtained from direct measurements expect above 700 nm where it should vanish. Note that the inverse method retrieved $A_{abs,\lambda}$ for each wavelength independently. Yet, the retrieved spectral absorption cross-section $A_{abs,\lambda}$ was a continuous and smooth function of wavelength. On the other hand, the retrieved transport scattering cross-section $(1-g_\lambda)S_{sca,\lambda}$ depended on the concentration considered and featured nonphysical fluctuations as a function of wavelength. It also exceeded significantly the values obtained from direct measurements.

Moreover, the same inverse procedure and algorithm was used to retrieve the three parameters $A_{abs,\lambda}$, $S_{sca,\lambda}$, and g_λ independently. This resulted in strongly oscillating values of $S_{sca,\lambda}$ and g_λ. However, the same values of $A_{abs,\lambda}$ and $(1-g_\lambda)S_{sca,\lambda}$ as those shown in Figures 3.6 were obtained. This can be attributed to the facts that (i) the solution of the inverse problem was not unique and (ii) the modified two-flux approximation for the expressions of $T_{nh,\lambda,pred}$ and $R_{nh,\lambda,pred}$ depended on the transport scattering coefficient $\sigma_{s,tr,\lambda}$ and not on $\sigma_{s,\lambda}$ and g_λ separately.

As argued earlier, the average mass absorption cross-section $A_{abs,\lambda}$ is the most important radiation characteristics in analyzing, predicting, and controlling coupled light transfer and growth kinetics in PBRs. In fact, Figure 3.7a shows the fluence rate ratio $G_\lambda(z)/G_{in,\lambda}$ at 435 nm in a 1 cm thick flat plate PBR illuminated normally on one side with a front transparent window and a back reflectivity $\rho_\lambda = 0.02$. The fluence rate ratio was predicted

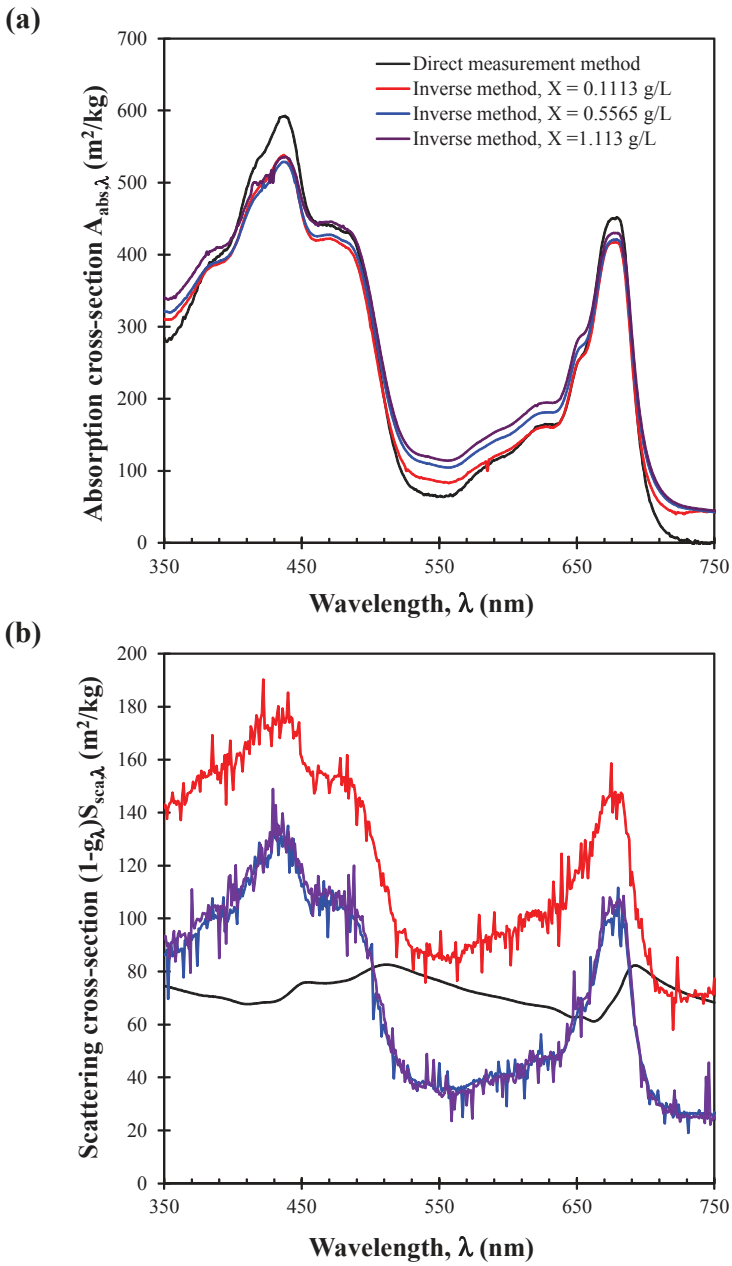

Figure 3.6: Retrieved average spectral mass absorption $A_{abs,\lambda}$ and transport scattering $(1 - g_\lambda)S_{sca,\lambda}$ cross-sections of *C. vulgaris* suspensions between 350 and 750 nm for biomass concentrations X of 0.1113, 0.5565, and 1.113 g/L.

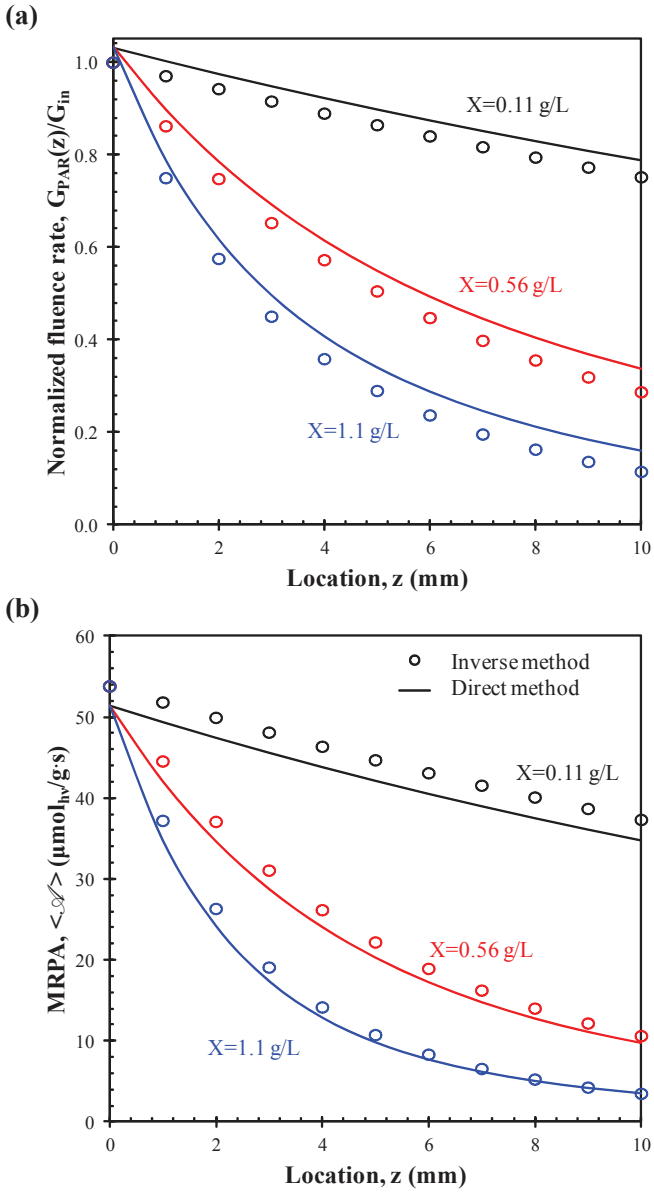

Figure 3.7: Comparison of (a) fluence rate ratio $G_{PAR}(z)/G_{in}$ and (b) mean rate of photon absorption (MRPA) as a function of depth in a 1 cm thick flat plate PBR predicted by Equations (1.10) and (1.27), respectively. The predictions used the radiation characteristics obtained from either direct measurements or retrieved by the inverse method for concentrations 0.11, 0.56, and 1.1 g/L.

by using either (i) the two-flux approximation given by Equation (1.10) based on the directly measured radiation characteristics $A_{abs,\lambda}$, $S_{sca,\lambda}$ with $b_\lambda = 0.0042$ or (ii) the simplified two-flux approximation based on the retrieved values of $A_{abs,\lambda}$ for concentrations 0.1113, 0.5565, and 1.113 g/L. The wavelength of 435 nm was chosen because it corresponded to Chl *a* absorption peak featuring the largest error of about 10% between direct measurements and retrieved value of $A_{abs,\lambda}$ by the inverse method.

Figure 3.7b compares the mean rate of photon absorption (MRPA) $\langle \mathscr{A} \rangle$ as a function of flat plate PBR thickness predicted by Equation (1.27) using the fluence rate shown in Figure 3.7a and the associated absorption and scattering cross-sections. Here, the light source was assumed to be white LEDs delivering a total incident flux of 200 $\mu mol_{h\nu}/\mathrm{m}^2\cdot\mathrm{s}$ as previously used experimentally [Soulies *et al.*(2016)]. Figure 3.7 indicates that the absorption cross-section retrieved by the inverse method combined with the simplified two-flux approximation led to acceptable predictions of the fluence rate and of the MRPA. This was achieved while requiring fewer experimental measurements and only an integrating sphere spectrometer.

Finally, Figures 3.8a and 3.8b show the volume averaged steady-state biomass productivity $\langle r_X \rangle$ of *C. vulgaris* as a function of steady-state biomass concentration X and dilution rate D, respectively. Productivity was predicted using Equations (1.30)-(1.33) combined with either (i) the two-flux approximation given by Equation (1.10) and the directly measured radiation characteristics $\bar{A}_{abs,\lambda}$, $\bar{S}_{sca,\lambda}$ with $b_\lambda = 0.0042$ or (ii) the simplified two-flux approximation and the retrieved values of $\bar{A}_{abs,\lambda}$. A torus type 4 cm thick flat-plate PBR in continuous mode was simulated exposed to 200 or 500 $\mu\mathrm{mol}_{h_\nu}/\mathrm{m}^2\cdot\mathrm{s}$ of white LEDs and the dilution rate D varied from 0.02 to 0.1 h^{-1} as previously used experimentally [Soulies *et al.*(2016)]. Figure 3.8 illustrates that the productivity predicted using the fluence rate estimated with the simplified two-flux approximation and the absorption cross-section retrieved by the inverse method was very similar to productivity predictions using the fluence rate estimated by the two-flux approximation and the directly measured radiation characteristics. Indeed, the relative difference between these two methods was less than 10% for all dilution rates D investigated and for both realistic incident irradiance considered.

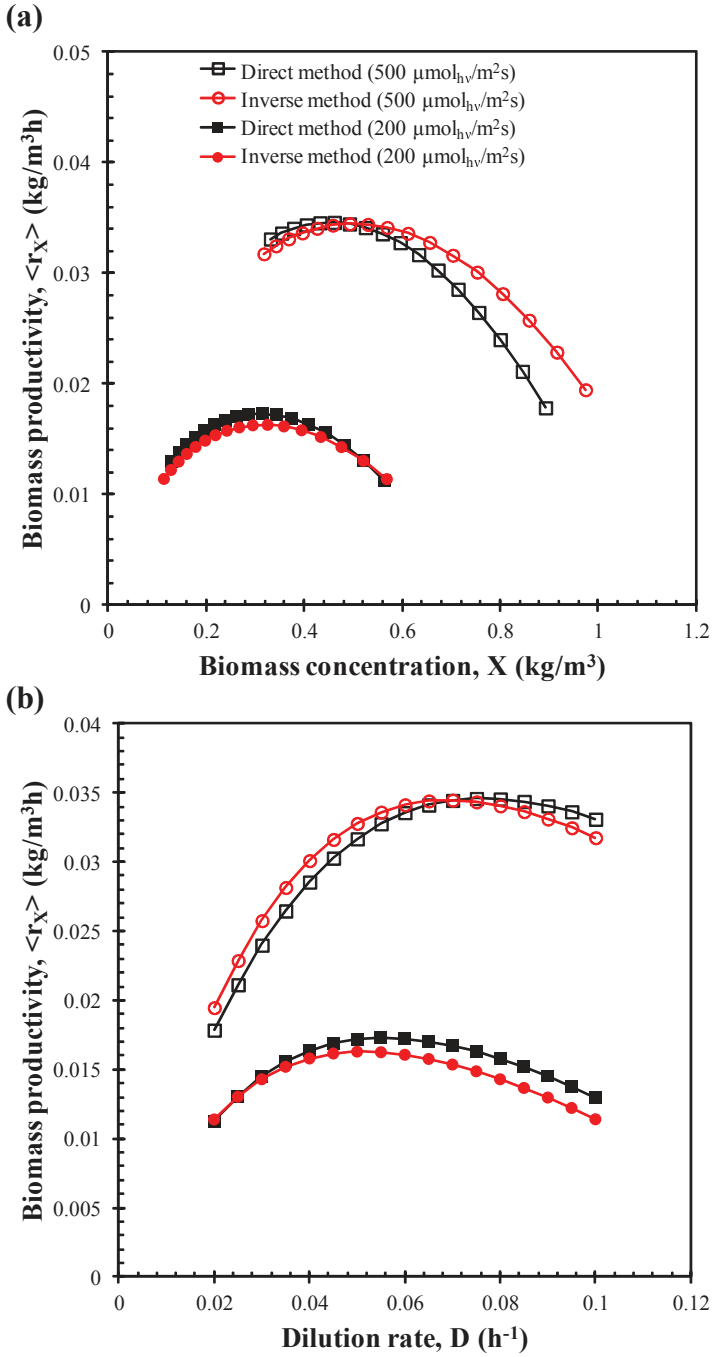

Figure 3.8: Comparison of biomass productivity $\langle r_X \rangle$ of *C. vulgaris* grown in a 1 cm thick flat-plate PBRs exposed to 200 or 500 $\mu\text{mol}_{h\nu}/\text{m}^2\cdot\text{s}$ incident white LED light, predicted using Equations (1.30) to (1.33) as a function of either (a) the steady-state biomass concentration X or (b) the dilution rate D. The predictions used the radiation characteristics obtained from either direct measurements or retrieved by the inverse method.

3.6 Conclusion

This Chapter presented a method to easily measure the spectral absorption cross-section of randomly oriented microalgae of any shape from conventional normal-hemispherical transmittance and reflectance measurements of well-mixed suspensions in conventional cuvettes. It was successfully demonstrated with suspension of *Chlorella vulgaris* with relatively large biomass concentrations such that multiple scattering prevailed. Even though the method was unable to properly retrieve the transport scattering cross-section, the retrieval of the absorption cross-section combined with the simplified two-flux approximation was sufficient to predict accurately the local fluence rate and the MRPA in flat plate PBRs. This new method can also be applied to other absorbing and scattering particles of various shapes with large enough size parameter to ensure strong forward scattering and therefore a small transport scattering cross-section compared with the absorption cross-section.

CHAPTER 4

Influence of Light Absorption Rate by *Nannochloropsis oculata* on Triglyceride Production During Nitrogen Starvation

his study aims to understand the role of light transfer in triacylglycerol (TAG) cell content and productivity from microalgae during nitrogen starvation. Large amounts of TAG lipids can be produced via nitrogen starvation of microalgae in photobioreactors exposed to intense light. First, spectral absorption and scattering cross-sections of *N. oculata* were measured at different times during nitrogen starvation. They were used to relate the mean rate of photon absorption (MRPA) per unit mass of microalgae to the TAG productivity and cell content. TAG productivity correlated with the MRPA and reached a maximum for MRPA of 13 $\mu\text{mol}_{h\nu}$/g·s. This indicated that TAG synthesis was limited by the photon absorption rate in the PBR. A minimum MRPA of 13 $\mu\text{mol}_{h\nu}$/g·s was also necessary at the onset of nitrogen starvation to trigger large accumulation of TAG in cells. These results will be instrumental in defining protocols for TAG production in scaled-up photobioreactors.

4.1 Introduction

Previous studies established the existence of a relationship between the light attenuation conditions in the PBR and lipid or TAG accumulation in the cells. In order to examine this link further, it is necessary to perform light transfer analysis in the PBR and relate it to the kinetics of lipid accumulation in the cells. To do so, the radiation characteristics of the

microalgae as a function of time are necessary during nitrogen starvation [Pilon *et al.*(2011)]. Because the cells undergo large changes in pigment concentrations and composition, theoretical predictions could be difficult to obtain and may be inaccurate [Berberoğlu *et al.*(2007)]. Therefore, experimental measurements were preferred in this study.

4.2 Background

4.2.1 Determination of radiation characteristics

4.2.1.1 Semi-empirical determination

The average mass absorption cross-section $\bar{A}_{abs,\lambda}$ of a phytoplanktonic suspension can be estimated as a weighted sum of the effective mass absorption cross-sections $a^*_{i,\lambda}$ of pigment i present in the microalgae cells [Bidigare *et al.*(1990),Nelson *et al.*(1993),Bricaud *et al.*(2004)]

$$\bar{A}_{abs,\lambda} = \sum_{i=1}^{n} C_i a^*_{i,\lambda} + \omega_\lambda \tag{4.1}$$

Here, C_i is the concentration of pigment i and ω_λ is a semi-empirical function independent of any pigment concentration [Nelson *et al.*(1993),Bricaud *et al.*(2004)]. This average mass absorption cross-section takes into account the package effect responsible for a decrease in the effective absorption cross-section of the pigments once they are packaged into the cells [Nelson *et al.*(1993),Bricaud *et al.*(2004)]. It can be estimated by considering the ratio of the *in-vivo* and *ex-vivo* absorption cross-sections of the cell's pigments [Bricaud *et al.*(2004)]. Bricaud *et al.* [Bricaud *et al.*(2004)] and Nelson *et al.* [Nelson *et al.*(1993)] measured the absorption cross-section $\bar{A}_{abs,\lambda}$ of various microalgae cells as well as the cells' pigment concentrations using high precision liquid chromatography (HPLC). The authors then compared the measured absorption cross-section $\bar{A}_{abs,\lambda}$ to that predicted by Equation (4.1) accounting for 20 different pigments. To minimize the error between the predicted and measured average spectral absorption cross-sections $\bar{A}_{abs,\lambda}$, both studies reported the necessity to introduce the term ω_λ in Equation (4.1) [Nelson *et al.*(1993), Bricaud *et al.*(2004)]. However, there is no

clear consensus in the literature on the origin of this term. It has been attributed to (i) intracellular pigments that cannot be extracted by solvents such as methanol or acetone [Bricaud *et al.*(2004)] and (ii) to absorption by the cell walls and cytoplasm that are filtered out during pigment extraction [Bissett *et al.*(1997), Bricaud *et al.*(2004)].

4.2.1.2 Theoretical predictions

Theoretical predictions of $\bar{A}_{abs,\lambda}$ and $\bar{S}_{sca,\lambda}$ can be obtained by Lorenz-Mie theory based on the cell size distribution and on the effective complex index of refraction of the microalgae on spectral basis over the PAR region [Pottier *et al.*(2005),Berberoğlu *et al.*(2007),Jonasz and Fournier(2007)]. Flynn *et al.* [Flynn *et al.*(1993)] observed a 30% increase in the volume of *N. oculata* cells during NH_4^+ starvation. Unfortunately, changes in the real part of the complex index of refraction due to nitrogen starvation have not been reported in the literature. However, it is a function of the cell's composition including lipid, protein, and carbohydrates mass fractions [Jonasz and Fournier(2007)]. Thus, a large increase in cell lipid content would lead to changes in the cell's effective refraction index and therefore in its average spectral scattering cross-section. Therefore, experimentally measuring the absorption and scattering cross-sections appeared to provide a more reliable and accurate method of accounting for changes in composition and cell size distribution during nitrogen starvation.

4.3 Materials and methods

4.3.1 Species and culture medium

A strain of *Nannochloropsis oculata* was obtained from Alphabiotech collection (Asserac, France). The microalgae were cultivated in a modified Conway medium using an artificial seawater (ASW) base [Berges *et al.*(2001)] with salinity of 25 g/L. The Conway medium composition was (in mM) : $Na_2EDTA{\cdot}2H_2O$, 0.36 ; H_3BO_3, 1.63 ; NaH_2PO_4, 1.50 ; $FeCl_3{\cdot}6H_2O$, 0.01 ; $MnCl_2{\cdot}4H_2O$, 0.91 ; $ZnCl_2$, 0.023 ; $CoCl_2{\cdot}6H_2O$, 0.013 ; $CuSO_4{\cdot}5H_2O$, 0.012 ; $Na_2MoO_4{\cdot}5H_2O$,

0.008. The medium was filter-sterilized using 0.22 μm liquid filter (AcroPak 20, Pall Corp., Port Washington, NY).

Sudden starvation experiments were performed by inoculating the PBRs with *N. oculata* produced by a continuous PBR illuminated with 150 $\mu mol_{h\nu}/m^2 \cdot s$. A specific volume of culture was harvested and centrifuged at 10,000 g (ThermoScientific Sorvall RC 6 Plus, Massachusetts, USA) for 5 minutes at 4^oC, washed with nitrogen-free Conway medium and injected into the PBR filled with the nitrogen-free medium. The volume of culture was chosen based on the desired initial biomass concentration of the nitrogen starvation batch.

4.3.2 Photobioreactor

The nitrogen starvation experiments were performed in batch mode in a 1L airlift-type flat-panel PBR with thickness of 3 cm. The PBR was described in more detail by Pruvost *et al.* [Pruvost *et al.*(2009)]. Illumination was provided on one face of the PBR by a white LED light panel (P4 Cool White, Seoul Semiconductor) with adjustable PFD. The illuminated surface of the PBR was made of transparent polymethyl methacrylate (PMMA) and the backwall of diffuse stainless steel with diffuse reflectance ρ_λ of 0.2 over the PAR region [Takache *et al.*(2010)]. The incident PFD was measured over the PAR region at 12 different locations on the inside surface of the PBR using a quantum light sensor (LI-250A, LI-COR, Lincoln, NE). The measured PFD varied by less than 10% for the different locations measured the average PFDs was reported. The pH was continuously measured using a pH sensor (Mettler Toledo SG 3253) and was maintained at 8 by automatic CO_2 injection when the culture pH exceeded 8. Mixing in the PBR was provided by injecting air at a flow rate of 80 mL/min. The PBR was maintained at room temperature (approximately 22.5^oC) by forced air convection on the back of the PBR. Before starting each experiment, the PBR was sterilized for 30 minutes using a 5 mM peroxyacetic acid solution and rinsed twice with sterile deionized water.

4.3.3 Biomass concentration

Microorganisms dry biomass concentration X was determined gravimetrically by filtering 5 mL of culture through a pre-dried and pre-weighed 0.45 μm pore size glass-fiber filter (Whatman GF/F). The filters were dried overnight in an oven at 105^{o}C and weighed after being cooled in a desiccator for 20 minutes. The samples were analyzed in triplicates and the reported biomass concentration corresponded to the mean value.

4.3.4 Pigment concentration

Pigments were extracted in pure methanol and quantified spectrophotometrically. A volume of 0.5 mL of culture was first centrifuged at 13,400 rpm (12,100 g) for 15 minutes. The medium was discarded and the cells were resuspended in 1.25 mL pure methanol and sonicated for 10 seconds. Pigments were extracted for a period of 1 hour at 45^{o}C and the extract was centrifuged. The optical density OD_λ of the supernatant was measured at wavelengths 750, 665, 652, and 480 nm using a UV-VIS-NIR spectrophotometer (Agilent Cary 5000, Santa Clara, CA). All extractions were performed in triplicates. Chlorophyll a concentration, denoted by C_{chla}, was estimated according to the correlation [Ritchie(2006)]

$$C_{chla}[mg/L] = -8.0962(OD_{652} - OD_{750}) + 16.5169(OD_{665} - OD_{750}) \tag{4.2}$$

Similarly, photo-protective carotenoid (PPC) concentration C_{PPC} was estimated according to [Strickland and Parsons(1968b)]

$$C_{PPC}[mg/L] = 4(OD_{480} - OD_{750}) \tag{4.3}$$

4.3.5 Lipid extraction

Lipid extraction was performed according to the whole cell analytic method outlined by Van Vooren *et al.* [Van Vooren *et al.*(2012)]. Briefly, 2 mL of culture were centrifuged for 10 minutes at 3,600 g and the supernatant was discarded. The cells were then resuspended in chloroform/methanol mixture (2 :1 by volume) and sonicated for 30 seconds followed by

6 hours of light agitation on a tube roller. The extracts were dried under pure nitrogen and recovered with 1 mL of chloroform/methanol mixture (2 :1 by volume). Triglyceride lipids were separated from the other lipids by solid phase extraction. Finally, the lipids were transesterified and their concentration was measured by gas chromatography with a flame ionization detector (Thermo-Fisher).

The areal TAG productivity R (in g/m^2·day) of a culture can be expressed as

$$R(t) = L\frac{d[\text{TAG}](t)}{dt} \tag{4.4}$$

where [TAG](t) (in kg/m^3) corresponds to the culture's TAG concentration at time t. In practice, with daily sampling of the culture, the areal daily average TAG productivity $\bar{R}$ of a batch culture can be written as

$$\bar{R}(t_i) = L\frac{[\text{TAG}](t_i) - [\text{TAG}](t_{i-1})}{(t_i - t_{i-1})} \tag{4.5}$$

where t_i and t_{i-1} correspond to two consecutive sampling times 24 hours apart.

4.4 Results

Three sudden starvation experiments were performed with different initial biomass concentrations X_0. In all cases, the front face of the PBR was exposed to an incident PFD of 250 $\mu\text{mol}_{h\nu}$/m^2·s.

4.4.1 Biomass concentration

Figure 4.1a shows the temporal evolution of the biomass concentration of *N. oculata* grown in batch mode and subjected to sudden nitrogen starvation with initial biomass concentrations X_0 of 0.23, 0.41, and 0.85 kg/m^3. It indicates that the biomass concentration increased nearly linearly with time in the nitrogen-free medium. Cells were able to divide despite the absence of nitrogen as previously demonstrated and discussed by Flynn *et al.* [Flynn *et al.*(1993)]. Note that nitrogen starved *N. oculata* cells featured approximately one to two

orders of magnitude smaller biomass productivity than those cultivated in nitrogen replete media. The three batches reached biomass concentrations of 0.84, 1.3, and 2.18 kg/m^3 after 96 hours of cultivation, respectively. For comparison purposes, biomass concentrations reported by Van Vooren *et al.* [Van Vooren *et al.*(2012)] for experiments with initial concentration X_0 equal to 0.23 and 0.41 kg/m^3 were added to Figure 4.1. The values obtained in the present study agreed with those reported by Van Vooren *et al.* [Van Vooren *et al.*(2012)] for identical growth conditions. This confirms the repeatability of the measurements. The present study provides additional and more detailed information on the temporal evolution of *N. oculata* during nitrogen starvation.

4.4.2 Pigment concentrations

Figures 4.1b and 4.1c show the temporal evolution of chl*a* and carotenoid concentrations during sudden starvation cultivation for the three different initial biomass concentrations X_0 considered. They indicate that the cell pigment concentration decreased immediately after the microalgae were suspended in the nitrogen-free medium. Most of this decrease occurred within the first 24 hours. Here also, the pigment concentrations were similar to those reported by Van Vooren *et al.* [Van Vooren *et al.*(2012)]. Moreover, it is apparent that the rate of pigment loss was correlated with the initial biomass concentration. In fact, after 96 hours of cultivation, the chl*a* concentration C_{chla} in culture with X_0=0.23 kg/m^3 was 0.23 wt.% compared with 0.31 and 0.59 wt.% for cells cultivated in the same PBR with initial concentration X_0 of 0.41 and 0.85 kg/m^3, respectively. This was due to the fact that batches with smaller initial biomass concentration had larger cell growth rates. This resulted in faster decrease of cell nitrogen content thus increasing the rate of chl*a* loss in cells. Indeed, by 96 hours, the biomass concentration had grown by 3.6 times for the batch with initial concentration X_0 of 0.23 kg/m^3 while it had increased by only 3.1 and 2.4 times for batches with X_0 equal to 0.41 and 0.85 kg/m^3, respectively. These corresponded to a time-averaged growth rates of 27.6 $\times 10^{-3}$, 22.6 $\times 10^{-3}$, and 16.2 $\times 10^{-3}$ 1/h, respectively.

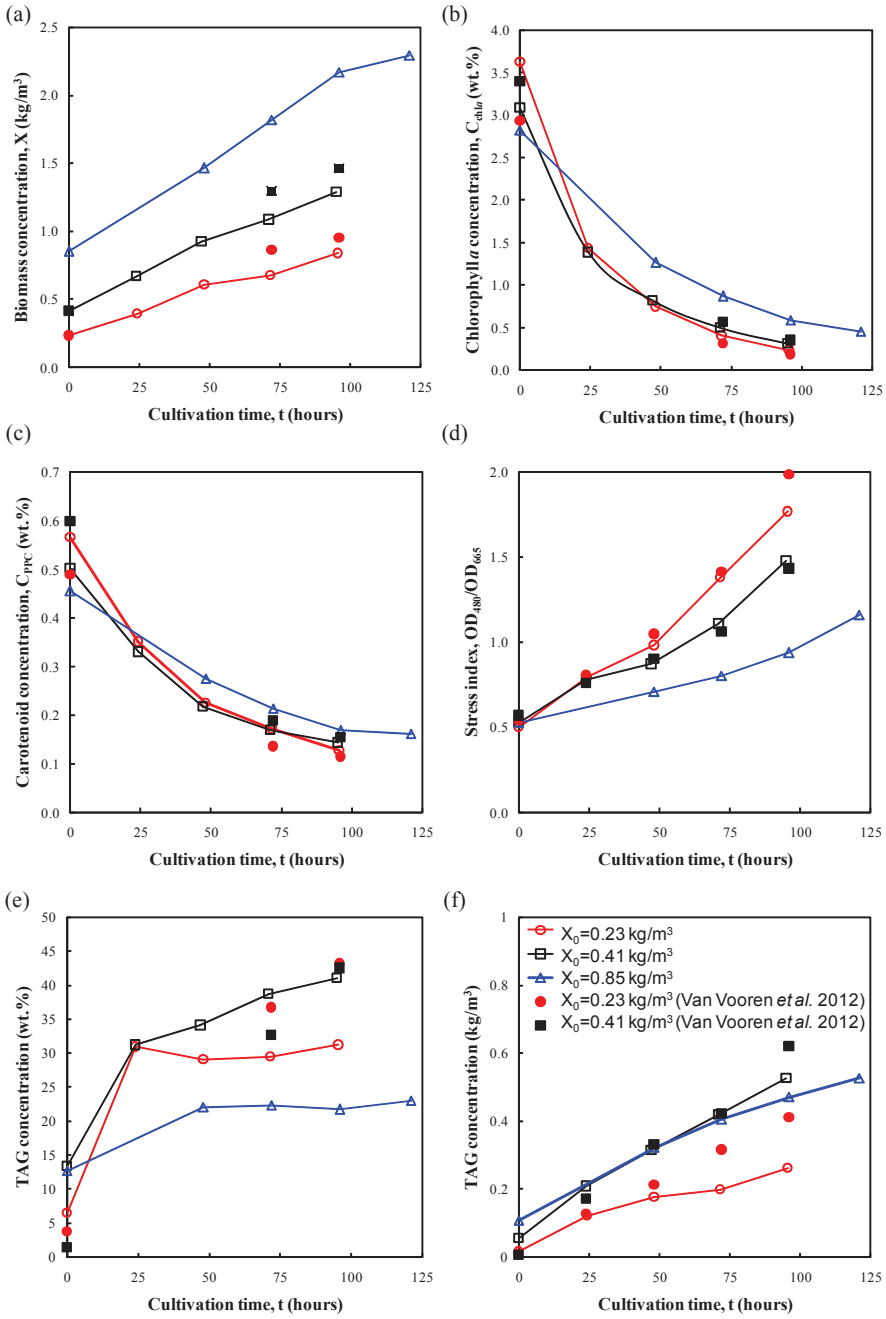

Figure 4.1: Temporal evolution of (a) biomass concentration X, (b) chlorophyll a concentration C_{chla}, (c) carotenoid concentration C_{PPC}, (d) the stress index, (e) TAG concentration (dry wt.%), and (f) TAG concentration (kg/m^3) during sudden nitrogen starvation of batch culture exposed to 250 μmol$_{h\nu}$/m^2·s with initial biomass concentrations X_0 equal to 0.23, 0.41, and 0.85 kg/m^3. Data reported by Van Vooren *et al.* [Van Vooren *et al.*(2012)] for experiments with initial concentration X_0 = 0.23 and 0.41 kg/m^3 were added for reference.

4.4.3 Stress index

The stress index is defined as the ratio of the optical densities (OD) of the cells' pigment extract at wavelengths 480 and 665 nm [Heath *et al.*(1990)]. It is an indicator of the "nutrient status" of the cells as proposed by Heath *et al.* [Heath *et al.*(1990)]. It is an indirect measure of the carotenoid to chl*a* ratio and it is inversely correlated to the C/N ratio of the cells [Heath *et al.*(1990)]. Figure 4.1d shows the stress index for the three batch cultivations previously described. In nutrient replete conditions, corresponding to cultivation time t =0, the stress index was approximately 0.5. For all sudden starvation experiments it increased with time and was larger for cultures with smaller initial biomass concentration X_0. In fact, the stress index after 96 hours of cultivation was 1.8, 1.5, and 0.9 for cultures with initial biomass concentration X_0 of 0.23, 0.41 and 0.85 kg/m^3, respectively. This indicates that cells in the culture with initial concentration $X_0 = 0.23$ kg/m^3 had undergone more cell divisions and thus featured a larger C/N ratio.

4.4.4 TAG concentration

Figures 4.1e and 4.1f show the temporal evolution of the TAG concentration in dry wt.% and in kg/m^3, respectively, for *N. oculata* grown in batch mode and subjected to sudden nitrogen starvation with initial biomass concentrations X_0 of 0.23, 0.41, and 0.85 kg/m^3. It indicates an immediate increase in TAG concentration in cells following their suspension in nitrogen-free medium. Indeed, experiments with initial concentration X_0 of 0.23, 0.41, and 0.85 kg/m^3 featured cells that reached a TAG concentration of 30, 31, and 21 dry wt.% after 24 hours, respectively. The culture with initial concentration X_0 equal to 0.41 kg/m^3 reached a final TAG concentration of 41.2 dry wt.%. This compared well with the TAG concentration of 42 dry wt.% reported by Van Vooren *et al.* [Van Vooren *et al.*(2012)] for an identical experiment. On the other hand Van Vooren *et al.* [Van Vooren *et al.*(2012)] reported a final TAG concentration of 43% for sudden starvation experiment with initial biomass concentration X_0 of 0.23 k/m^3. This was significantly different from the 30 dry wt.%

obtained here. In addition, it is unusual to observe a decrease in the TAG concentration such as that seen after 48 hours of cultivation in continuously illuminated cultures. This may be attributed to experimental uncertainties in the lipid extraction or analysis. Note, however, that other measurements (Figure 4.1a to 4.1d) were consistent with data reported by Van Vooren *et al.* [Van Vooren *et al.*(2012)].

4.4.5 Radiation characteristics

Figures 4.2a and 4.2b show the temporal evolution of the measured average mass absorption and scattering cross-sections in the spectral region from 350 to 750 nm for *N. oculata* during sudden nitrogen starvation of the batch culture with an initial biomass concentration X_0 of 0.23 kg/m^3. Overall, the mass absorption cross-section decreased as a function of time for all wavelengths in the PAR region. Similar results were obtained for experiments with different initial biomass concentrations. The decrease in absorption cross-section was consistent with the continuous decrease in pigment concentrations over time observed in Figures 4.1b and 4.1c. For example, the chl$a$ absorption peak at 676 nm decreased from 544 m^2/kg at the start of cultivation to only 43 m^2/kg after 96 hours for the culture with initial concentration X_0=0.23 kg/m^3. During the same time period, the chl$a$ concentration decreased from 3.6 wt.% to 0.23 wt.%. Such sharp decrease in the mass absorption cross-section had a significant effect on the PAR-averaged fluence rate $G_{PAR}(z)$ in the PBR.

Moreover, the magnitude and shape of the average mass scattering cross-section changed slightly over time. For example, it decreased by 20% at 555 nm corresponding to the lowest absorption cross-section. However, it increased by 5.5% at wavelength 437 nm corresponding to one of chlorophyll *a* absorption peaks. Changes in the scattering cross-section overtime could be due to changes in size, shape, cellular composition, and pigment concentrations of the cells [Jonasz and Fournier(2007)]. However, it is difficult to attribute the observed changes specifically to any one or more of those parameters due to the complexity of the biological response to nitrogen starvation [Flynn *et al.*(1993)].

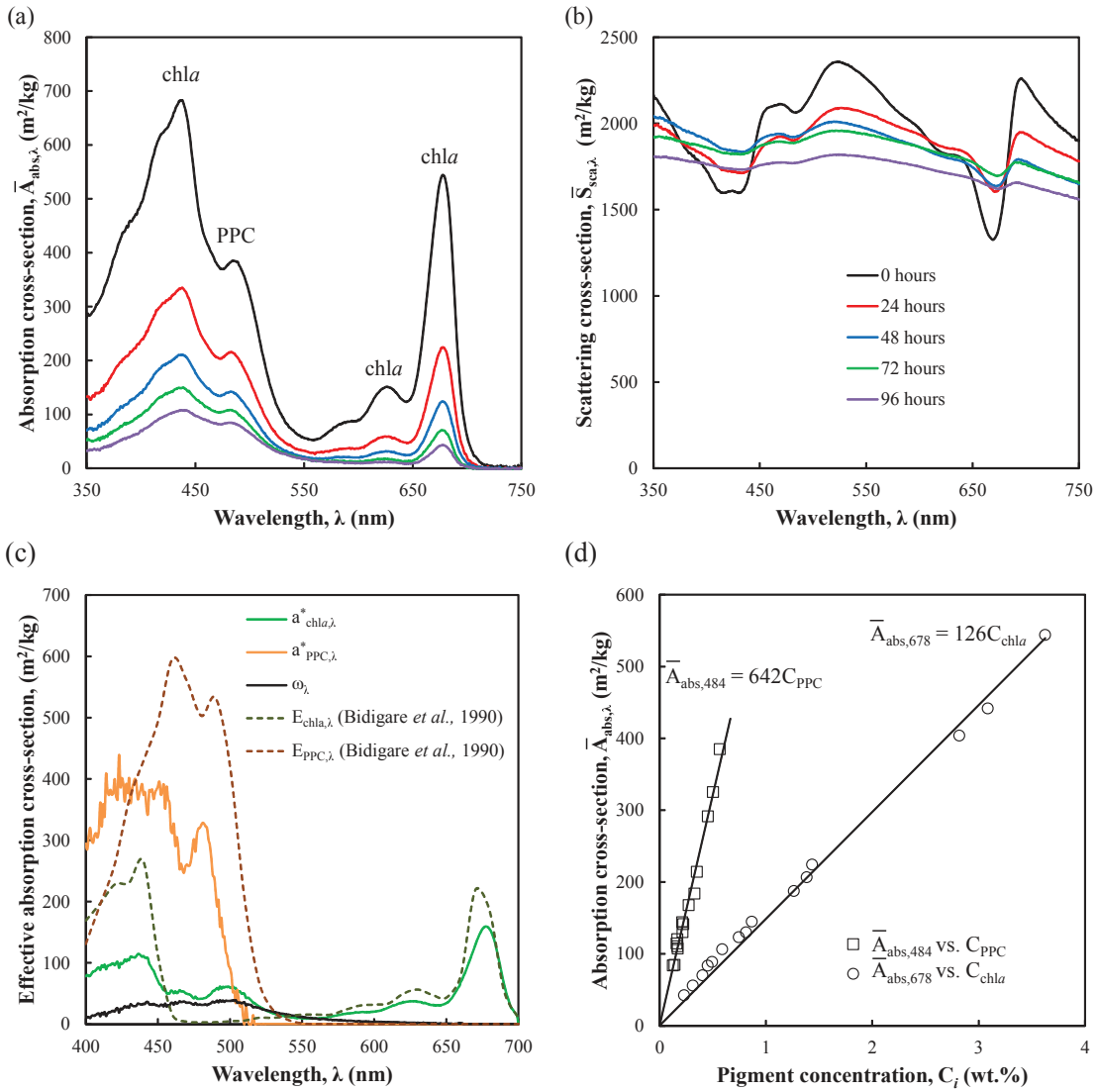

Figure 4.2: Average mass (a) absorption and (b) scattering cross-sections of *N. oculata* after 0, 24, 48, 72, and 96 hours of cultivation during sudden nitrogen starvation of batch culture exposed to 250 $\mu\text{mol}_{h\nu}/\text{m}^2\cdot\text{s}$ with an initial biomass concentration $X_0 = 0.23$ kg/m^3. (c) Retrieved pigment effective absorption cross-sections $a^*_{chla,\lambda}$, $a^*_{PPC,\lambda}$, and coefficient ω_λ used in Equation (4.6). (d) Absorption cross-section at 676 nm $\bar{A}_{abs,676}$ as a function of chl*a* concentration C_{chla} and absorption cross-section at 484 nm $\bar{A}_{abs,484}$ as a function of carotenoid concentration C_{PPC} compiled from all three experiments.

In the present study, the concentrations of chlorophyll *a* C_{chla} and the photo-protective carotenoids C_{PPC} were measured. Then Equation (4.1) can be written as

$$\bar{A}_{abs,\lambda} = a^*_{chla,\lambda} C_{chla} + a^*_{PPC,\lambda} C_{PPC} + \omega_\lambda \tag{4.6}$$

Here, $a^*_{chla,\lambda}$ and $a^*_{PPC,\lambda}$ (in m^2/kg) correspond to the effective specific absorption cross-sections of chl*a* and PPC, respectively. Figure 4.2c presents the coefficients $a^*_{chla,\lambda}$, $a^*_{PPC,\lambda}$, and ω_λ obtained by fitting 15 experimentally measured spectral mass absorption cross-sections to Equation (4.6) using the least squares method. It also shows the *ex-vivo* absorption cross-sections of chl*a*, $Ea_{chla,\lambda}$, and PPC, $Ea_{PPC,\lambda}$, (in m^2/kg) reported by [Bidigare *et al.*(1990)]. The retrieved pigment effective absorption cross-sections $a^*_{chla,\lambda}$ and $a^*_{PPC,\lambda}$ show similar trends but were smaller than those reported by Bidigare *et al.* [Bidigare *et al.*(1990)]. The differences can be attributed to the package effect and was indirectly accounted for by $a^*_{i,\lambda}$ and ω_λ. Note that during nitrogen starvation the specific types of carotenoid pigments in the cells change shifting the wavelength and the magnitude of their absorption peaks [Cohen(1999)]. However, this cannot be accounted for with spectrophotometric pigment measurements. Consequently, the absorption cross-section of carotenoids $a^*_{PPC,\lambda}$ should be considered as a mean cross-section for the various carotenoids produced by *N. oculata* during nitrogen starvation. Figure 4.2d show the measured average mass absorption cross-sections $\bar{A}_{abs,676}$ and $\bar{A}_{abs,484}$ at wavelengths 676 and 484 nm versus the simultaneously measured chl*a* and PPC concentrations C_{chla} and C_{PPC}, respectively. Linear relationships were found between $\bar{A}_{abs,676}$ and C_{chla} and between $\bar{A}_{abs,484}$ and C_{PPC} with coefficient of determination R^2 exceeding 0.98. This provided confidence in the accuracy and the consistency of the measured radiation characteristics as well as the measured pigment concentrations for the different experiments.

4.4.6 Fluence rate and MRPA

Figure 4.3a shows the PAR-averaged fluence rate $G_{PAR}(z)$ predicted by Equations (1.10) to (1.12) as a function of PBR depth z using the radiation characteristics measured after 0

and 96 hours during sudden starvation experiments with initial biomass concentration X_0 of 0.23, 0.41, and 0.85 kg/m^3. As expected, the fluence rate $G_{PAR}(z)$, at any given time, was larger for the cultures with smaller biomass concentration. In addition, for all three batches, the fluence rate after 96 hours of cultivation was larger than the initial fluence rate despite the significantly larger biomass concentration (Figure 4.1a). This was due to the decrease in the absorption cross-section (Figure 4.2a) whose magnitude was significantly larger than the increase in biomass concentration. A similar increase in fluence rate as a function of time was experimentally observed by Pruvost *et al.* [Pruvost *et al.*(2009)] during nitrogen starvation cultivation of *Neochloris oleoabundans* in a flat-plate PBR. However, the fluence rate alone is not indicative of the amount of light absorbed by the cells [Pruvost and Cornet(2012)]. Indeed, the absorption cross-section must also be considered as it accounts for the average amount of light absorbed by the cells. In fact, this is an important consideration during nitrogen starvation given the sharp decrease in absorption cross-section and the simultaneous increase in biomass concentration.

Figure 4.3b shows the mean rate of photon absorption (MRPA) $\langle \mathscr{A} \rangle$, as a function of time for each sudden nitrogen starvation cultivation. It was estimated by Equations (1.27) to (1.11) using the corresponding experimentally measured average spectral mass absorption and scattering cross-sections $\bar{A}_{abs,\lambda}$ and $\bar{S}_{sca,\lambda}$. Here also, $\langle \mathscr{A} \rangle$ was larger for batches with smaller initial biomass concentration at all times. This could be attributed to the correspondingly larger fluence rate in the PBR (Figure 4.3a). In addition, $\langle \mathscr{A} \rangle$ decreased with time for all three experiments. For example, in the sudden nitrogen starvation experiment with X_0= 0.23 kg/m^3, $\langle \mathscr{A} \rangle$ was 24 μmol$_{h\nu}$/g·s initially but decreased to 6.6 and 5.4 μmol$_{h\nu}$/g·s after 72 and 96 hours, respectively. This may seem counterintuitive since the fluence rate increased during nitrogen starvation (Figure 4.3a). However, the decrease in the absorption cross-section dominated over the increase in the fluence rate. As previously suggested, MRPA $\langle \mathscr{A} \rangle$ is indicative of the amount of energy absorbed by the microalgae, unlike the fluence rate $G_{PAR}(z)$. The decrease in MRPA $\langle \mathscr{A} \rangle$ demonstrates that, on average, the energy absorbed per cell decreased during nitrogen starvation. This may negatively impact both cell division

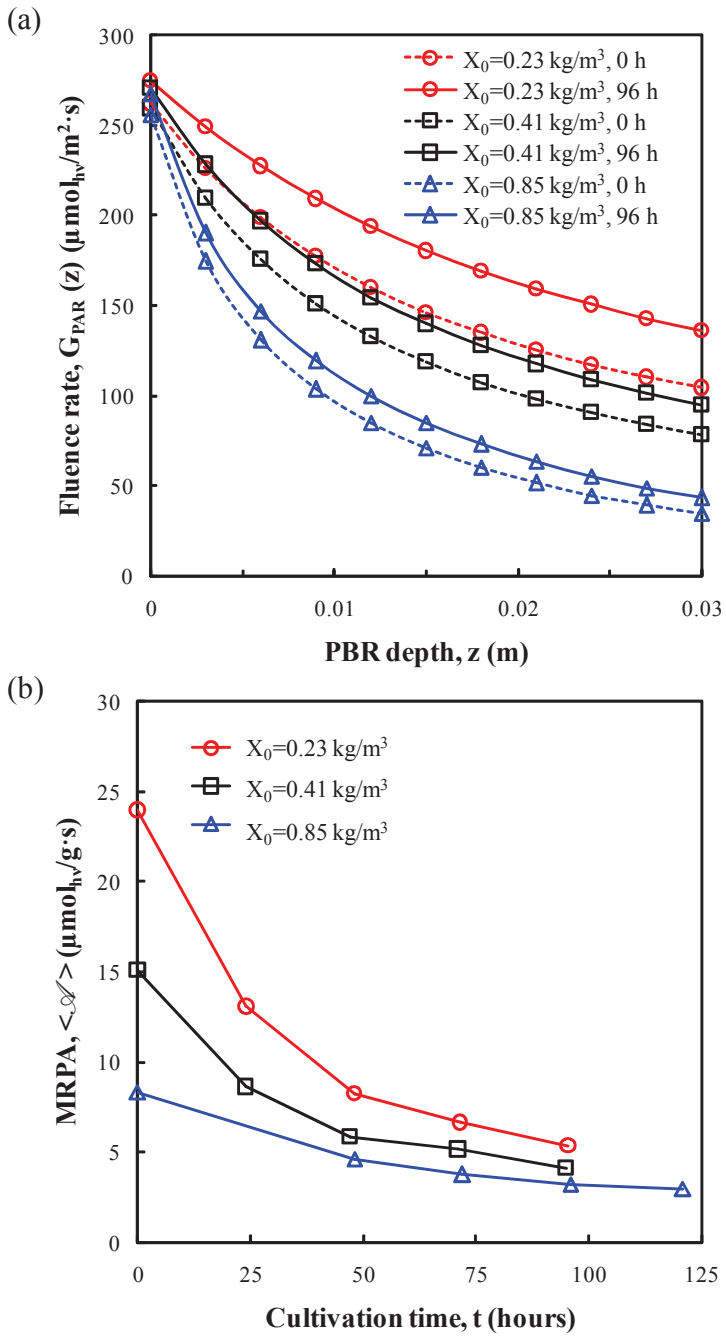

Figure 4.3: (a) Fluence rate $G_{PAR}(z)$ in the PBR at the start of the cultivation (0 hours) and after 96 hours and (b) temporal evolution of MRPA $\langle\mathscr{A}\rangle$ for sudden starvation experiments with initial biomass concentration X_0 equal to 0.23, 0.41, and 0.85 kg/m^3.

and lipid synthesis [Pruvost and Cornet(2012)]. Indeed, microalgae rely on the absorption of incident photons to carry out biochemical reactions. Their inability to absorb light could reduce their efficacy in performing photosynthesis and in fixating inorganic carbon [Williams and Laurens(2010)].

4.4.7 TAG productivity

As previously discussed, cells synthesize TAG to store carbon and energy. Thus, the rate of TAG production should correlate with the mean rate of photon absorption (MRPA). The daily areal average productivity $\bar{R}(t_i)$ was estimated from experimental measurements at discrete time t_i according to Equation (4.5). Similarly, the average daily MRPA was defined as $\langle\bar{\mathscr{A}}\rangle(t_i)= [\langle\mathscr{A}\rangle(t_i)+\langle\mathscr{A}\rangle(t_{i-1})]/2$ where $t_i - t_{i-1} = 24$ hours. Figure 4.4 shows the daily average areal TAG production rate $\bar{R}$ versus the daily average MRPA $\langle\bar{\mathscr{A}}\rangle$ for the sudden starvation experiments with three different initial concentrations X_0. For each experiment, the maximum daily productivity corresponded to the maximum MRPA $\langle\bar{\mathscr{A}}\rangle$ occurring on the first day of cultivation. Interestingly, data for the different experiments were consistent with one another. A parabolic relationship between TAG productivity $\bar{R}$ and daily average MRPA $\langle\bar{\mathscr{A}}\rangle$ was fitted to the experimental data for convenience and for a lack of a better model. The peak productivity of 4.6 g/m^2·day was observed for MRPA equal to 13 μmol$_{h\nu}$/g·s.

This relationship indicates that nitrogen starvation alone does not guarantee large TAG production rate. The TAG biosynthesis kinetics appears to be limited by the photon absorption rate represented by MRPA $\langle\bar{\mathscr{A}}\rangle$. This is analogous to microalgae grown under optimal growth conditions (i.e., without nutrient deprivation) when biomass productivity is only limited by light. Increasing MRPA per unit mass of microalgae can be achieved by reducing the biomass concentration. However, below a certain optimum value, the biomass productivity decreases and the light incident on the PBR is not fully absorbed [Takache *et al.*(2012), Pruvost and Cornet(2012)]. In this so-called kinetic regime, biomass productivity is limited by the biosynthesis rate of the microalgae. Similarly, increasing the daily average MRPA beyond its optimal value resulted in a decrease in the daily TAG productivity $\bar{R}$. However, due to

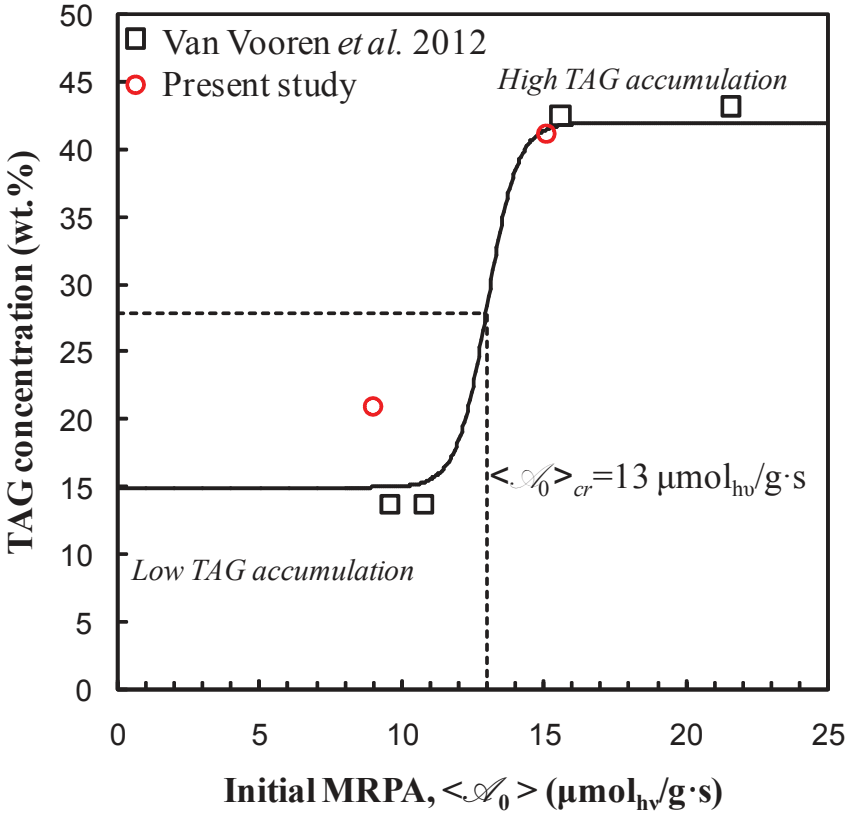

Figure 4.4: Daily average areal TAG productivity $\bar{R}$ (in g/m^2·day) versus daily average MRPA $\langle \bar{\mathscr{A}} \rangle$ for sudden starvation experiments with incident PDF of 250 μmol$_{h\nu}$/m^2·s and initial biomass concentrations X_0 equal to 0.23, 0.41, and 0.85 kg/m^3.

the reduction in pigment content and in absorption cross-section, it was not possible to achieve complete light absorption in the PBR during nitrogen starvation. Here, the process was biologically limited by the maximum TAG accumulation allowed in cells. For example, increasing daily average MRPA $\langle \bar{\mathscr{A}} \rangle$ on the first day of cultivation from 15 to 24 μmol$_{h\nu}$/g·s was achieved by lowering the initial biomass concentration X_0 from 0.41 to 0.23 kg/m^3. Both experiments yielded cells with 31 dry wt.% TAG concentration after 24 hours of cultivation. However, the corresponding TAG concentration in the PBR was 0.21 and 0.12 kg/m^3, respectively. Thus, increasing MRPA $\langle \bar{\mathscr{A}} \rangle$ did not affect the TAG concentration per cell but

resulted in a smaller PBR daily TAG productivity due to the smaller biomass concentration.

Furthermore, there was a large difference in the temporal evolution of biomass concentration for experiments with initial biomass concentration X_0 of 0.41 and 0.85 kg/m^3 for the duration of the batch culture. By contrast, both experiments featured a similar TAG concentration after 24 and 48 hours of cultivation. However, the daily TAG productivity of the PBR with X_0=0.41 kg/m^3 during the first 24 hours of cultivation was much larger than that of the PBR with X_0=0.85 kg/m^3 due to its lower initial TAG concentration. On the other hand, between 24 and 48 hours both experiments featured a similar TAG concentration and therefore a similar daily TAG productivity. It is interesting to note that they both featured similar values of daily average MRPA $\langle \bar{\mathscr{A}} \rangle$. This was illustrated in Figure 4.4 for daily average MRPA $\langle \bar{\mathscr{A}} \rangle$ values of 5.5-7.5 $\mu\text{mol}_{h\nu}$/g·s where data from both experiments were clustered. This exemplifies the value of our proposed method of correlating the MRPA with the TAG productivity. Despite the differing biomass and pigment concentrations, cultures with comparable values in MRPA featured similar TAG productivities.

Finally, During sudden starvation batch cultivations the TAG productivity $R(t)$ decreased due to the decrease in MRPA $\langle \mathscr{A} \rangle$ (Figure 4.3b). Thus, in batch cultivation it is not possible to maintain a constant TAG productivity. Instead, the TAG productivity can be optimized through the initial value of MRPA denoted by $\langle \mathscr{A}_0 \rangle$. The latter can be adjusted by changing the initial biomass concentration according to the incident PFD and PBR thickness.

4.4.8 TAG accumulation

Here, the data reported by Van Vooren *et al.* [Van Vooren *et al.*(2012)] was used in addition to those reported in this study to elucidate the relationship between initial value of MRPA $\langle \mathscr{A}_0 \rangle$ and TAG cell content. The authors performed a total of fourteen progressive and sudden starvation experiments using the same microalgae species, strain, and PBR as those used in the present study. The pigment and biomass concentrations were analyzed using the same protocols. In addition, the authors reported the pigment concentrations and the TAG

concentrations in the cells for a wide range of nitrogen starvation experiments. However, they did not measure the radiation characteristics of *N. oculata*. Therefore, in order to extend the present light transfer analysis to experiments reported by Van Vooren *et al.* [Van Vooren *et al.*(2012)], Equation (4.6) was used to estimate the average mass absorption cross-section of cultures based on the reported pigment concentrations.

4.4.8.1 Sudden nitrogen starvation

Van Vooren *et al.* [Van Vooren *et al.*(2012)] performed a total of four sudden starvation experiments in a PBR exposed to 250 $\mu\text{mol}_{h\nu}/\text{m}^2\cdot\text{s}$. The initial biomass concentrations were 0.23, 0.41, 0.65, and 0.75 kg/m^3. The four experiments yielded cultures with a TAG concentration of 44, 45, 14, and 13 dry wt.%, after 96 hours respectively. Figure 4.5 shows the TAG cell content (in wt.%) after 96 hours as a function of the initial MRPA $\langle \mathscr{A}_0 \rangle$ for sudden starvation experiments performed in the present study and those reported by Van Vooren *et al.* [Van Vooren *et al.*(2012)].

It suggests that there exists a critical initial MRPA $\langle \mathscr{A}_0 \rangle_{cr}$ beyond which the cells accumulated large amounts of TAG. Here, $\langle \mathscr{A}_0 \rangle_{cr}$ was estimated to be 13 $\mu\text{mol}_{h\nu}/\text{g}\cdot\text{s}$. Note that it is generally not possible to exceed this critical initial MRPA $\langle \mathscr{A}_0 \rangle_{cr}$ on the second day of sudden starvation cultivation. Indeed, a sharp decrease in $\langle \mathscr{A} \rangle$ was observed in the first 24 hours of cultivation (Figure 4.3b) due to the rapid decrease in pigment concentrations (Figures 4.1b and 4.1c) and increase in biomass concentration. Therefore, in order to produce cells with large TAG content in a batch culture, the initial mass concentration X_0 of the batch culture must be adjusted carefully in order to achieve values of $\langle \mathscr{A}_0 \rangle$ that exceed the critical MRPA $\langle \mathscr{A}_0 \rangle_{cr}$=13 $\mu\text{mol}_{h\nu}/\text{g}\cdot\text{s}$.

The critical MRPA under nitrogen starvation could correspond to conditions when the cells' TAG synthesis rate increases with respect to the synthesis rate of carbohydrate, protein, etc. In fact, the TAG synthesis pathway is activated under nitrogen starvation to act as an electron sink and prevent creation of excess free-radicals in the photosynthetic electron

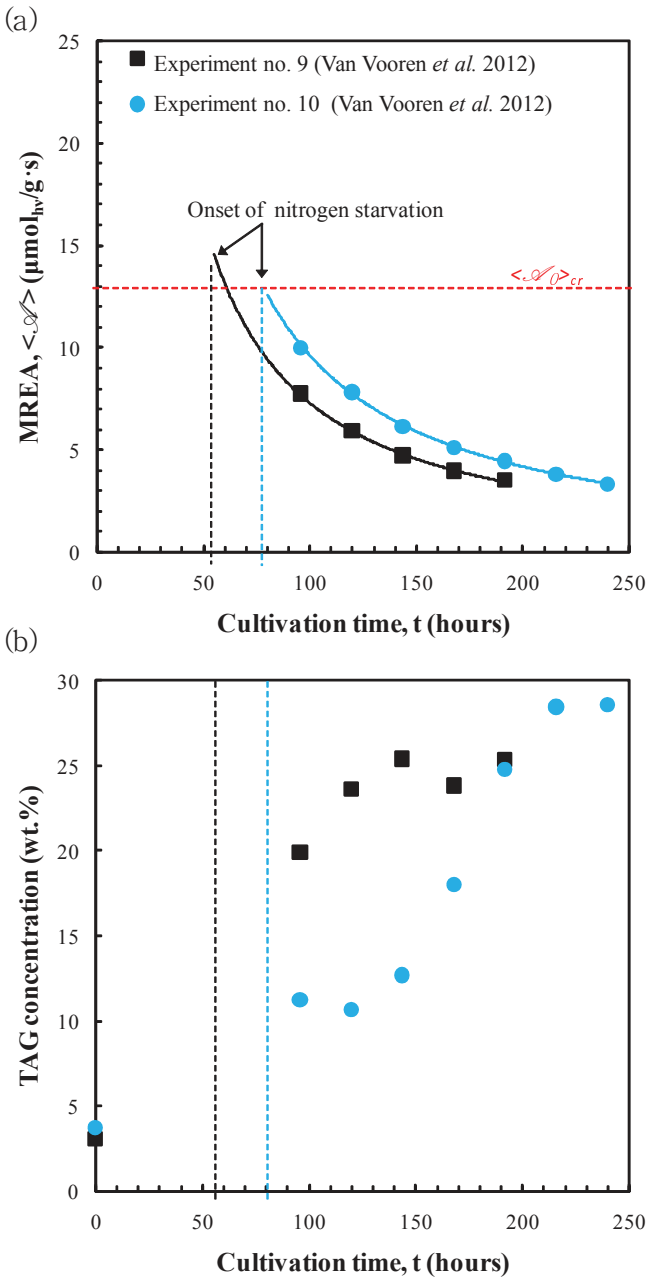

Figure 4.5: TAG concentration (in wt.%) after 96 hours of sudden nitrogen starvation as a function of initial MRPA $\langle \mathscr{A}_0 \rangle$. A critical value $\langle \mathscr{A}_0 \rangle_{cr}$ of 13 $\mu\text{mol}_{h\nu}$/g·s was necessary to trigger large TAG accumulation in cells.

transport chain [Hu *et al.*(2008)]. In addition, it takes twice as much light energy to produce TAG as it does to produce protein or carbohydrate of equal mass [Hu *et al.*(2008)]. However, it remains unclear how cells distribute the absorbed energy during nitrogen starvation [Hu *et al.*(2008)]. By setting the initial MRPA in excess of $\langle \mathscr{A}_0 \rangle_{cr}$ in batch experiments, the average MRPA was sufficient to ensure the average production rate of TAG was at least 40-45% of the biomass production rate for the duration of the experiment and produced cells with 40-45 dry wt.% TAG.

The similarity between the critical initial MRPA $\langle \mathscr{A}_0 \rangle_{cr}$ for maximum TAG cell content and the daily MRPA $\langle \bar{\mathscr{A}} \rangle$ corresponding to peak daily average areal productivity $\bar{R}$ is interesting but unsurprising. It can be explained by the fact that the largest increase in TAG concentration in cells and maximum daily productivity for each cultivation occurred in the first 24 hours of nitrogen starvation. Since, the daily average MRPA $\langle \bar{\mathscr{A}} \rangle$ for the first 24 hours of cultivation corresponded approximately to the initial MRPA $\langle \mathscr{A}_0 \rangle$, the optimum values for both were equal.

4.4.8.2 Progressive starvation

Van Vooren *et al.* [Van Vooren *et al.*(2012)] performed a total of 10 progressive starvation experiments as summarized in Table 2 of their manuscript. Experiments no. 9 and 10 used a modified Conway medium with an initial NO_3^- concentration of 0.92 and 1.65 mM, respectively. In both cases, the initial biomass concentration was 0.02 kg/m^3 and the microorganisms were cultivated in a 150 L PBR, 5 cm in thickness, exposed to a PFD of 222 $\mu\text{mol}_{h\nu}/\text{m}^2\cdot\text{s}$. Note that the biomass concentration at the culture's onset of nitrogen starvation was not reported in experiments no. 1 to 8. Therefore, it was not possible to estimate the radiation characteristics and the MRPA $\langle \mathscr{A} \rangle$ for those experiments.

Figures 4.6a and 4.6b respectively present the temporal evolution of the MRPA $\langle \mathscr{A} \rangle$ and of the cellular TAG concentration during the course of experiments no. 9 and 10. The approximate time at which nitrogen starvation began was estimated from elemental analysis

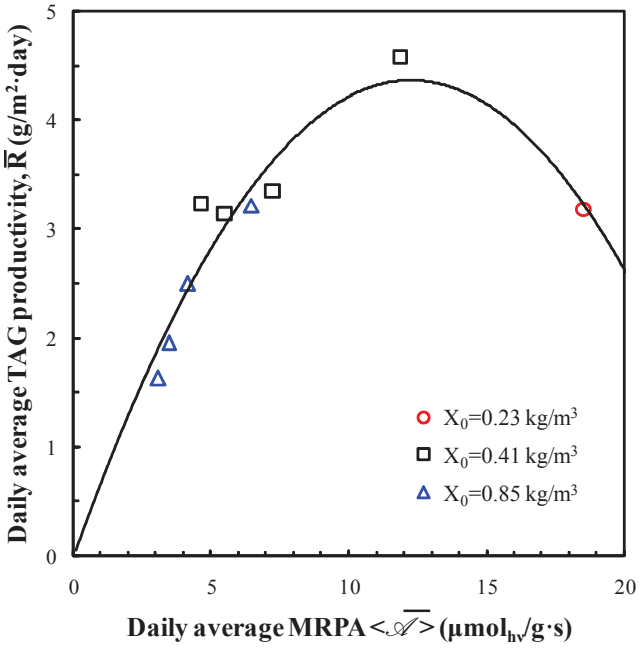

Figure 4.6: Temporal evolution of (a) MRPA $\langle\mathscr{A}\rangle$ and (b) cellular TAG concentration for progressive starvation batch cultures grown in a 150 L PBR, 5 cm in thickness, in modified Conway medium with an initial NO_3^- concentration of 0.93 mM (experiment no. 9) and 1.65 mM (experiment no. 10) by Van Vooren *et al.* [Van Vooren *et al.*(2012)]. The dashed lines indicate the estimated time at which nitrogen starvation began.

assuming that *N. oculata* was composed of 10 dry wt.% nitrogen in nutrient replete conditions [Takache *et al.*(2012)]. Nitrogen starvation occurred later in experiment no. 10 than in experiment no. 9 because of the larger initial nitrate concentration. For both experiments, the extrapolated MRPA $\langle \mathscr{A}_0 \rangle$ at the onset of the nitrogen starvation fell between 12 and 15 $\mu\text{mol}_{h\nu}/\text{g}\cdot\text{s}$. This corresponded, approximately, to the value of the critical MRPA $\langle \mathscr{A}_0 \rangle_{cr}$ observed in the sudden starvation experiments. The intracellular TAG concentration increased sharply after nitrogen starvation began and reached 28 dry wt.%. It is remarkable that both progressive and sudden starvation experiments had a similar MRPA at the onset of nitrogen starvation since it is not possible to control and set MRPA at the onset of nitrogen starvation $\langle \mathscr{A}_0 \rangle$ for progressive nitrogen starvation experiments. This provided further evidence in the relevance of MRPA $\langle \mathscr{A}_0 \rangle$ in predicting the TAG accumulation in cells.

Along with nitrogen starvation, the term "light stress" has often been used in the literature as a necessary condition for large TAG productivity [Hu *et al.*(2008)]. However, the concept of "light stress" has remained qualitative. The present study addressed this issue by defining the physical variable to quantify "light stress", namely the rate of photon absorption (MRPA). It also reported the critical value of the MRPA necessary for large TAG productivity.

The maximum batch averaged areal TAG and biomass productivities achieved were respectively 2.9 and 7.5 $\text{g/m}^2\cdot\text{day}$, obtained for the experiment with initial biomass concentration X_0=0.41 kg/m^3. The associated volumetric TAG and biomass productivities were 0.1 and 0.25 $\text{kg/m}^3\cdot\text{day}$, respectively. These productivities could be significantly increased by optimizing the MRPA in the PBR using the proposed relation between TAG productivity R and MRPA $\langle \mathscr{A} \rangle$. The latter can also be used to predict the TAG productivity of PBRs of all scales and optimize them as long as rigorous radiation transfer analysis is performed to estimate MRPA $\langle \mathscr{A} \rangle$. Pruvost and Cornet [Pruvost and Cornet(2012)] validated this approach by optimizing and predicting both biomass concentration and productivity of microorganisms in PBRs scaling from 1 to 150 L.

Future studies should focus on validating the present observations and quantitative ana-

lysis for other microalgae species and developing novel methods of optimizing the instantaneous TAG production rate R with respect to MRPA $\langle \mathscr{A} \rangle$. The latter depends on biomass concentration, cell pigment content, and incident PFD. These parameters are dynamic and interdependent. They will be difficult to control, especially in a batch cultivation exposed to solar radiation. Therefore, while an optimum value of MRPA exists that maximizes TAG productivity, it may not be trivial to control and optimize MRPA $\langle \mathscr{A} \rangle$. Moreover, the optimum and critical MRPA may depend on culture conditions such as medium salinity, pH, or temperature. In the present study, the microalgae were cultivated under conditions leading to maximal biomass and TAG productivity reported by Van vooren *et al.* [Van Vooren *et al.*(2012)] and Pruvost *et al.* [Pruvost *et al.*(2009)]. The methodology presented here could be extended to investigate the effects of cultivation conditions on the optimal and critical MRPA.

4.5 Conclusion

This study demonstrated the existence of a relation between the mean rate of photon absorption (MRPA) per unit mass of microalgae and the daily TAG productivity of *N. oculata* cultures. It indicated that TAG synthesis in the PBR was physically limited by the photon absorption rate per unit mass of microalgae. The TAG productivity reached a maximum of 4.5 g/m^2·day corresponding to MRPA equal to 13 $\mu\text{mol}_{h\nu}$/g·s. In addition, a critical initial MRPA $\langle \mathscr{A}_0 \rangle_{cr}$ in excess of also 13 $\mu\text{mol}_{h\nu}$/g·s was required to trigger a large accumulation of TAG in cells in both sudden and progressive nitrogen starvation.

CHAPTER 5

Influence of light absorption on TAG accumulation and TAG productivity by nitrogen limited continuous cultures grown in photobioreactors

abstract

This study aims to elucidate the role of light absorption rate on the triacyglycerol (TAG) accumulation in cells and TAG productivity in nitrogen limited *Parachlorella kessleri* cultures. In nitrogen starvation batch cultures the cells accumulate large amounts of TAGs at the expense of cell multiplication and growth. In continuous nitrogen limited cultures, microalgae cells can simultaneously accumulate TAG and grow, albeit at a slower rate. First, *P. kessleri* were cultivated in flat-plate PBR with a constant dilution rate of 0.01 1/h and feed-medium nitrate concentration ranging from 16 to 1 mM. For each culture, the stead-state biomass, pigment, and TAG concentration as well as the absorption and scattering cross-sections of the microalgae were measured. The TAG productivity depended on both biomass productivity and cellular TAG concentration. The former depended on the rate of photon absorption in the PBR and the later depended on the nitrate concentration in the feed medium and the light attenuation profile in the PBR. The maximum areal TAG productivity of 2.6 $g/m^2 \cdot day$ was obtained for the culture with feed-medium nitrate concentration of 3.65 mM. To the best of our knowledge this is the largest continuous TAG productivity reported to date using photosynthetic microorganisms. The TAG productivity can be further increased by optimizing the culture dilution rate and the feed-medium nitrogen concentration.

5.1 Introduction

We demonstrated in the previous chapter that there was a correlation between the TAG accumulation in cells or the TAG productivity in the PBR and the mean rate of photon absorption in the PBR. The latter depends on the incident irradiance on the surface of the PBR and the light attenuation inside the PBR influenced by the biomass concentration and the cell pigment concentration. Optimization of the energy absorption rate in the PBR in batch processes was found to be complex due to the interdependency of pigment and biomass concentrations and the light attenuation in the PBR and due to continuous temporal evolution of the aforementioned parameters. Therefore, continuous cultures where all physiological parameters of the culture are in steady-state presents an ideal scenario to study TAG metabolism with respect to light absorption by cells and to optimize these culture conditions for maximum TAG productivity for the biodiesel production process.

5.2 Materials and methods

All experiments were conducted using the microalgae *Parachlorella kessleri* UTEX2229 from the culture collection of UTEX (Austin, TX). It was cultivated in a modified Bold Basal medium with the following composition (in mM) $NaNO_3$ 8.02, $Na_2EDTA{\cdot}2H_2O$ 0.122, $MgSO_4{\cdot}7H_2O$ 0.83, K_2HPO_4 0.78, KH_2PO_4 0.88, $CaCl_2{\cdot}2H_2O$ 0.155, $FeSO_4{\cdot}7H_2O$ 0.046, $ZnSO_4\,\mathrm{cot}7H_2O$ 7.72 $\times 10^{-4}$, $CuSO_4$ 4.95 $\times 10^{-4}$, $MnCl_2{\cdot}4H_2O$ 9.15 $\times 10^{-3}$, H_3BO_3 4.63 $\times 10^{-2}$, $Co(NO_3)_2{\cdot}6H_2O$ 1.51 $\times 10^{-4}$, Na_2MoO_4 1.06 $\times 10^{-3}$, and $NaHCO_3$ 0.005.

All experiments were performed in a 3 cm thick, 1 L airlift-type flat-panel PBR (Figure 1.8a). The pH was measured using a pH sensor (Mettler Toledo SG 3253) and was set to 8 by the injection of CO_2 in the culture medium when the pH exceeded the desired set value. The temperature was maintained at approximately 22 ^{o}C by forced air convection at the back of the PBR. Mixing was achieved by injecting air in the PBR at the rate of 80 ml/min. The PBR was illuminated from the front side by a white LED light panel (P4 Cool White, Seoul Semiconductor) with a photon flux density (PFD) over the PAR region equal

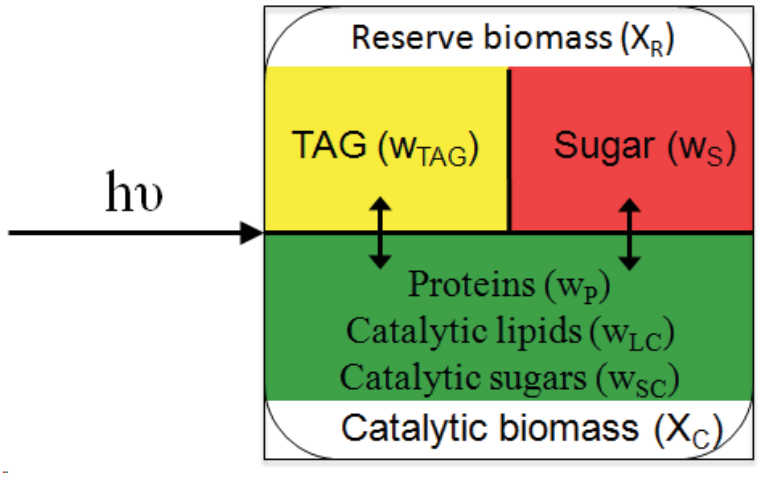

Figure 5.1: Representation of the different partitions of biomass in the cell.

to 250 $\mu\text{mol}_{h\nu}/\text{m}^2\cdot\text{s}$. The incident PFD was measured on the inside surface of the PBR at twelve different locations using a quantum light sensor (Li-250A, Li-COR, Lincoln, NE). The reported PFD was averaged over the 12 locations and showed a variation of less than 10%.

All continuous cultures were operated in chemostat mode. A Stepdos pump (08/RC, KNF, Freiburg, Germany) was used to continuously pump fresh medium in the PBR at a culture dilution rate D of 0.01 h^{-1} (10 ml/h). The culture was harvested by overflowing the PBR. All the measurements were performed in triplicates and were described in detail in the previous chapter.

The steady-state TAG productivity R_{TAG} was estimated according to

$$R_{TAG} = D \cdot X \cdot w_{TAG} \tag{5.1}$$

where X is the dry biomass concentration (in kg/m^3) and w_{TAG} is the cellular TAG concentration (in dry wt.%).

The PAR averaged fluence rate $G_{PAR}(z)$ in the PBR was estimated according to the two-flux approximation [Pottier *et al.*(2005), Kandilian *et al.*(2014a)]. The MRPA $\mathscr{A}$ was estimated by

$$\mathscr{A}(z) = \frac{\mathscr{A}_\gamma}{X_C} \tag{5.2}$$

Here, X_C (in kg/m^3) is the catalytic biomass concentration and $\mathscr{A}_Y$ is the MVRPA given by Equation (1.27). The biomass X of a microalgal culture can be partitioned into the catalytic X_C and the reserve X_R biomass [Cornet *et al.*(1998)] as shown in Figure 5.1.

$$X = X_C + X_R \tag{5.3}$$

The major components of the cell are proteins, carbohydrates or sugars, and lipids [Cornet *et al.*(1998)]. The sugar or carbohydrates can be located in the cell walls where they have an active function or they can be stored intracellularly as reserves [Cornet *et al.*(1998)]. Similarly, lipids can be divided into membrane and storage lipids [Cornet *et al.*(1998)].

The reserve biomass X_R is the cells' carbon storage and they are accumulated as a response to stress. These include TAG lipids as well as intracellular sugar reserves expressed as

$$X_R = w_{TAG}X + w_S X - w_{SC}X_C \tag{5.4}$$

Here, the reserve biomass consisted of both sugars and TAG lipids. It was assumed that in optimally grown cultures the cells did not accumulate sugar reserves. Thus, the catalytic mass fraction of sugar w_{sc} was estimated from cultures grown in optimal conditions according to $w_{SC} = X_S/X$ where X_S was the concentration of sugar. The fraction of catalytic biomass that was made up of sugar w_{SC} was assumed to be constant for all the nitrogen limited cultures and it was subtracted from the total sugar concentration in the biomass $w_s X$. Finally, by combining Equations (5.3) and (5.4), the catalytic biomass can be expressed as a function of the total biomass X according to

$$X_C = \frac{1 - w_{TAG} - w_S}{1 - w_{SC}} X \tag{5.5}$$

5.3 Results

5.3.1 Biomass, pigments, and TAG concentrations

Figure 5.2 shows the biomass and total pigment concentrations of *P. kessleri* during nitrogen limitation during approximately 1600 hours of operation. The culture was considered to be in steady-state when biomass, pigment, and TAG concentrations were approximately constant during three consecutive days or measurements. Once the culture reached steady-state, the nitrate concentration in the feed medium was changed and the culture was allowed to reach its new steady-state. The experiment was repeated to obtain the steady-state characteristics of the culture at feed-medium nitrate concentration of 5 mM (data not shown). Table 5.1 summarized the biomass, pigment, total lipid, TAG, sugar, and protein concentrations at the different feed-medium nitrate concentrations. The culture reached a steady-state biomass and pigment concentrations of 2.2 kg/m^3 and 184 mg/m^3, respectively, when nitrate was supplied in excess (16 mM). There was a slight increase in the biomass concentration reaching 2.6 kg/m^3 at the beginning stages of nitrate limitation between days 14 and 20 of cultivation. This may be attributed to the increase in the rate of photon absorption in the PBR in response to the decrease in pigment concentration. Once the culture reached steady-state conditions, the biomass concentration had decreased to 1.8 kg/m^3. Indeed, both biomass and pigment concentrations decreased in response to nitrogen limitation. The pigment concentration decreased by approximately two orders of magnitude when the feed-medium nitrate concentration was reduced from 16 mM to 1 mM while the biomass concentration decreased by 50%. The biomass concentration decreased to 1.9, 1.8, 1.55, and 1.0 kg/m^3 when the nitrate concentration in the feed medium was adjusted to 5, 3.56, 2.3, and 1 mM, respectively. Moreover, both biomass and pigment concentrations decreased non-linearly with decreasing nitrate concentration in the feed-medium. For example, a large decrease in biomass concentration coincided with a small decrease in the pigment concentration and *vice versa*. In fact, the biomass concentration decreased by 13% and 37% when the nitrate concentration was reduced from 3.56 mM to 2.3 mM and from 2.3 to 1 mM, respectively. Conversely, for the

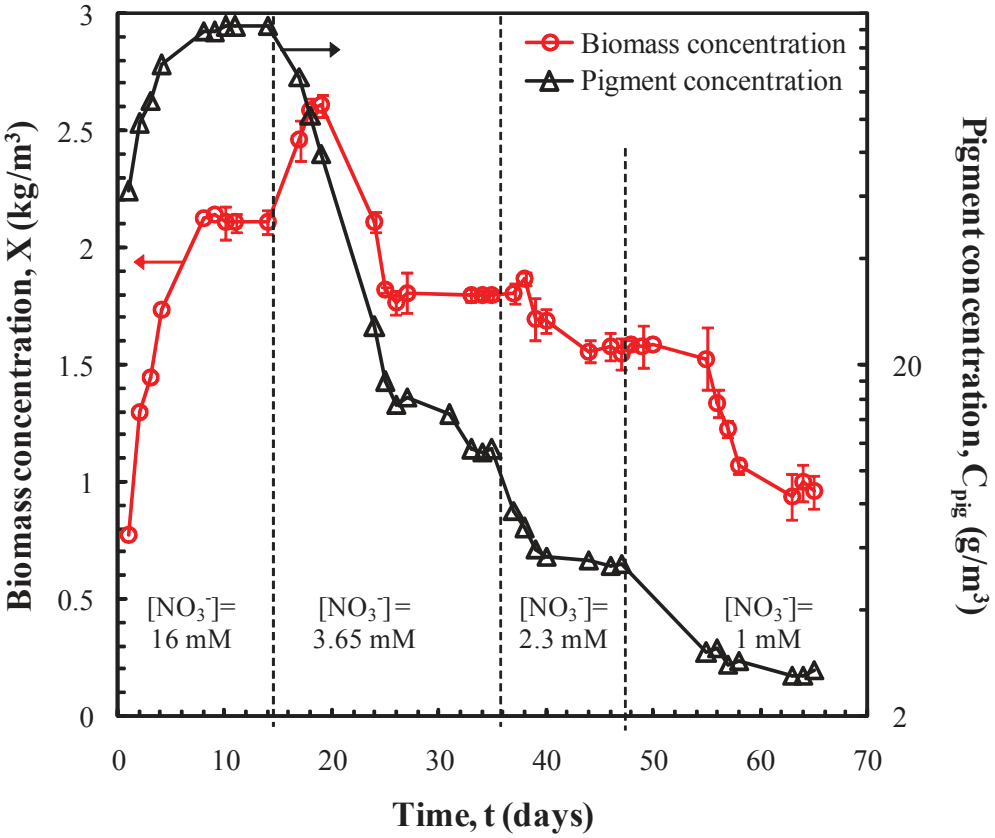

Figure 5.2: Biomass and pigment concentration of *P. kessleri* culture during nitrogen limitation in continuous a PBR [Taleb(2015)].

same conditions, the pigment concentration decreased by 52% and 22%, respectively. This disparity in reduction of biomass and pigment concentrations will alter the rate of photon absorption in the PBR in an unpredictable way in response to the feed-medium nitrate concentration.

The protein and sugar concentrations in the culture in optimum conditions were 58 and 25 wt.%, respectively. However, the sugar concentration increased up to 64 wt.% in nitrate limited culture. This indicates that the cells accumulate sugar as carbon reserve in response to nitrogen limitation. Moreover, as feed-medium nitrate concentration decreased the sugar concentration in the biomass decreased to 46 wt.% and the cells showed more

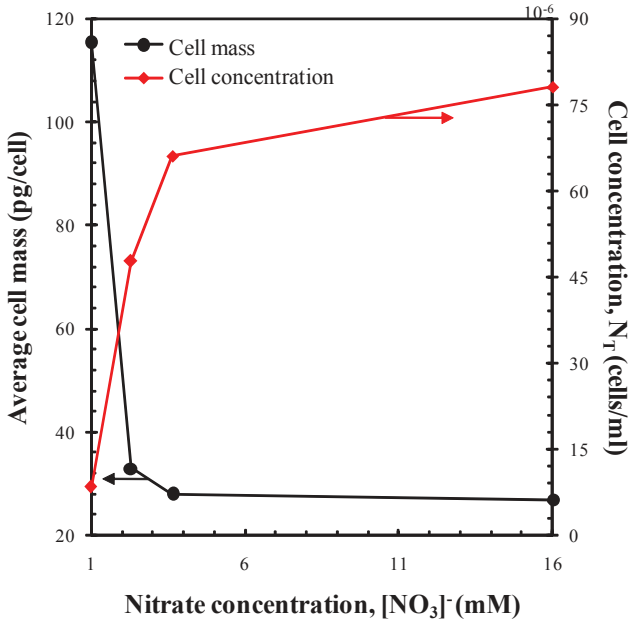

Figure 5.3: Average cell mass and cell concentration in continuous *P. kessleri* cultures grown with feed-medium nitrate concentration 1, 2.2, 3.65, or 16 mM.

affinity to accumulating TAG lipids. Moreover, the protein concentration in nitrogen limited cultures decreased to 9 wt.% for cultures with feed-medium nitrate concentration of 1 mM. This indicates that majority of the biomass in these cultures were in the form of carbon reserves. Table 5.1 also shows the catalytic biomass concentration estimated using Equation (5.5). It illustrates the decline in the catalytic biomass concentration as the cells became limited in nitrogen. For example, in optimal growth conditions, approximately 90% of the biomass was catalytic. By contrast, only 21% of the biomass of the culture fed with nitrate concentration of 3.65 mM was catalytic. This may impact negatively on the cells ability to perform photosynthesis. Note that the sugar concentration of the culture fed with 5 mM of nitrates was not measure but it was estimated as 50 dry wt.% by linearly interpolating the sugar concentration of the culture fed with nitrate replete medium and the one with nitrate concentration equal to 3.65 mM .

Figure 5.3 plots the average cell mass and cell concentration in continuous *P. kessleri*

Table 5.1: Total and catalytic biomass, pigment, protein, lipid, and sugar concentrations of *P. kessleri* cultivated in nitrogen limited conditions with feed-medium nitrogen concentration ranging from 1 mM to 16 mM, dilution rate of 0.01 1/h, and an incident photon flux density of 250 $\mu\text{mol}_{h\nu}/\text{m}^2\cdot\text{s}$.

Nitrate	Biomass	Cell	Pigment	Chla	Chlb	Carotnoids	Total lipid	TAG	Sugar	Protein	Cat. biomass
$[NO_3^-]$	X	N_T	C_{pig}	C_{chla}	C_{chlb}	C_{PPC}	w_L	w_{TAG}	w_S	w_P	X_C
(mM)	(kg/m3)	(cells/ml)	(g/m^3)	(wt. %)	(wt. %)	(wt. %)	(wt. %)	(wt. %)	(wt. %)	(wt. %)	(kg/m^3)
16	2.25	7.8×10^7	184	5.2	1.1	1.3	11	7	25	58	2.05
5	1.9	-	58	2.0	0.49	0.61	13	8.6	-	-	1.05
3.65	1.8	6.6×10^7	11	0.39	0.084	0.15	21	20	64	14	0.41
2.3	1.6	4.8×10^7	5.5	0.24	0.04	0.1	19	16	50	9	0.72
1	0.98	8.4×10^6	2.6	0.16	0.032	0.093	27	24	46	9	0.39

cultures grown with feed-medium nitrate concentration 1, 2.2, 3.65, or 16 mM. The cell concentration was larger in cultures grown with larger feed-medium nitrate concentration. It also illustrates the increase in average cell mass when the culture was subjected in nitrogen limitation. Indeed, the average cell mass was equal to 27 pg/cell during optimal growth conditions. It increased 4.25 fold to 115 pg/cell for cells grown in nitrogen limited conditions. This can be attributed to the accumulation of biomass reserve in cells in response to the nitrogen limited conditions.

Figure 5.4 plots the TAG concentration in the cells and TAG productivity as a function of nitrate concentration in the feed medium. The TAG concentration w_{TAG} was 7 dry wt.% and TAG productivity R_{TAG} was 1.1 g/m^2·day when the cells were cultivated in nutrient replete conditions. For nitrogen limited cultures, the maximum TAG concentration in cells w_{TAG} peaked at $[NO_3]^-$=1 mM, i.e., the smallest concentration of nitrates in the feed-medium tested. On the other hand, the maximum areal productivity R_{TAG} peaked at 2.6 g/m^2·day when the nitrate concentration was 3.65 mM. This suggests that to achieve large TAG productivity, the culture must feature both a large biomass productivity and a relatively large TAG concentration. Indeed, while the PBR fed with 1 mM of nitrates featured the largest TAG accumulation in cells, 24 dry wt.%, it suffered from the lowest areal biomass productivity corresponding to 7 g/m^2·day. This resulted in a relatively small TAG productivity. Note that there was no clear relationship between nitrate concentration in the feed medium and the TAG concentration or productivity indicating that nitrogen limitation was not the only factor affecting TAG accumulation in cells. This is consistent with previous findings suggesting that nitrogen limitation was necessary but not a sufficient condition for producing cells rich in TAG lipids [Pruvost *et al.*(2009), Van Vooren *et al.*(2012), Kandilian *et al.*(2014b)]. This was illustrated more clearly with the culture fed with nitrate concentration of 5 mM. Here, the cells were nitrate limited as evident by the 68% reduction in pigment concentration in the culture. However, the cells did not accumulate large amounts of TAG lipids. Indeed, a large mean rate of photon absorption was necessary to produce biomass containing large concentrations of TAG [Kandilian *et al.*(2014b)].

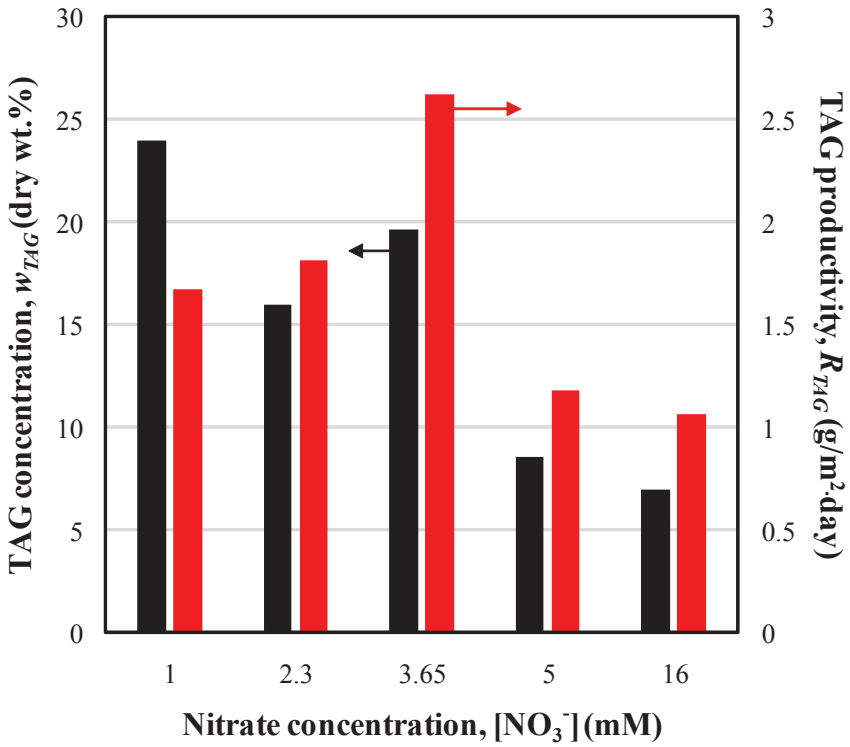

Figure 5.4: TAG concentration w_{TAG} and TAG productivity R_{TAG} of *P. kessleri* of continuous cultures with feed medium nitrate concentration of 1, 2.3, 3.56, 5, and 16 mM.

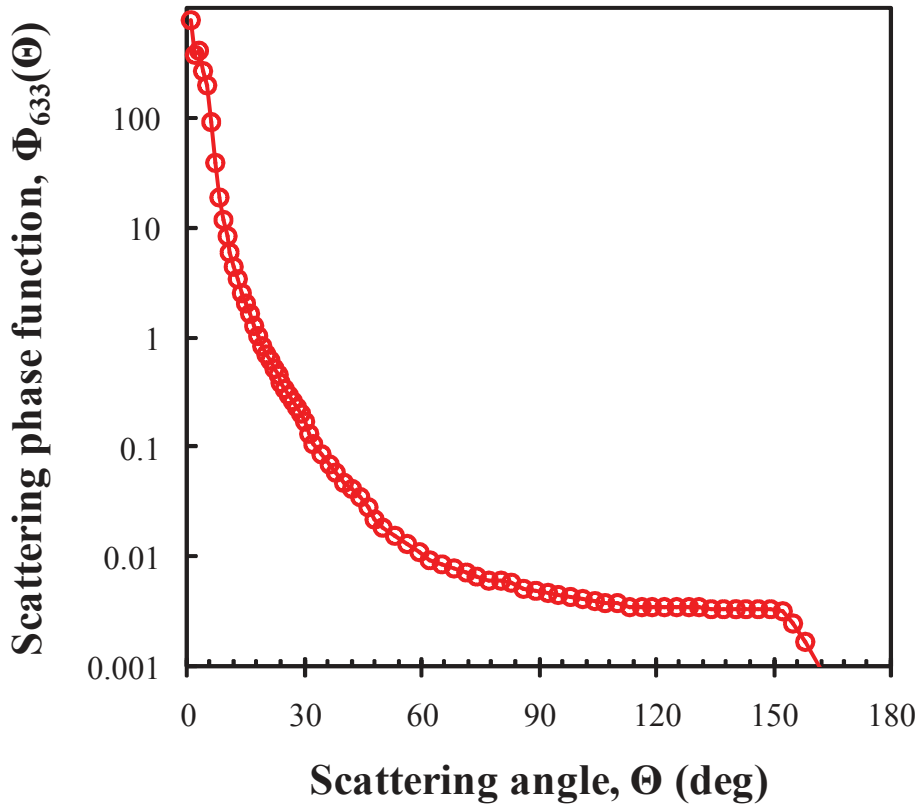

Figure 5.5: The scattering phase function of *P. kessleri* culture during nutrient replete phase.

5.3.2 Radiation characteristics of *P. kessleri*

5.3.2.1 Scattering phase function

Figure 5.5 shows the measured scattering phase function of *P. kessleri* suspension at 633 nm grown in nutrient replete conditions. It was assumed that the scattering phase function did not change as a function of nitrate concentration in the feed medium [Kandilian *et al.*(2013)]. As expected, given the large cell diameter compared with the wavelength of light, scattering was mainly in the forward direction with asymmetry factor found to be $g_{633} = 0.989$ at 633 nm. Furthermore, the backward scattering ratio was very small and

equal to $b_{633} = 0.002$.

5.3.2.2 Absorption and scattering cross-sections

Figure 5.6a and 5.6b, respectively, show the absorption $A_{abs,\lambda}$ and scattering $S_{sca,\lambda}$ cross-sections of *P. kessleri* cells grown in continuous cultures with feed-medium nitrate concentration corresponding to 5, 3.65, 2.3, 1 mM. As previously observed with *Nannochloropsis oculata*, the absorption cross-section decreased across all wavelengths with decreasing nitrogen concentration in the medium [Kandilian *et al.*(2013), Kandilian *et al.*(2014b)]. The decrease in absorption cross-section was consistent with the decrease in the pigment concentration of the cells. The absorption cross-section at 435 nm $A_{abs,435}$ decreased by 75% when the feed-medium nitrate concentration was reduced from 5 mM to 1 mM. Moreover, the magnitude and the shape of the scattering cross-section changed slightly with feed-medium nitrogen concentration. For example, the scattering cross-section at 550 nm, corresponding to the wavelength with lowest absorption cross-section, decreased by 20% when the nitrate concentration in the feed-medium was reduced from 16 mM to 1 mM. However, it increased by 40% at 435 nm corresponding to one of chlorophyll*a* absorption peaks. The changes in the shape and magnitude of the scattering cross-section can be due to changes in the pigment concentration of cells, or cell size and shape, or biochemical composition of the cells [Jonasz and Fournier(2007)]. The changes in absorption and scattering cross-sections of cells during nitrogen limitation will have significant effect on the light availability and light absorption rate in the PBR.

5.3.3 Mean rate of photon absorption

Figure 5.7a and 5.7b show the TAG concentration in dry wt.% as a function of the mean rate of photon absorption $\langle \mathscr{A} \rangle$ in the PBR for the *P. kessleri* cultures with different feed-medium nitrate concentration per unit biomass and per unit catalytic biomass, respectively. There is no clear relation between cellular TAG concentration w_{TAG} and MRPA $\langle \mathscr{A} \rangle$ when

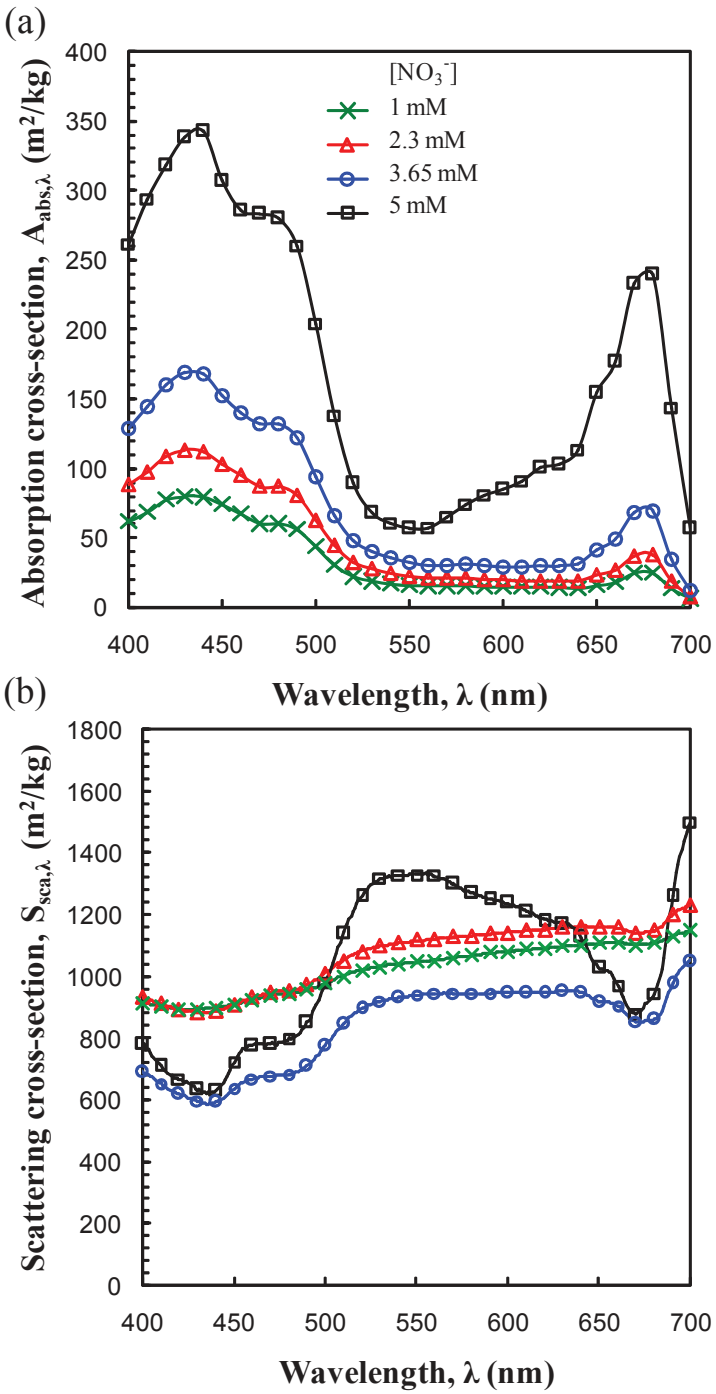

Figure 5.6: The absorption and scattering cross-sections of *P. kessleri* for various nitrogen limited cultures.

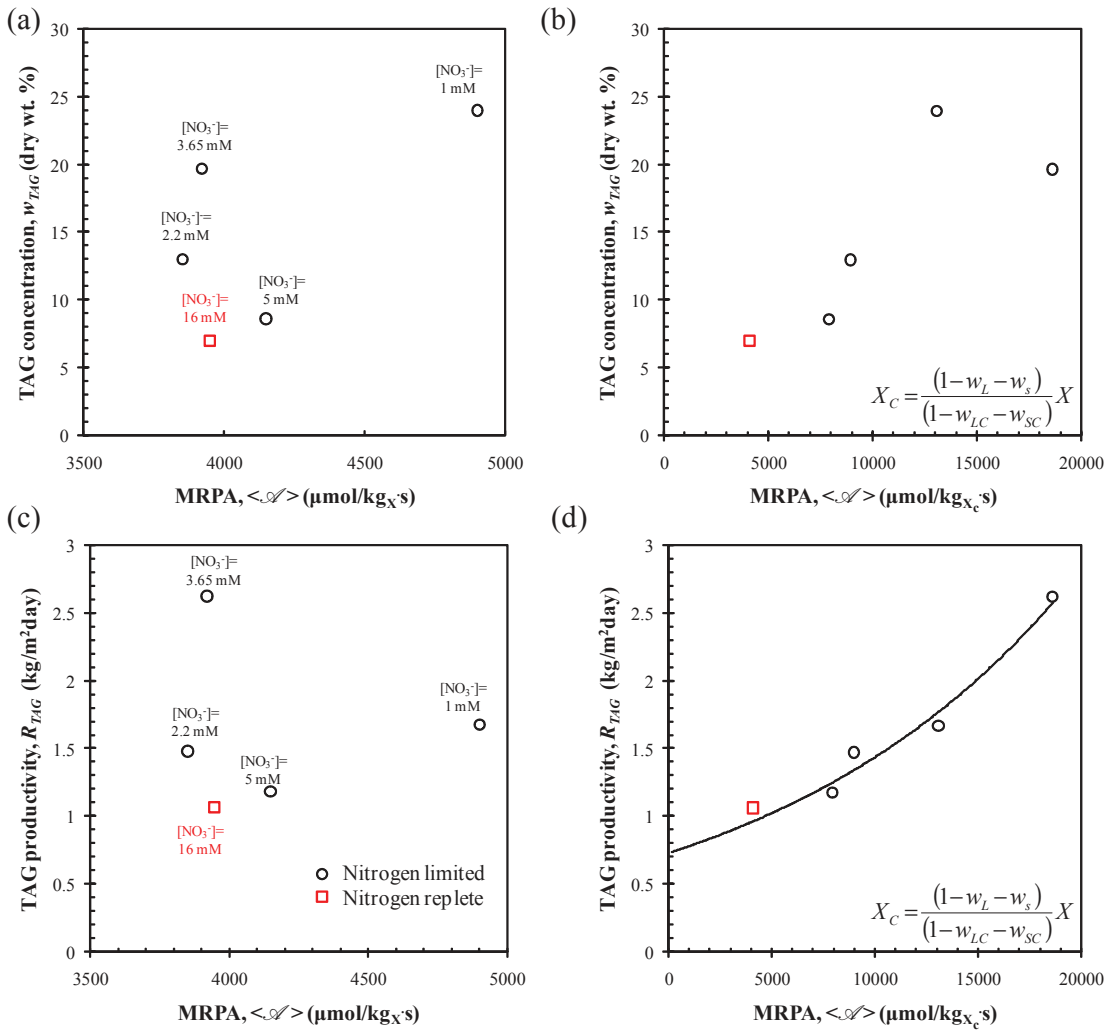

Figure 5.7: TAG concentration as a function of MRPA expressed per (a) kg of total biomass and (b) kg of catalytic biomass and TAG productivity as a function of MRPA expressed per (c) kg of total biomass (d) kg of catalytic biomass.

the latter was estimated per gram of total biomass. However, there was a correlation between the TAG concentration and w_{TAG} and MRPA $\langle \mathscr{A} \rangle$ expressed per kg of catalytic biomass X_C. The TAG concentration w_{TAG} increased with increasing MRPA $\langle \mathscr{A} \rangle$. On the other hand, the culture with feed-medium of 3.65 mM had the largest MRPA $\langle \mathscr{A} \rangle$ but not the largest TAG concentration w_{TAG}. Here, despite the large rate of photon absorption by cells, the culture did not accumulate the most amount of TAG lipids. In this case, the cells may have used the absorbed energy to synthesize sugar instead of TAGs. Indeed, as previously discussed the culture fed with 3.56 mM of nitrates accumulated approximately 65 dry wt.% sugars and was presumed to have higher affinity to accumulating sugars than TAG lipids as the form of carbon storage. This observation is consistent with previous findings in Chapter 4 indicating that a large MRPA $\langle \mathscr{A} \rangle$ was necessary for cells to accumulate large amount of TAG lipids by dry weight. This effect was more apparent and more clearly illustrated here as the continuous culture had achieved steady-state and the physical conditions such as the pH, the nutrient concentration, the fluence rate $G_{PAR}(z)$ and LRPA $\mathscr{A}(z)$ in the PBR remained constant with time. The increase in TAG accumulation in cells with increasing MRPA $\langle \mathscr{A} \rangle$ is consistent with the hypothesis that *de novo* TAG synthesis pathway is activated to quench the excess electrons generated in the photosynthetic electron transport chain when cells absorb large quantities of light [Hu *et al.*(2008)]. It is presumed that energy is sunk in TAG synthesis to prevent damage to the cells by reactive oxygen species. Indeed, the synthesis of fatty acids require significantly more energy in the form of NADPH to synthesize compared to proteins and carbohydrates of similar mass [Hu *et al.*(2008)]. This may also be the reason for activation of secondary carotenoid synthesis pathway along with TAG production. Carotenoids such as β-carotene, lutein, astaxanthin are esterified along with TAG and stored in lipid bodies to protect the cell from large irradiances [Hu *et al.*(2008)]. This can be observed by the increase in the carotenoids to chlorophyll ratio seen in cultures with smaller feed-medium nitrate concentration.

Figure 5.7c and 5.7d show the TAG productivity R_{TAG} as a function of the mean rate of photon absorption $\langle \mathscr{A} \rangle$ in the PBR for the *P. kessleri* cultures with different feed-medium

nitrate concentration per unit biomass and per unit catalytic biomass, respectively. Similar to TAG concentration, there is no clear relation between TAG productivity and MRPA $\langle \mathscr{A} \rangle$ per kg of total biomass. However, the TAG productivity increased with increasing MRPA $\langle \mathscr{A} \rangle$ per kg of catalytic biomass. This indicates that the TAG production rate is light limited. In other words, as the light absorption rate increased so did the TAG production rate. In Chapter 4 TAG productivity and MRPA had a parabolic relation. This may be due to the different method of estimating the MRPA and it may be due to differences between batch and continuous cultures. Note that in outdoor batch or continuous cultures it is complex to control the MRPA of the culture. Here it was demonstrated that it may be possible to set the MRPA of the cultures cultivated in continuous mode by adjusting the nitrate concentration. However, as previously discussed the latter also modifies the carbon flux in the cell reserves thus further complicating any effort to optimize the TAG production rate by controlling the MRPA in the PBR.

5.3.4 Local fluence rate and rate of photon absorption

Figures 5.8a and 5.8b show the PAR averaged fluence rate $G_{PAR}(z)$ in the PBR and the rate of photon absorption $\mathscr{A}(z)$, respectively, for cultures with nitrate concentration equal to 5, 3.65, 2.3, and 1 mM. The fluence rate in the PBR $G_{PAR}(z)$ increased as the feed-medium nitrate concentration decreased. This was due to the decrease in the biomass and pigment concentration in the cells as previously mentioned. Similarly, the rate of photon absorption of cells at the back wall of the PBR $\mathscr{A}(L)$ was smaller for cultures with larger nitrate concentration in the feed medium. Note that cultures with smaller back wall fluence rate $G_{PAR}(L)$ or rate of photon absorption $\mathscr{A}(L)$ featured larger biomass productivity. Moreover, these cultures with strong light attenuation also suffered from relatively small MRPA $\langle \mathscr{A} \rangle$ leading to the production of cells with relatively small TAG concentration w_{TAG}.

When the cells are exposed to large RPA A, incident light to biomass or light to TAG conversion may be inhibited due to the dissipation of energy by cells through fluorescence and heat. In this case, the absorbed light can be wasted as heat and light rather than being

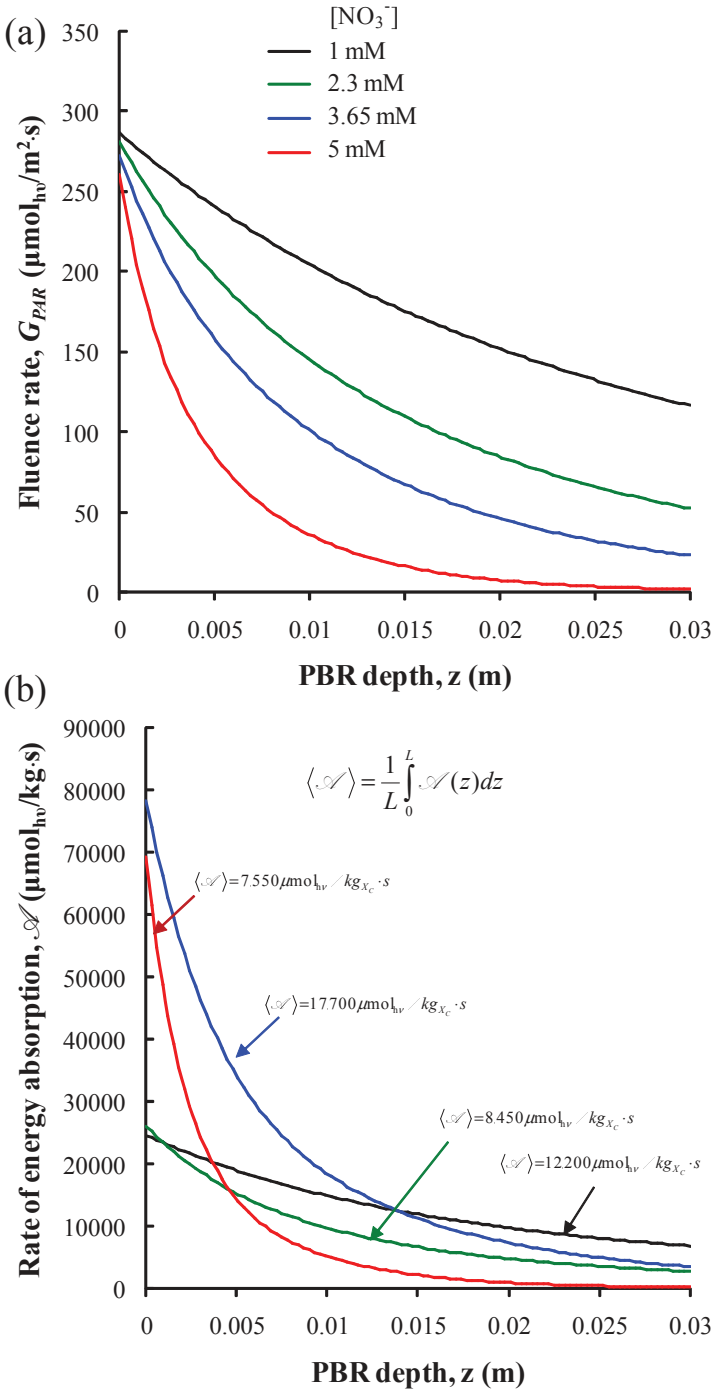

Figure 5.8: The PAR averaged fluence rate $G_{PAR}(z)$ and the rate of photon absorption $\mathscr{A}(z)$ as a function of PBR depth for nitrogen limited *P. kessleri* cultures.

directed into, for example, TAG synthesis thus decreasing TAG productivity. Indeed, the cells in the culture with smaller feed-medium nitrogen concentration should be affected more by this phenomenon due to their severely degraded photosystem and their significantly smaller chlorophyll concentration which may explain the decline in biomass productivity of these cultures. During nitrogen starvation, the cells synthesize photoprotective carotenoids and place them in lipid droplets along with the TAGs [Hu *et al.*(2008)]. These photoprotective carotenoids are not part of the photosystem and only absorb the incident radiant energy in order to quench it and protect the photosystem [Dubinsky and Stambler(2000)]. Therefore, it is reasonable to expect that some of the absorbed radiant energy will not be used for metabolism but it will rather be released as heat.

5.4 Discussion

The maximum TAG productivity of 2.6 g/m^2·day obtained in this study is significantly larger than the 0.64 g/m^2·day reported for *Neochloris oleoabundans* culture grown in turbidostat mode in a 2 cm thick flat-plate PBR exposed to 200 $\mu\text{mol}_{h\nu}$/m^2·s and supplied with a 0.013 g/L·day of potassium nitrate. Note that in turbidostat mode, a constant turbiditiy is maintained in the culture at all times. However, this does not guarantee a constant light absorption rate $\mathscr{A}(z)$ in the PBR across cultures with different feed-medium nitrate concentration. This is due to the decrease in pigment concentration in the cells when feed-medium nitrogen concentration is decreased. The maximum TAG productivity obtained here was also slightly smaller than the maximum TAG productivity of 3.6 g/m^2·day achieved in sudden starvation batch culture of *Nannochloropsis oculata* with an initial biomass concentration of 0.4 kg/m^3 and an incident irradiance of 250 $\mu\text{mol}_{h\nu}$/m^2·s obtained in Chapter 4 and reported by Van Vooren *et al.* [Van Vooren *et al.*(2012)]. Note that the Eustigmatophyte *N. oculata* and the chlorophyte *P. kessleri* belong to different classes of microalgae and may have different TAG metabolism and TAG synthesis pathways and therefore they will most likely respond differently to the method of nitrogen deprivation.

The maximum TAG accumulation in cells was 24 dry wt.% and it was obtained for the

culture with feed-medium nitrate concentration equal to 1 mM. This was significantly smaller than the reported cellular TAG concentration in batch nitrogen starved cultures which can typically reach between 40 and 50 dry wt.% [Pruvost *et al.*(2009),Pruvost *et al.*(2011),Breuer *et al.*(2012),Van Vooren *et al.*(2012),Kandilian *et al.*(2014b),Taleb(2015),Taleb *et al.*(2015)]. The major reason for the low TAG accumulation in the cells may be due to the affinity of the cells in nitrogen limited cultures to accumulate sugar as the carbon storage instead of TAG. A similar trend was observed in batch sudden nitrogen starved *P. kessleri* cultures [Taleb(2015)]. During the initial period of nitrogen starvation (first 4 days of cultivation) when the C/N of the cells was relatively large, the cells accumulated up to 60 dry wt.% sugar and 20 dry wt.% of TAGs. However, as the carbon to nitrogen ratio of the cells increased, the cells catabolized the sugars and they synthesized TAG lipids. In fact, after 14 days of cultivation the biomass featured final sugar and TAG concentrations of 30 and 55 dry wt.%, respectively [Taleb(2015)]. Similar observation can be made, as illustrated in Table 5.1 the cells accumulated sugar as the form of carbon reserves instead of TAGs in nitrogen limitation. The concentration of sugar decreased as the nitrate concentration in the feed-medium decreased. Another reason for the low TAG concentration in the biomass is the fact that the cells do not convert membrane lipids to TAG lipids. Indeed, TAG production occurs via two methods the *de novo* synthesis of TAG (acyl CoA-dependent pathway) or by recycling the membrane lipids (acyl CoA-independent pathway) [Fang(2013)]. The latter reaction is catalyzed by the enzyme phospholipid :diacylglycerol acyltransferase (PDAT) [Hu *et al.*(2008)]. In *C. reinhardtii* and *Nannochloropsis oceanica* overexpression of the PDAT enzyme has been observed during the early stages of nitrogen starvation [Yoon *et al.*(2012),Jia *et al.*(2015)]. However, in continuous nitrogen limited cultures cells need to maintain their membrane lipids. Thus, most of the TAG produced in nitrogen limited cultures must come from the *de novo* synthesis pathway. This may also modify the TAG lipid profile and the quality of the produced biodiesel.

Another significant finding was the disproportionate decrease in biomass and pigment concentrations in response to the decrease in nitrate concentration in the feed-medium. This

suggest that there is no linear or obvious relationship between the fluence rate and the rate of photon absorption in the PBR and the feed-medium nitrate concentration. This complex relationship causes the optimization of light attenuation conditions in the PBR challenging.

Moreover, as much as 420% increase in the average mass of a cell was observed in nitrogen limited cultures compared to ones grown in optimal conditions. A more thorough investigation must be performed to determine if the radius of the cells increased. In fact, cells grown in optimal conditions are typically composed of 78% of water by volume [Dauchet *et al.*(2015)]. The increase in the average mass of the cells may be due to the decrease in the water fraction of cells which can be replaced by solid matter. The density of the latter is much larger than the density of water suggesting that the cells can increase their mass and maintain their size by replacing water with, for example, TAG or sugar. Or the cells could maintain their water volume fraction and instead increase their size to accommodate the increase in the mass of the cells. Either way, the effects may be significant with respect to theoretical determination of the radiation characteristics of the cells. The latter may be useful when performing radiation transfer analysis in nitrogen limited cultures to predict their growth or TAG accumulation kinetics.

As previously stated, the two carbon reserve partitions in the biomass are sugar and TAG lipids. It was demonstrated that depending on the concentration of nitrates in the feed-medium the cells preferred to synthesize more sugar or more TAG. The total amount of reserve biomass synthesized can be correlated to the mean rate of photon absorbed. However, different types of reserve biomass requires different amount of energy to synthesize. For example, TAG lipids may necessitate twice the amount of energy as sugars [Hu *et al.*(2008)]. Therefore, it may be inaccurate to simply correlate the mean rate of photon absorbed (MRPA) to the reserve biomass productivity. The relationship between MRPA and reserve production could be refined by introducing a more detailed modeling the partitioning of TAG vs sugar accumulation during nitrogen limitation.

Several parameters such as the feed-medium nitrate concentration or the dilution rate of the culture can be optimized to increase TAG productivity in nitrogen limited chemostat

cultures. Indeed, such an endeavor may be facilitated by first developing kinetic models that could predict biomass, pigment, and TAG productivity of the cultures during nitrogen limitation. Note that, stable nitrogen limited continuous cultures have not been demonstrated in diurnal light conditions in outdoor PBRs and due to the non-steady illumination condition it may not be possible to produce microalgae in continuous mode under solar conditions. Finally, the chemostat system presented in this study can be used for transcriptional expression study where the steady-state conditions may enable the better understanding of TAG metabolism and TAG synthesis pathways in microalgae.

5.5 Conclusions

This study demonstrated that cellular TAG concentration in continuous *P. kessleri* cultures depended on mean rate of photon absorption in the PBR. First, it was demonstrated that the correct definition of mean rate of photon absorption MRPA should be expressed per kg of catalytic biomass instead of per kg of total biomass. Moreover, the cellular TAG concentration and TAG productivity did not solely depend on the MRPA but it also depended on the nitrate concentration in the culture. Indeed, for relatively large nitrogen concentration in the feed-medium, i.e., $[NO_3^-] \geq 3.65$ mM, the cells preferred to store carbon in the form of sugars. However, as the nitrate concentration in the feed-medium decreased, the cellular concentration of sugars decreased in cells and the TAG concentration in the cells increased. Therefore, TAG accumulation in cells and TAG productivity in the culture are influenced in a complex manner by both the MRPA and the nitrate concentration in the feed-medium. Thus, the light absorption rate in the PBR and nitrate concentration in the medium must be carefully controlled to maximize TAG productivity.

Conclusion

Liquid biofuels, especially biodiesel, produced by photosynthetic microorganisms is touted as the renewable energy sources that will satisfy the transportation fuel needs of the future. However, it has so far proved to be uneconomical to produce biomass in PBRs or raceways exposed to solar radiation. This is in part due to the low biomass and TAG productivity of cultures grown in outdoor photobioreactors. Indeed, large-scale reactors often have productivities that are fraction of those corresponding to lab-scale cultures as well as the maximum theoretical yields. These reductions in biodiesel and biomass productivity are mainly attributed to inefficiency in light utilization by the PBRs. This work addressed some of the outstanding issues preventing from economical large scale outdoor biodiesel production by elucidating the role of light absorption by microalgae cells on their triglyceride synthesis and productivity.

The first part of the study focused on the interaction between light and photosynthetic microorganisms on a fundamental level to develop methods and procedures for measuring or predicting the radiation characteristics of microorganisms. The radiation characteristics of microorganisms were then utilized to perform radiation transfer analysis on microalgae cultures with the goal understanding the process of TAG production using nitrogen limited microalgae cultures and conceiving rules for optimizing the biodiesel production process.

First, the study presented the validation of a model based on the Lorenz-Mie theory for predicting the radiation characteristics of microorganisms by comparing them to experimentally measured ones. A full set of radiation characteristics, including the absorption and scattering cross-sections and the scattering phase function, were measured experimentally for the microalgae *Chlamydomonas reinhardtii* grown in both optimal and nutrient limited conditions and for the microalgae *Chlorella vulgaris*. The validation was successfully carried out for *C. reinhardtii* grown in optimal or nitrogen limited conditions. However, the theoretical model did not predict the radiation characteristics of *C. vulgaris* accurately. The latter is known to have a thick, rigid cell wall. Modeling the *C. vulgaris* cells as coated spheres with

non-absorbing outer shell resulted in absorption cross-sections that were approximately 15% smaller than the ones predicted for the *C. vulgaris* cells modeled as homogenous spheres. The decrease in the absorption cross-section was most likely due to the package effect. The latter causes a decrease in the effective absorption cross-section due to the dense packing of pigments in the cell. Finally, the mean rate of photon absorption and the illuminated fraction of the PBR were estimated using the radiation characteristics determined by measurement or by prediction. The maximum relative differences in these parameters were less than 6%, 15%, and 5% using radiation characteristics of *C. reinhardtii* grown in optimal conditions, *C. reinhardtii* grown in nitrogen limited conditions, and *C. vulgaris*, respectively.

Then, a simple experimental procedure was developed for retrieving the average spectral absorption cross-section of concentrated microalga suspensions featuring single or multiple scattering samples. The method combined experimental measurements of the normal-hemispherical transmittance and reflectance of the suspensions in conventional cuvettes, using an integrating sphere attached to a UV-VIS spectrometer, and an inverse method based on genetic algorithm and analytical expressions obtained from the modified two-flux approximation. The method was validated with direct measurements of the scattering phase function and of the absorption and scattering cross-sections of freshwater microalgae *Chlorella vulgaris*. It was able to retrieve the absorption cross section with adequate accuracy for correct estimation of mean and local rates of energy absorption in the PBR.

The second part of the work focused on the determination of the relation between light absorption rate and the TAG production by two distinct species, namely, the seawater eustigmatophyceae *Nannochloropsis oculata* and the freshwater species *Parachlorella kessleri* in batch and continuous cultures, respectively. First, a relationship was unraveled between the mean rate of photon absorption (MRPA) per unit mass of microalgae and the daily TAG productivity of n° cultures. This relationship indicated that nitrogen starvation alone does not guarantee large TAG production rate. The TAG biosynthesis kinetics appeared to be limited by the photon absorption rate of the cultures represented by MRPA. The TAG productivity reached a maximum of 4.5 g/m^2·day corresponding to MRPA equal to 13 $\mu\text{mol}_{h\nu}$/gs. In

addition, a critical initial MRPA $\langle \mathscr{A} \rangle$ in excess of also 13 $\mu\text{mol}_{h\nu}$/g was required to trigger a large accumulation of TAG in cells in both sudden and progressive nitrogen starvation. However, in batch cultures, the biomass and pigment concentrations evolved significantly with time and thus MRPA varied significantly during the cultivation period. This obscured the effects of light absorption rate and MRPA on the TAG accumulation of cells. This led to an uncertainty over the exact relation between MRPA and TAG accumulation by cells. Therefore, the concept of critical MRPA was proposed for batch cultures. It suggested that cultures that featured MRPA greater than the critical MRPA at the beginning of nitrogen starvation were guaranteed to achieve the maximum TAG accumulation.

To clarify this relation further, the TAG accumulation and productivity of cells were finally studied in continuous nitrogen limited cultures where all physiological parameters remained in steady-state and did not vary with time. First, a detailed analysis of light attenuation regimes in the cultures revealed that the correct definition of mean rate of photon absorption MRPA was to express it per kg of catalytic biomass instead of per kg of total biomass. Moreover, the cellular TAG concentration and TAG productivity did not solely depend on the MRPA but it also depended on the nitrate concentration in the culture. Indeed, for relatively large nitrogen concentration in the feed-medium, i.e., $[NO_3^-] \geq 3.65$ mM, the cells preferred to store carbon in the form of sugars. However, as the nitrate concentration in the feed-medium decreased, the cellular concentration of sugars decreased in cells and the TAG concentration in the cells increased. Therefore, TAG accumulation in cells and TAG productivity in the culture are influenced in a complex manner by both the MRPA and the nitrate concentration in the feed-medium. Thus, the light absorption rate in the PBR must be carefully controlled to maximize TAG productivity.

Future studies concerning to the radiation characteristics of microalgae should focus on determining the cell wall thickness and the cell wall material of *Chlorella vulgaris* more accurately. Moreover, the cell homogeneity assumption must be investigated more thoroughly. For example, can microalgae cells of all sizes and shapes be assumed to be homogenous ? In addition, the necessity to model the chloroplast as a separate entity inside the cell must be

investigated in the context of cell size and cell pigment concentration. Finally, the relation between MRPA and TAG productivity accumulation can be confirmed in large scale outdoor reactors. The continuous biodiesel production process can also be further enhanced by optimizing the feed-medium nitrate concentration and the dilution rate of the culture. The latter may require the development of kinetic models predicting the biomass and pigment concentration as a function of nitrate concentration. Finally, the successful development of downstream processes (biomass concentration, lipid extraction, conversion to biodiesel, etc.) may be the key for economical biodiesel production from microalgae.

Nomenclature

$\mathscr{A}$	local rate of photon absorption, $\mu\text{mol}_{h\nu}$/g·s
$<\mathscr{A}>$	mean rate of photon absorption, $\mu\text{mol}_{h\nu}$/g·s
$\bar{A}_{abs}$	average mass absorption cross-section, m^2/kg
b_λ	backward scattering ratio
c	speed of light, m/s
Ea	*in vivo* pigment specific absorption cross-section, m^2/kg
f	number frequency distribution
G_{in}	incident irradiance, $\mu\text{mol}_{h\nu}/\text{m}^2$·s
G	fluence rate, $\mu\text{mol}_{h\nu}/\text{m}^2$·s
g_λ	Henyey-Greenstein asymmetry factor
I	radiation intensity, W/m^2·nm·sr
k	absorption index
k_c	absorption index of core
L	PBR thickness, cm
l	cuvette pathlength, cm
m	relative complex index of refraction
N_λ	normalized spectral distribution of light source
n	refractive index
N_T	cell number density, cells/m^3
P	Cauchy principal value
Q_{abs}	absorption efficiency factor
r_{TAG}	areal TAG productivity, kg/m^2·day
R	areal TAG productivity, kg/m^2·day
$\hat{s}$	direction vector
$\bar{S}_{sca}$	average mass scattering cross-section, m^2/kg
T	transmittance

t	time, hours
X	biomass concentration, kg/m^3
V	microalgae sample volume, m^3
v	volume of solvent, m^3
w	pigment mass fraction
x_w	water fraction of cells
z	PBR depth coordinate, cm

Greek symbols

β	extinction coefficient, m^{-1}
κ	absorption coefficient, m^{-1}
ϵ	spheroid aspect ratio
ϵ_n	spectrometer correction factor
ϵ_h	integrating sphere correction factor
γ	illuminated fraction of PBR
λ	wavelength, nm
ν	frequency of radiation, s^{-1}
Ω	solid angle, sr
Φ_λ	scattering phase function
ρ_{dry}	dry biomass density, kg/m^3
σ_s	single scattering coefficient, m^{-1}
Θ	scattering angle, degrees
τ	batch cultivation duration, days
ξ	apparent extinction coefficient, m^{-1}

Subscripts

0	initial
32	Sauter mean

avg	refers to average
c	compensation point
cr	critical
eq	volume equivalent
f	final
h	normal-hemispherical
i	inner radius
inc	incident
n	normal-normal
o	outer radius
p	anchor point
sca	scattered

Acronyms and abbreviations

ASW	artificial sea water
chl$a$	chlorophyll a
LRPA	local rate of photon absorption
MRPA	mean rate of photon absorption
MVRPA	mean volumetric rate of photon absorption
OD	optical density
PAR	Photosynthetically active radiation
PBR	photobioreactor
PPC	photoprotective carotenoids
PSC	photosynthetic carotenoids
PS I	Photosystem I
PS II	Photosystem II
TAG	triglyceride fatty acid

References

[Adams *et al.*(2013)] Adams, C., Godfrey, V., Wahlen, B., Seefeldt, L., and Bugbee, B. (2013). Understanding precision nitrogen stress to optimize the growth and lipid content tradeoff in oleaginous green microalgae. *Bioresource Technology*, 131(1), 188–194.

[Administration(2013)] Administration, U. S. E. I. (2013). Annual energy review. "http ://www.eia.gov/totalenergy/data/monthly/pdf/sec1_3.pdf".

[Aiba(1982)] Aiba, S. (1982). Growth kinetics of photosynthetic microorganisms. In *Microbial Reactions*, volume 23 of *Advances in Biochemical Engineering*, pages 85–156. Springer Berlin Heidelberg.

[Allen(2004)] Allen, J. (2004). Cytochrome b6f : structure for signalling and vectorial metabolism. *Trends in Plant Science*, 9(3), 130–137.

[ASU(2014)] ASU, A. S. U. (2014). Vertical flat-plate photobioreactors. http ://biofuels.asu.edu/biomaterials.shtml.

[Atkinson *et al.*(1972)] Atkinson, A., Gunning, B., and John, P. (1972). Sporopollenin in the cell wall of *Chlorella* and other algae : Ultrastructure, chemistry, and incorporation of 14C-acetate, studied in synchronous cultures. *Planta*, 107(1), 1–32.

[Baeck(1996)] Baeck, T. (1996). *Genetic Algorithms in Theory and Practice*. The Oxford University Press, Oxford, UK.

[Baroli and Melis(1996)] Baroli, I. and Melis, A. (1996). Photoinhibition and repair in *Dunaliella salina* acclimated to different growth irradiances. *Planta*, 198, 640–646.

[Béchet *et al.*(2013)] Béchet, Q., Shilton, A., and Guieysse, B. (2013). Modeling the effects of light and temperature on algae growth : State of the art and critical assessment for productivity prediction during outdoor cultivation. *Biotechnology Advances*, 31(8), 1648 – 1663.

[Bellini *et al.*(2014)] Bellini, S., Bendoula, R., Latrille, E., and Roger, J.-M. (2014). Potential of a spectroscopic measurement method using adding-doubling to retrieve the bulk optical properties of dense microalgal media. *Applied Spectroscopy*, 68(10), 1154–1167.

[Berberoğlu *et al.*(2007)] Berberoğlu, H., Yin, J., and Pilon, L. (2007). Light transfer in bubble sparged photobioreactors for H_2 production and CO_2 mitigation. *International Journal of Hydrogen Energy*, 32(13), 2273–2285.

[Berberoğlu *et al.*(2008)] Berberoğlu, H., Pilon, L., and Melis, A. (2008). Radiation characteristics of *Chlamydomonas reinhardtii* CC125 and its truncated chlorophyll antenna transformants *tla1, tlaX* and *tla1-CW+*. *International Journal of Hydrogen Energy*, 33(22), 6467–6483.

[Berges *et al.*(2001)] Berges, J., Franklin, D., and Harrison, P. (2001). Evolution of an artificial seawater medium : Improvements in enriched seawater, artificial water over the last two decades. *Journal of Phycology*, 37(6), 1138–1145.

[Bidigare *et al.*(1990)] Bidigare, R. R., Ondrusek, M. E. E., Morrow, J. H. H., and Kiefer, D. A. A. (1990). *In-vivo* absorption properties of algal pigments. *Proceedings of the SPIE*, 1302, 290–302.

[Bissett *et al.*(1997)] Bissett, W., Patch, J., Carder, K., and Lee, Z. (1997). Pigment packaging and chlorophyll a-specific absorption in high-light oceanic waters. *Limnology and Oceanography*, 42(5), 961–968.

[Björkman(1981)] Björkman, O. (1981). Responses to different quantum flux densities. In O. Lange, P. Nobel, C. Osmond, and H. Ziegler, editors, *Physiological Plant Ecology I : Responses to the Physical Environment*, volume 12A of *Encyclopedia of Plant Physiology New Series*, pages 57–107. Springer-Verlag, Berlin.

[BP(2014)] BP (2014). Energy outlook 2035. bp.com/energyoutlook.

[Brennan and Owende(2013)] Brennan, L. and Owende, P. (2013). Biofuels from microalgae : Towards meeting advanced fuel standards. In J. W. Lee, editor, *Advanced Biofuels and Bioproducts*, pages 553–599. Springer New York.

[Breuer *et al.*(2012)] Breuer, G., Lamers, P. P., Martens, D. E., Draaisma, R. B., and Wijffels, R. H. (2012). The impact of nitrogen starvation on the dynamics of triacylglycerol accumulation in nine microalgae strains. *Bioresource Technology*, 124, 217–226.

[Breuer *et al.*(2013)] Breuer, G., Lamers, P. P., Martens, D., Draaisma, R., and Wijffels, R. (2013). Effect of light intensity, pH, and temperature on triacylglycerol (TAG) accumulation induced by nitrogen starvation in *Scenedesmus obliquus*. *Bioresource Technology*, 143, 1–9.

[Briassoulis *et al.*(2010)] Briassoulis, D., Panagakis, P., Chionidis, M., Tzenos, D., Lalos, A., Tsinos, C., Berberidis, K., and Jacobsen, A. (2010). An experimental helical-tubular photobioreactor for continuous production of *Nannochloropsis sp. Bioresource Technology*, 101(17), 6768–6777.

[Bricaud *et al.*(2004)] Bricaud, A., Claustre, H., Ras, J., and Oubelkheir, K. (2004). Natural variability of phytoplanktonic absorption in oceanic waters : Influence of the size structure of algal populations. *Journal of Geophysical Research*, 109(C11), 1947–1960.

[Carvalho *et al.*(2011)] Carvalho, A., Silva, S., Baptista, J., and Malcata, F. (2011). Light requirements in microalgal photobioreactors : an overview of biophotonic aspects. *Applied Microbiology and Biotechnology*, 89, 1275–1288.

[Cassano *et al.*(1995)] Cassano, A., Martin, C., Brandi, R., and Alfano, O. (1995). Photoreactor analysis and design : Fundamentals and applications. *Industrial & Engineering Chemistry Research*, 34(7), 2155–2201.

[Charbonneau(1995)] Charbonneau, P. (1995). Genetic algorithms in astronomy and astrophysics. *The Astrophysical Journal Supplement Series*, 101, 309–334.

[Charbonneau(2002a)] Charbonneau, P. (2002a). An Introduction to Genetic Algorithms for Numerical Optimization. Technical Report NCAR Technical Note 450+IA, National Center for Atmospheric Research.

[Charbonneau(2002b)] Charbonneau, P. (2002b). Release Notes for PIKAIA 1.2. Technical Report NCAR Technical Note 451+STR, National Center for Atmospheric Research.

[Charbonneau and Knapp(1995)] Charbonneau, P. and Knapp, B. (1995). A User's guide to PIKAIA 1.0. Technical Report NCAR Technical Note 418+IA, National Center for Atmospheric Research.

[Chen *et al.*(2011)] Chen, C., Yeh, K., A., R., Lee, D., and Chang, J. (2011). Cultivation, photobioreactor design and harvesting of microalgae for biodiesel production : A critical review. *Bioresource Technology*, 102(1), 71–81.

[Chisti(2007)] Chisti, Y. (2007). Biodiesel from algae. *Biotechnology Advances*, 25, 294–306.

[Chisti(2012)] Chisti, Y. (2012). Raceways-based production of algal crude oil. In C. Posten and C. Walter, editors, *Microalgal Biotechnology : Potential and Production*, pages 113–144. De Gruyter, Berlin, Germany.

[Chisti(2013)] Chisti, Y. (2013). Constraints to commercialization of algal fuels. *Journal of Biotechnology*, 167(3), 201–214.

[Cohen(1999)] Cohen, Z. (1999). *Chemicals from Microalgae*. Taylor & Francis, London, UK.

[Cornet and Dussap(2009)] Cornet, J. and Dussap, C. (2009). A simple and reliable formula for assessment of maximum volumetric productivities in photobioreactors. *Biotechnology Progress*, 25, 424–435.

[Cornet *et al.*(1992a)] Cornet, J.-F., Dussap, C., and Dubertret, G. (1992a). A structured model for simulation of cultures of the cyanobacterium *Spirulina platensis* in photobioreactors : I. Coupling between light transfer and growth kinetics. *Biotechnology and Bioengineering*, 40, 817–825.

[Cornet *et al.*(1992b)] Cornet, J.-F., Dussap, C., Cluzel, P., and Dubertret, G. (1992b). A structured model for simulation of cultures of the cyanobacterium *Spirulina platensis* in photobioreactors : II. Identification of kinetic parameters under light and mineral limitations. *Biotechnology and Bioengineering*, 40, 826–834.

[Cornet *et al.*(1995)] Cornet, J.-F., Dussap, C., Gross, J., Binois, C., and Lasseur, C. (1995). A simplified monodimensional approach for modeling coupling between radiant light transfer and growth kinetics in photobioreactors. *Chemical Engineering Science*, 50, 1489–1500.

[Cornet *et al.*(1998)] Cornet, J.-F., Dussap, C., and Gros, J.-B. (1998). Kinetics and energetics of photosynthetic micro-organisms in photobioreactors. In *Bioprocess and Algae Reactor Technology, Apoptosis*, volume 59 of *Advances in Biochemical Engineering Biotechnology*, pages 153–224. Springer Berlin Heidelberg.

[Croughan *et al.*(2015)] Croughan, M., Konstantinov, K., and Cooney, C. (2015). The future of industrial bioprocessing : Batch or continuous ? *Biotechnology and Bioengineering*, 112(4), 648–651.

[Dauchet(2012)] Dauchet, J. (2012). *Analyse Radiative des Photobioréacteurs*. Ph.D. thesis, Université Blaise Pascal, Clermont Ferrand, France.

[Dauchet *et al.*(2013)] Dauchet, J., Blanco, S., Cornet, J., Hafi, M. E., Eymet, V., and Fournier, R. (2013). The practice of recent radiative transfer Monte Carlo advances and its contribution to the field of microorganisms cultivation in photobioreactors. *Journal of Quantitative Spectroscopy and Radiative Transfer*, 128, 52–59.

[Dauchet *et al.*(2015)] Dauchet, J., Blanco, S., Cornet, J.-F., and Fournier, R. (2015). Calculation of the radiative properties of photosynthetic microorganisms. *Journal of Quantitative Spectroscopy and Radiative Transfer*, 161, 60–84.

[Dombrovsky *et al.*(2005)] Dombrovsky, L., Randrianalisoa, J., Baillis, D., and Pilon, L. (2005). Use of Mie theory to analyze experimental data to identify infrared properties of fused quartz containing bubbles. *Applied Optics*, 44(33), 7021–7031.

[Dubinsky and Stambler(2000)] Dubinsky, Z. and Stambler, N. (2000). Photoacclimation processes in phytoplankton : mechanisms, consequences, and applications. *Aquatic Microbial Ecology*, 56, 163–176.

[EU(2013)] EU, E. C. (2013). Renewable energy progress report. REPORT# COM(2013) 175 final.

[EU(2009)] EU, T. E. P. . T. C. O. T. E. U. (2009). Directive 2009/28/ec of the european parliament and of the council.

[Fang(2013)] Fang, S.-C. (2013). Biofuels from algae. chapter Metabolic Engineering and Molecular Biotechnology of Microalgae for Fuel Production, pages 47–65. Elsevier, San Diego, CA, first edition.

[Feng *et al.*(2011)] Feng, Y., Li, C., and Zhang, D. (2011). Lipid production of *Chlorella vulgaris* cultured in artificial wastewater medium. *Bioresource Technology*, 102(1), 101 – 105.

[Ferrell and Sarisky-Reed(2010)] Ferrell, J. and Sarisky-Reed, V. (2010). National Algal Biofuels Technology Roadmap. Technical Report DOE/EE-0332, Department of Energy, Office of Energy Efficiency and Renewable Energy, Biomass Program, Maryland, Washington DC.

[Fisher *et al.*(1996)] Fisher, T., Minnaard, J., and Dubinsky, Z. (1996). Photoacclimation in the marine alga *Nannochloropsis* sp. (eustigmatophyte) : a kinetic study. *Journal of Plankton Research*, 18(10), 1797–1818.

[Flynn *et al.*(1993)] Flynn, K., Davidson, K., and Cunningham, A. (1993). Relations between carbon and nitrogen during growth of *Nannochloropsis oculata* (droop) Hibberd under continuous illumination. *New Phytologist*, 125(4), 717–722.

[Francis *et al.*(1975)] Francis, G., Strand, L., Lien, T., and Knutsen, G. (1975). Variations in the carotenoid content of *Chlamydomonas reinhardii* throughout the cell cycle. *Archives of Microbiology*, 104(1), 249–254.

[Frank *et al.*(2013)] Frank, E., Elgowainy, A., Han, J., and Wang, Z. (2013). Life cycle comparison of hydrothermal liquefaction and lipid extraction pathways to renewable diesel from algae. *Mitigation and Adaptation Strategies for Global Change*, 18(1), 137–158.

[Geken *et al.*(2013)] Geken, H., Donohoe, B., and Knoshaug, E. (2013). Enzymatic cell wall degradation of *Chlorella vulgaris* and other microalgae for biofuels production. *Planta*, 237(1), 239–253.

[Gentile and Blanch(2001)] Gentile, M.-P. and Blanch, H. W. (2001). Physiology and xanthophyll cycle activity of *Nannochloropsis gaditana*. *Biotechnology and Bioengineering*, 75(1), 1–12.

[Griffiths and Harrison(2009)] Griffiths, M. and Harrison, S. (2009). Lipid productivity as a key characteristic for choosing algal species for biodiesel production. *Journal of Applied Phycology*, 21(5), 493–507.

[Heath *et al.*(1990)] Heath, M., Richardson, K., and Kiørboe, T. (1990). Optical assessment of phytoplankton nutrient depletion. *Journal of Plankton Research*, 12(2), 381–396.

[Heng and Pilon(2014)] Heng, R.-L. and Pilon, L. (2014). Time-dependent radiation characteristics of *Nannochloropsis oculata* during batch culture. *Journal of Quantitative Spectroscopy and Radiative Transfer*, 144, 154 – 163.

[Heng *et al.*(2014a)] Heng, R.-L., Sy, K., and Pilon, L. (2014a). Absorption and scattering by bispheres, quadspheres, and circular rings of spheres and their equivalent coated spheres. *Journal of Optical Society of America A*. (under review).

[Heng *et al.*(2014b)] Heng, R.-L., Lee, E., and Pilon, L. (2014b). Radiation characteristics and optical properties of filamentous cyanobacteria *Anabaena cylindrica*. *Journal of the Optical Society of America A*, 31(4), 836–845.

[Hodgson *et al.*(1991)] Hodgson, P., Henderson, R., Sargent, J., and Leftley, J. (1991). Patterns of variation in the lipid class and fatty acid composition of *Nannochloropsis oculata* (eustigmatophyceae) during batch culture. *Journal of Applied Phycology*, 3, 169–181.

[Hoffmann *et al.*(2010)] Hoffmann, M., Marxen, K., Schulz, R., and Vanselow, K. (2010). TFA and EPA productivities of *Nannochloropsis salina* influenced by temperature and nitrate stimuli in turbidostatic controlled experiments. *Marine Drugs*, 8(9), 2526–2545.

[Hu *et al.*(2008)] Hu, Q., Sommerfeld, M., Jarvis, E., Ghirardi, M., Posewitz, M., Seibert, M., and Darzins, A. (2008). Microalgal triacylglycerols as feedstocks for biofuel production : perspectives and advances. *The Plant Journal*, 54(4), 621–639.

[Hulst(1957)] Hulst, H. V. D. (1957). *Light Scattering by Small Particles*. Wiley, New York, NY.

[IPCC(2007)] IPCC (2007). *Climate Change 2007 : Impacts, Adaptation and Vulnerability. Contribution of Working Group II to the Fourth Assessment Report of the Intergovernmental Panel on Climate Change*. Cambridge University Press, Cambridge, UK.

[Jia *et al.*(2015)] Jia, J., Han, D., Gerken, H., Li, Y., Sommerfeld, M., Hu, Q., and Xu, J. (2015). Molecular mechanisms for photosynthetic carbon partitioning into storage neutral lipids in *Nannochloropsis oceanica* under nitrogen-depletion conditions. *Algal Research*, 7, 66 – 77.

[Jonasz and Fournier(2007)] Jonasz, M. and Fournier, G. (2007). *Light Scattering By Particles In Water : Theoretical and Experimental Foundations*. Academic Press, San Diego, CA.

[Jones and Mayfield(2012)] Jones, C. and Mayfield, S. (2012). Algae biofuels : versatility for the future of bioenergy. *Current Opinion in Biotechnology*, 23(3), 346–351.

[Jones(2010)] Jones, M. (2010). Calvin cycle. http ://commons.wikimedia.org/wiki/File :Calvin-cycle4.svg.

[Kandilian *et al.*(2013)] Kandilian, R., Lee, E., and Pilon, L. (2013). Radiation and optical properties of *Nannochloropsis oculata* grown under different irradiances and spectra. *Bioresource Technology*, 137, 63 – 73.

[Kandilian *et al.*(2014a)] Kandilian, R., Tsao, T.-C., and Pilon, L. (2014a). Control of incident irradiance on a batch operated flat-plate photobioreactor. *Chemical Engineering Science*, 119, 99 – 108.

[Kandilian *et al.*(2014b)] Kandilian, R., Pruvost, J., Legrand, J., and Pilon, L. (2014b). Influence of light absorption rate by *Nannochloropsis oculata* on triglyceride production during nitrogen starvation. *Bioresource Technology*, 163, 308 – 319.

[Kanehisa Laboratories(2014)] Kanehisa Laboratories (2014). Photosynthesis - reference pathway. http ://www.genome.jp/kegg/pathway/map/map00195.html.

[Ke(2001)] Ke, B. (2001). *Photosynthesis : Photobiochemistry and Photobiophysics*. Advances in Photosynthesis. Kluwer Academic Publishers, Dordrecht, The Netherlands.

[Kellar and Box(1981)] Kellar, B. M. and Box, M. (1981). The scaling group of the radiative transfer equation. *Journal of the Atmospheric Sciences*, pages 1063–1068.

[Khozin-Goldberg and Cohen(2011)] Khozin-Goldberg, I. and Cohen, Z. (2011). Unraveling algal lipid metabolism : Recent advances in gene identification. *Biochimie*, 93(1), 91 – 100.

[Klok *et al.*(2013)] Klok, A. J., Martens, D. E., Wijffels, R. H., and Lamers, P. P. (2013). Simultaneous growth and neutral lipid accumulation in microalgae. *Bioresource Technology*, 134, 233 – 243.

[Kong and Vigil(2014)] Kong, B. and Vigil, R. D. (2014). Simulation of photosynthetically active radiation distribution in algal photobioreactors using a multidimensional spectral radiation model. *Bioresource Technology*, 158, 141–148.

[Krinsky and Levine(1964)] Krinsky, N. and Levine, R. (1964). Carotenoids of wild type and mutant strains of the green alga, *Chlamydomonas reinhardtii*. *Plant Physiology*, 39(4), 680–687.

[Lee *et al.*(2013)] Lee, E., Heng, R.-L., and Pilon, L. (2013). Spectral optical properties of selected photosynthetic microalgae producing biofuels. *Journal of Quantitative Spectroscopy and Radiative Transfer*, 114, 122 – 135.

[Lee *et al.*(2014)] Lee, E., Pruvost, J., He, X., Ramakanth, R., and Pilon, L. (2014). Design tool and guidelines for outdoor photobioreactors. *Chemical Engineering Science*, 106, 18–29.

[Lehana(1990)] Lehana, M. (1990). Kinetic analysis of the growth of *Chlorella vulgaris*. *Biotechnology and Bioengineering*, 36(2), 198–206.

[Li *et al.*(2013)] Li, X., Pribyl, P., Bisova, K., Kawano, S., Cepak, V., Zachleder, V., Cizkova, M., Branyikova, I., and Vitova, M. (2013). The microalga *Parachlorella kessleri* a novel highly efficient lipid producer. *Biotechnology and Bioengineering*, 110(1), 97–107.

[Liska *et al.*(2014)] Liska, A., Yang, H., Milner, M., Goddard, S., Blanco-Canqui, H., Pelton, M., Fang, X., Zhu, H., and Suyker, A. (2014). Biofuels from crop residue can reduce soil carbon and increase CO_2 emissions. *Nature Climate Change*, 4, 398–401.

[Liu *et al.*(2013a)] Liu, F., Wong, C., Snelling, D., and Smallwood, G. (2013a). Investigation of absorption and scattering properties of soot aggregates of different fractal dimension at 532 nm using RDG and GMM. *Aerosol Science and Technology*, 47(12), 1393–1405.

[Liu *et al.*(2013b)] Liu, X., Saydah, B., Eranki, P., Colosi, L., Mitchell, B., Rhodes, J., and Clarens, A. (2013b). Pilot-scale data provide enhanced estimates of the life cycle energy and emissions profile of algae biofuels produced via hydrothermal liquefaction. *Bioresource Technology*, 148, 163 – 171.

[Lubián *et al.*(2000)] Lubián, L. M., Montero, O., Moreno-Garrido, I., Huertas, I. E., Sobrino, C., del Valle, M. G., and Pares, G. (2000). *Nannochloropsis* (eustigmatophyceae) as source of commercially valuable pigments. *Journal of Applied Phycology*, 12, 249–255.

[Melis *et al.*(1998)] Melis, A., Neidhardt, J., and Benemann, J. (1998). *Dunaliella salina (Chlorophyta)* with small chlorophyll antenna sizes exhibit higher photosynthetic productivities and photon use efficiencies than normally pigmented cells. *Journal of Applied Phycology*, 10, 515–525.

[Mendes *et al.*(2003)] Mendes, R., Nobre, B., Cardoso, M., Pereira, A., and Palavra, A. (2003). Supercritical carbon dioxide extraction of compounds with pharmaceutical importance from microalgae. *Inorganica Chimica Acta*, 356(0), 328 – 334.

[Merchant *et al.*(2012)] Merchant, S., Kropat, J., Liu, B., Shaw, J., and Warakanont, J. (2012). TAG, you're it ! *Chlamydomonas* as a reference organism for understanding algal triacylglycerol accumulation. *Current Opinion in Biotechnology*, 23(3), 352 – 363.

[Modest(2003)] Modest, M. (2003). *Radiative Heat Transfer*. Academic Press, San Diego, CA.

[Modest(2013)] Modest, M. (2013). *Radiative Heat Transfer*. Elsevier, Oxford, UK, third edition.

[Mohan *et al.*(2013)] Mohan, S., Devi, M., Subhash, G., and Chandra, R. (2013). Biofuels from algae. chapter Algae Oils as Fuels, pages 155–187. Elsevier, San Diego, CA, first edition.

[Moody *et al.*(2014)] Moody, J., McGinty, C., and Quinn, J. (2014). Global evaluation of biofuel potential from microalgae. *Proceedings of the National Academy of Sciences*, 111(23), 8691–8696.

[Murphy and Berberoğlu(2011)] Murphy, T. and Berberoğlu, H. (2011). Effect of algae pigmentation on photobioreactor productivity and scale-up : A light transfer perspective. *Journal of Quantitative Spectroscopy and Radiative Transfer*, 112(18), 2826 – 2834.

[Nelson *et al.*(1993)] Nelson, N., Prezelinl, B., and Bidigare, R. (1993). Phytoplankton light absorption and the package effect in California coastal waters. *Marine Ecology Progress Series*, 94, 217–227.

[Oeschger and Posten(2012)] Oeschger, L. and Posten, C. (2012). Construction and assessment parameters of photobioreactors. In C. Posten and C. Walter, editors, *Microalgal Biotechnology : Potential and Production*, pages 225–236. De Gruyter, Berlin, Germany.

[Pal *et al.*(2011)] Pal, D., Khozin-Goldberg, I., Cohen, Z., and Boussiba, S. (2011). The effect of light, salinity, and nitrogen availability on lipid production by *Nannochloropsis sp.* *Applied Microbiology and Biotechnology*, 90(4), 1429–1441.

[Pilon and Kandilian(2015)] Pilon, L. and Kandilian, R. (2015). Interaction between light and photosynthetic microorganisms. In J. Legrand, editor, *Thematic Issue on Photobioreaction Engineering*, volume 46 of *Advances in Chemical Engineering*. Elsevier, The Netherlands.

[Pilon *et al.*(2011)] Pilon, L., Berberoğlu, H., and Kandilian, R. (2011). Radiation transfer in photobiological carbon dioxide fixation and fuel production by microalgae. *Journal of Quantitative Spectroscopy and Radiative Transfer*, 112(17), 2639–2660.

[Pottier *et al.*(2005)] Pottier, L., Pruvost, J., Deremetz, J., Cornet, J.-F., Legrand, J., and Dussap, C. (2005). A fully predictive model for one-dimensional light attenuation by C*hlamydomonas reinhardtii* in a torous photobioreactor. *Biotechnology and Bioengineering*, 91, 569–582.

[Prahl *et al.*(1993)] Prahl, S., van Gemert, M., and Welch, A. (1993). Determining the optical properties of turbid media by using the adding-doubling method. *Applied Optics*, 32(4), 559–568.

[Pruvost and Cornet(2012)] Pruvost, J. and Cornet, J. (2012). Knowledge models for the engineering and optimization of photobioreactors. In C. Posten and C. Walter, editors, *Microalgal Biotechnology : Potential and Production*, pages 181–224. De Gruyter, Berlin, Germany.

[Pruvost *et al.*(2006)] Pruvost, J., Pottier, L., and Legrand, J. (2006). Numerical investigation of hydrodynamic and mixing conditions in a torus photobioreactor. *Chemical Engineering Science*, 61, 4476–4489.

[Pruvost *et al.*(2009)] Pruvost, J., Vooren, G. V., Cogne, G., and Legrand, J. (2009). Investigation of biomass and lipids production with *Neochloris oleoabundans* in photobioreactor. *Bioresource Technology*, 100(23), 5988–5995.

[Pruvost *et al.*(2011)] Pruvost, J., Cornet, J., Goetz, V., and Legrand, J. (2011). Modeling dynamic functioning of rectangular photobioreactors in solar conditions. *AIChE Journal*, 57(7), 1947–1960.

[Pruvost *et al.*(2016)] Pruvost, J., Gouic, B. L., Lepine, O., Legrand, J., and Borgne, F. L. (2016). Microalgae culture in building-integrated photobioreactors : Biomass production modelling and energetic analysis. *Chemical Engineering Journal*, 284, 850 – 861.

[Quirantes and Bernard(2006)] Quirantes, A. and Bernard, S. (2006). Light-scattering methods for modeling algal particles as a collection of coated and/or nonspherical scatterers. *Journal of Quantitative Spectroscopy and Radiative Transfer*, 100(1-3), 315–324.

[Ritchie(2006)] Ritchie, R. (2006). Consistent sets of spectrophotometric chlorophyll equations for acetone, methanol and ethanol solvents. *Photosynthesis Research*, 89(1), 27–41.

[Rodolfi *et al.*(2009)] Rodolfi, L., Zittelli, G. C., Bassi, N., Padovani, G., Biondi, N., Bonini, G., and Tredici, M. R. (2009). Microalgae for oil : Strain selection, induction of lipid synthesis and outdoor mass cultivation in a low-cost photobioreactor. *Biotechnology and Bioengineering*, 102(1), 100–112.

[Rodriguez-Amaya(2001)] Rodriguez-Amaya, D. (2001). *A Guide to Carotenoid Analysis in Foods*. ILSI Press, Washington D.C.

[Seambiotic Ltd.(2014)] Seambiotic Ltd., I. (2014). Open ponds. http ://www.seambiotic.com/.

[Soulies(2014)] Soulies, A. (2014). *Contribution à L'étude hydrodynamique et à la modélisation des photobioréacteurs à haute productivité volumique*. Ph.D. thesis, Université de Nantes, Saint Nazaire, France.

[Souliés *et al.*(2013)] Souliés, A., Pruvost, J., Legrand, J., Castelain, C., and Burghelea, T. (2013). Rheological properties of suspensions of the green microalga *Chlorella vulgaris* at various volume fractions. *Rheologica Acta*, 52(6), 589–605.

[Soulies *et al.*(2016)] Soulies, A., Pruvost, J., Castelain, C., Burghelea, T., and Legrand, J. (2016). Impact and modeling of using red or white radiations and applying an incident angle on *Chlorella vulgaris* microalga growth in intensified photobioreactors. *Biotechnology and Bioengineering*. in review.

[Stephens *et al.*(2010)] Stephens, E., Ross, I., King, Z., Mussgnug, J., Kruse, O., Posten, C., Borowitzka, M., and Hankamer, B. (2010). An economic and technical evaluation of microalgal biofuels. *Nature Biotechnology*, 28(2), 126–128.

[Strickland and Parsons(1968a)] Strickland, J. and Parsons, T. (1968a). *A Practical Handbook of Seawater Analysis*. Fisheries Research Board of Canada, Ottawa, Canada.

[Strickland and Parsons(1968b)] Strickland, J. and Parsons, T. (1968b). *A Practical Handbook of Seawater Analysis : Pigment Analysis*. Bulletin of Fisheries Research Board of Canada. Fisheries Research Board of Canada.

[Sydney *et al.*(2013)] Sydney, E., Novak, A., de Carvalho, J., and Soccol, C. (2013). Biofuels from algae. chapter Respirometric Balance and Carbon Fixation of Industrially Important Algae, pages 67–84. Elsevier, San Diego, CA, first edition.

[Takache *et al.*(2010)] Takache, H., Christophe, G., J.-F.Cornet, and Pruvost, J. (2010). Experimental and theoretical assessment of maximum productivities for the microalgae *Chlamydomonas reinhardtii* in two different geometries of photobioreactors. *Biotechnology Progress*, 26(2), 431–440.

[Takache *et al.*(2012)] Takache, H., Pruvost, J., and Cornet, J.-F. (2012). Kinetic modeling of the photosynthetic growth of *Chlamydomonas reinhardtii* in a photobioreactor. *Biotechnology Progress*, 28(3), 681–692.

[Taleb(2015)] Taleb, A. (2015). *Production de Biodiesel à Partir des Microalgues : Recherche de Souches Accumulatrices de lipides et Optimisation des Conditions de Culture en Photobioréacteurs*. Ph.D. thesis, Université de Nantes, Nantes, France.

[Taleb *et al.*(2015)] Taleb, A., Pruvost, J., Legrand, J., Marec, H., Le-Gouic, B., Mirabella, B., Legeret, B., Bouvet, S., Peltier, G., Li-Beisson, Y., Taha, S., and Takache, H. (2015). Development and validation of a screening procedure of microalgae for biodiesel production : Application to the genus of marine microalgae *Nannochloropsis*. *Bioresource Technology*, 177, 224 – 232.

[Tokuşoglu and Ünal(2003)] Tokuşoglu, O. and Ünal, M. (2003). Biomass nutrient profiles of three microalgae : *Spirulina platensis*, *Chlorella vulgaris*, and *Isochrisis galbana*. *Journal of Food Science*, 68(4), 1144–1148.

[Traverse(2007)] Traverse, A. (2007). *Paleopalynology*. Springer, Dordrecht, The Netherlands.

[Van Vooren *et al.*(2012)] Van Vooren, G., Grand, F. L., Legrand, J., Cuine, S., Peltier, G., and Pruvost, J. (2012). Investigation of fatty acids accumulation in *Nannochloropsis oculata* for biodiesel application. *Bioresource Technology*, 124, 421–432.

[Wheaton and Krishnamoorthy(2012)] Wheaton, Z. and Krishnamoorthy, G. (2012). Modeling radiative transfer in photobioreactors for algal growth. *Computers and Electronics in Agriculture*, 87, 64 – 73.

[Williams and Laurens(2010)] Williams, P. J. and Laurens, L. (2010). Microalgae as biodiesel and biomass feedstocks : Review and analysis of the biochemistry, energetics and economics. *Energy Environmental Science*, 3, 554–590.

[Yoon *et al.*(2012)] Yoon, K., Han, D., Li, Y., Sommerfeld, M., and Hu, Q. (2012). Phospholipid :diacylglycerol acyltransferase is a multifunctional enzyme involved in membrane lipid turnover and degradation while synthesizing triacylglycerol in the unicellular green microalga *Chlamydomonas reinhardtii*. *The Plant Cell*, 24(9), 3708–3724.

[Yun and Park(2003)] Yun, Y.-S. and Park, J. (2003). Kinetic modeling of the light-dependent photosynthetic activity of the green microalga *Chlorella vulgaris*. *Biotechnology and Bioengineering*, 83(3), 303–311.

[Zhernovaya *et al.*(2011)] Zhernovaya, O., Sydoruk, O., Tuchin, V., and Douplik, A. (2011). The refractive index of human hemoglobin in the visible range. *Physics in Medicine and Biology*, 56(13), 4013–4021.

[Zou and Richmond(2000)] Zou, N. and Richmond, A. (2000). Light-path length and population density in photoacclimation of *Nannochloropsis sp.* (eustigmatophyceae). *Journal of Applied Phycology*, 12, 349–354.

l'université nantes angers le mans
COMMUNAUTÉ D'UNIVERSITÉS ET ÉTABLISSEMENTS

UNIVERSITÉ DE NANTES

Thèse de Doctorat

Razmig KANDILIAN

Etude du couplage entre limitation azotée et transfert de lumière pour la production de lipides par microalgues en photobioréacteur

Study of coupling between nitrogen limitation and light transport for lipid production by microalgae grown in photobioreactors

Résumé

Les microalgues sont connues pour leur fort potentiel à accumuler les TAG, qui peuvent se convertir en biodiesel. Cependant, la culture des microalgues en photobioréacteurs (PBRs) souffre généralement d'une perte au niveau de la productivité, en raison des limitations du transfert de la lumière au sein de la culture. Afin d'améliorer les productivités de TAG, l'analyse du transfert radiatif doit être effectuée afin d'étudies son rôle dans le processus. La première partie de cette étude a porté sur la détermination des propriétés optiques des microorganismes photosynthétiques. Des méthodes théoriques et expérimentales de détermination de ces propriétés ont été comparées. De plus, une nouvelle méthode expérimentale a été développée pour déterminer la section efficace d'absorption des cellules. La deuxième partie s'est focalisée sur la compréhension de la réalisation entre la vitesse spécifique des photons par la culture et la production intracellulaire de TAG pour des cultures de microalgues en limitation et carence azotées. Une forte accumulation en TAG ainsi qu'une productivité importante en TAG ont ainsi coïncidé avec une vitesse élevée d'absorption d'énergie, ce qui signifie que la production de TAG en carence ou limitation azotée est également limitée par la vitesse spécifique d'absorption des photons par la culture.

Mots clés : Transfert de lumière, photobioréacteur, microalgues, TAG, biodiesel, *Nannochloropsis*, limitation azotee

Abstract

Microalgae are tipped as the feedstock for biodiesel production due to their ability to produce large amounts of triacylglycerols (TAGs) that can be converted to biodiesel. However, microalgae cultivation in photobioreactors (PBRs) typically suffers from low productivity due to light transfer limitations. To optimize microalgae growth rate and productivity, radiation transfer analysis should be performed and light availability in PBR must be optimized. The first part of this study deals with the determination of the radiation characteristics of photosynthetic microorganisms. First, the radiation characteristics of two microalgae *Chlamydomonas reinhardtii* and *Chlorella vulgaris* were experimentally measured and theoretically predicted. Then, a new experimental method was developed to determine the absorption cross-section of the cells. The second part of the thesis focused on understanding how light absorption rate by the culture influences their TAG production rate. Microalgae were grown in nitrogen limited conditions in batch or continuous modes. Large TAG accumulation and productivity coincided with large rate of photon absorption suggesting that TAG production is limited by the light absorption rate in the PBR.

Keywords: Light transfer, photobioreactors, microalgae, TAG, Biodiesel, *Nannochloropsis*, Nitrogen limitation, photolimitation